



AD-A232 371

CUMENTATION PAGE

FORM 298
OCT 1988

1. REPORT DATE December 1990		2. REPORT TYPE AND DATES COVERED THESIS/DISSERTATION	
3. TITLE AND SUBTITLE Backscattering by Nonspherical Particles, Using the Coupled-Dipole Method: An Application in Radar Meteorology		5. FUNDING NUMBERS 	
6. AUTHOR(S) Clifton E. Dungey		7. PERFORMING ORGANIZATION NAME(S) AND ADDRESS(ES) AFIT Student Attending: Pennsylvania State University	
8. PERFORMING ORGANIZATION REPORT NUMBER AFIT/CI/CIA- 90-039D		9. SPONSORING MONITORING AGENCY NAME(S) AND ADDRESS(ES) AFIT/CI Wright-Patterson AFB OH 45433-6583	
10. SPONSORING/MONITORING AGENCY REPORT NUMBER		11. SUPPLEMENTARY NOTES	
12a. DISTRIBUTION AVAILABILITY STATEMENT Approved for Public Release IAW 190-1 Distributed Unlimited ERNEST A. HAYGOOD, 1st Lt, USAF Executive Officer		12b. DISTRIBUTION CODE	
13. ABSTRACT (Maximum 200 words) 			
14. SUBJECT TERMS		15. NUMBER OF PAGES 141	
		16. PRICE CODE	
17. SECURITY CLASSIFICATION OF REPORT	18. SECURITY CLASSIFICATION OF THIS PAGE	19. SECURITY CLASSIFICATION OF ABSTRACT	20. LIMITATION OF ABSTRACT

The Pennsylvania State University
The Graduate School
College of Earth and Mineral Science

BACKSCATTERING BY NONSPHERICAL PARTICLES,
USING THE COUPLED-DIPOLE METHOD:
AN APPLICATION IN RADAR METEOROLOGY

A Thesis in

Meteorology

by

Clifton E. Dungey

Accession For	
NTIS GRA&I	<input checked="" type="checkbox"/>
DTIC TAB	<input type="checkbox"/>
Unannounced	<input type="checkbox"/>
Justification	
By _____	
Distribution /	
Availability Codes	
Dist	Avail and/or Special
A-1	

Submitted in Partial Fulfillment
of the Requirements
for the Degree of

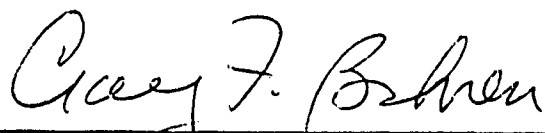
Doctor of Philosophy

December 1990




We approve the thesis of Clifton E. Dungey.

Date of Signature



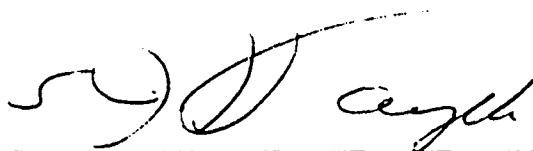
Craig F. Bohren
Distinguished Professor of Meteorology
Thesis Advisor
Chair of Committee

19 September 1990



Thomas P. Ackerman
Associate Professor of Meteorology

19 Sept 1990



Sabih I. Hayek
Professor of Engineering Mechanics

Sept 19, 1990



Akhlesh Lakhtakia
Assistant Professor of Engineering
Science and Mechanics

Sept 19, 1990



William M. Frank
Professor of Meteorology
Head of the Department of Meteorology

19 Sept 1990

ABSTRACT

In the coupled-dipole method, an arbitrary particle is modeled as an array of N polarizable subunits each of which gives rise to only electric dipole radiation. The total scattering is calculated by summing the waves scattered by each dipolar subunit excited by the incident wave and the waves of all the other dipolar subunits. By accounting for the dipolar interactions, the accuracy of the scattering calculations improves, but the mathematics become more complicated. The matrix inversion and scattering-order techniques are used to solve for the dipolar interactions.

The Clausius-Mosotti relation has been the most widely used effective-medium theory to relate the polarizability of the dipolar subunits to the refractive index of the bulk particle that the array represents. The polarizability of the dipolar subunits has been calculated using the electric dipole coefficient from Mie theory. This alternative expression for polarizability leads to scattering calculations that better agree with Mie theory.

Of all scattering angles, backscattering is the most sensitive to small changes in particle size and shape. The coupled-dipole method's ability and limitations for calculating backscattering are demonstrated. For particles with size parameter less than that associated with the first backscattering minimum, the coupled-dipole method agrees favorably with Mie theory. For particles

with larger size parameters the agreement decreases, but accuracy generally improves by increasing the number of dipolar subunits in the array.

Backscattering of 94 GHz Doppler radar by raindrops can be used to infer clear air velocity; backscattering by ice crystals may provide similar information. Backscattering at 94 GHz by randomly oriented ice plates or columns does not agree with backscattering by equal-volume ice spheres for size parameters greater than 0.8. Backscattering depends on zenith angle for ice crystals whose principle axes are confined to the horizontal plane. The relationship between first backscattering minimum and size parameter varies with particle shape and zenith angle. Backscattering of vertically polarized light is more sensitive to the presence of ice columns while horizontally polarized light is more sensitive to ice plates.

TABLE OF CONTENTS

LIST OF FIGURES	vii
LIST OF TABLES	x
ACKNOWLEDGEMENTS	xi
Chapter 1. INTRODUCTION	1
Motivation	5
Organization	6
Chapter 2. THE COUPLED-DIPOLE METHOD	8
Formulation of the Dipole Interaction Equation	9
Solution Techniques	13
Matrix Inversion Technique	13
Scattering-Order Technique	16
Other Techniques	20
Chapter 3. DOYLE'S METHOD FOR CALCULATION OF POLARIZABILITY	22
Chapter 4. SCATTERING CALCULATIONS USING THE COUPLED-DIPOLE METHOD	29
Particle Shape	29
Particle Size	39
Scattering Matrices	42
Cross Sections	47
Extinction	48
Scattering	49
Absorption	50
Backscattering	50

Chapter 5. BACKSCATTERING CALCULATIONS	53
Shape and Size Dependence of Backscattering	54
Limitations of the Coupled-Dipole Method	60
Backscattering by Equal-Volume Particles	66
Backscattering of 94GHz Radar by Ice Crystals	74
Ice Spheres	76
Hexagonal Columns and Plates	76
Chapter 6. SUMMARY AND CONCLUSION	94
Appendix A. LIGHT SCATTERING BY NONSPHERICAL PARTICLES: A REFINEMENT TO THE COUPLED-DIPOLE METHOD	100
Abstract	100
Introduction	101
Effective-Medium Theory	104
Surface Modes	112
Surface Modes for Spherical Particles	114
Shape Effects on Surface Modes	122
Conclusions	126
Acknowledgements	127
Appendix B. SUBROUTINES FOR BUILDING DIPOLAR ARRAYS	128
REFERENCES	136

LIST OF FIGURES

4.1	Arrays of dipoles arranged to represent spheres	32
4.2	Arrays of dipoles arranged to represent spheroids	33
4.3	Arrays of dipoles arranged to represent a rectangular solid and a cylinder	35
4.4	Arrays of dipoles arranged to represent hexagonal crystals	38
5.1	Diagram showing the relationship between the phase difference of two scattered waves and the distance between the scatterers	56
5.2	Importance of dipole interaction for backscattering calculations	58
5.3	Forward scattering and backscattering by spheres of increasing size parameter	59
5.4	Comparison of coupled-dipole method with Mie theory for spheres of increasing size parameter	62
5.5	Improvement of backscattering by increasing the number of dipoles	63
5.6	Backscattering of unpolarized light by equal-volume particles with aspect ratio 5:1 and refractive index $1.5 + i0.00$	68
5.7	Backscattering of horizontally polarized light by equal-volume particles with aspect ratio 5:1 and refractive index $1.5 + i0.00$	69
5.8	Backscattering of vertically polarized light by equal-volume particles with aspect ratio 5:1 and refractive index $1.5 + i0.00$	70
5.9	Backscattering of unpolarized light by equal-volume particles with aspect ratio 5:1 and refractive index $1.5 + i0.50$	71
5.10	Comparison of coupled-dipole method with Mie theory for an ice sphere at 94 GHz ($m = 1.878 + i0.0005$)	77

5.11	Backscattering of unpolarized light by randomly-oriented, equal-volume particles of increasing size parameter	79
5.12	Backscattering of unpolarized light by ice columns of increasing size parameter at various zenith angles	81
5.13	Backscattering of unpolarized light by ice columns of increasing size parameter at various zenith angles	82
5.14	Backscattering of horizontally polarized light by ice columns of increasing size parameter at various zenith angles	83
5.15	Backscattering of vertically polarized light by ice columns of increasing size parameter at various zenith angles	84
5.16	Backscattering by ice columns of increasing size parameter at zenith angle of 70°	85
5.17	Backscattering of unpolarized light by ice plates of increasing size parameter at various zenith angles	87
5.18	Backscattering of horizontally polarized light by ice plates of increasing size parameter at various zenith angles	88
5.19	Backscattering of vertically polarized light by ice plates of increasing size parameter at various zenith angles	89
5.20	Backscattering by ice plates of increasing size parameter at zenith angle of 50°	90
A.1	A spherical particle which has been represented by an array of 136 dipolar subunits	102
A.2	Comparison between Mie theory and the coupled-dipole method using different schemes to calculate polarizability while varying the number of dipolar subunits	108
A.3	Comparison between Mie theory and the coupled-dipole method using different schemes to calculate polarizability while varying the size of the dipolar subunits	109
A.4	Complex refractive index and dielectric function as a function of wavenumber for quartz	113

A.5	Extinction efficiency as a function of particle radius obtained from Mie theory and the coupled-dipole method	.115
A.6	Extinction cross section per unit volume as a function of wavenumber for spheres118
A.7	Pictorial representation of small-particle extinction for quartz	.123
A.8	Extinction cross section per unit volume as a function of wavenumber for spheroids125

LIST OF TABLES

2.1	An example of how the number of scattering orders necessary for series convergence increases with size parameter	19
4.1	Physical characteristics of dipolar arrays that are constructed by subroutine SPHERE	41
4.2	Results from the three independent equations used to determine C_{sca} , C_{abs} , and C_{ext}	51
5.1	Effect of small variations in shape on backscattering calculations	65
A.1	Comparison of Q_{ext} for nine spheres with different refractive indices as calculated by Mie theory and by the coupled-dipole method	111
A.2	Comparison of C_{ext}/v among seven dipolar arrays	120

ACKNOWLEDGEMENTS

I wish to express my sincere appreciation to my thesis advisor, Professor Craig F. Bohren, for his guidance and understanding during my graduate studies. I would like to thank Dr. Akhlesh Lakhtakia, Dr. Thomas Ackerman, and Dr. Sabih Hayek for serving as committee members. A special thanks is extended to Dr. Shermila Singham for providing several versions of the computer program that was adapted for use in my research.

I wish to thank fellow graduate students Andrew Vogelmann and Keith Kendall for their many valuable discussions. I would also like to acknowledge B. Scott Dickson and Louis Pepe of the Center for Academic Computing for providing the computer programs for drawing the dipole arrays.

Lastly, I am most deeply grateful to my wife, Carol. This research could not have been accomplished without her support. I pray that my daughters, Caryn and Colleen, will forgive me for spending many evenings in the big building.

This dissertation is dedicated to my parents.

Chapter 1

INTRODUCTION

Scattering and absorption of electromagnetic waves are due to the heterogeneity of matter. All matter is composed of discrete charged particles. When an electromagnetic wave excites a charged particle it oscillates; the acceleration of the particle gives rise to electromagnetic energy radiated in all directions. This radiation is called scattered radiation. If oscillation of the particle is not in phase with the incident wave, some of the incoming energy is absorbed.

Understanding this microscopic description of the scattering process is not a prerequisite for all scattering calculations. For example, the laws of specular reflection and of refraction were known empirically long before J. J. Thompson demonstrated that atoms contain electrons. In these cases the microscopic actions of charged particles can be described by empirically derived macroscopic equations. Although these macroscopic solutions to scattering problems are qualitatively simple to understand and use, they are easiest to apply to simple geometries such as optically smooth planes. Scattering by macroscopic particles can be calculated using macroscopic equations. If the shape of a particle can be described by one of the coordinate systems for which the technique of separation of variables can be exploited, an analytic solution for scattering may be found. Solutions exist for spheres

(Mie, 1908), infinite cylinders (Rayleigh, 1881), and spheroids (Asano and Yamamoto, 1975). Logan (1965) provided an interesting historical account of the solution for scattering by a sphere.

The task of calculating the scattering by an arbitrary particle becomes more difficult; several numerical methods are available. The T-matrix method is an integral formulation that obtains a solution by iteratively matching boundary conditions of the internal and scattered fields of the particle. The method was first developed by Waterman (1965) and later made less restrictive by Waterman (1971). Barber and Yeh (1975) applied the T-matrix method to scattering problems and renamed it the Extended Boundary Condition Method. In the point-matching method (Oguchi, 1973) the fields inside and outside the particle are calculated, and the tangential field components are required to be continuous or matched across the boundary. Perturbation methods treat nonspherical particles as spheres with a distorted boundary to estimate the scattered field (Yeh, 1964). The Purcell-Pennypacker method (Purcell and Pennypacker, 1973) solves the problem of scattering by an arbitrary particle by representing the particle as an array of polarizable subunits. The total scattered field is determined by summing the waves scattered by each dipolar subunit (also referred to as dipoles) that is excited by the incident wave as well as by the scattered waves of all the other dipoles.

In this dissertation, the Purcell-Pennypacker method is used. Recently, it has appeared in print under several different names: the coupled-dipole

approximation (Singham and Salzman, 1986); the digitized Green's function (Goedecke and O'Brien, 1988); and the discrete dipole approximation (Draine, 1988). Hereinafter it will be referred to as the coupled-dipole method, a name that better conveys the physical principles underlying the method.

Gray (1916), Kirkwood (1936), and Cassim and Taylor (1965) considered the interaction of dipoles, i.e. coupled dipoles; however, Purcell and Pennypacker were the first to include the interactions when calculating absorption and scattering by optically homogeneous particles and to compare the results with an analytic solution. Having a computer to perform the mathematical calculations was an advantage that Purcell and Pennypacker had over their predecessors, and the larger size and faster speed of today's computers continue to attract scientists and engineers to the coupled-dipole method. This is evident when examining the number of published papers which include calculations by or modifications to the coupled-dipole method.

In the first few years following 1973, most articles citing Purcell and Pennypacker contained simple applications of the method or only mentioned its existence. The number of citations from 1974 to 1977 totaled seven; nearly all were from articles published in astrophysical journals. Then, in an optics journal, Yung (1978) published an iterative technique for solving the dipole interactions. By exploiting the symmetry of a sphere and of the incident plane wave, he was able to increase the number of dipolar subunits to over 15,000 from the several hundred used by Purcell and Pennypacker. Shortly after this,

Chiappetta (1980) published another iterative solution that he referred to as a multiple scattering technique. The advantage of this technique is a substantial decrease of computer memory required to carry out the scattering calculations. The number of citations of the original Purcell-Pennypacker paper grew to ten from between 1978 and 1980; between 1981 and 1983 it decreased to three. The popularity of them again increased through the mid-1980s. Astronomers studying the characteristics of interstellar particulate matter (Wright, 1988; Draine, 1988) were joined by scientists interested in scattering by chiral particles and dielectric helices (e.g. Singham et al. 1986a; Chiappetta and Torresani, 1988), agglomerated soot particles (Jones, 1979; Drolen and Tien, 1987), dielectric cubes (Kattawar et al., 1987), fractal dust grains (Wright, 1987), foreign objects on a flat surface (Taubenblatt, 1990), and ice crystals (O'Brien and Goedecke, 1988; Flatau et al. 1988, 1990; Evans and Vivekanandan, 1990; Vogelmann et al., 1990).

During the last few years several alternative solution techniques were published. Singham et al. (1986b) showed how the scattering properties of randomly oriented particles could be calculated quickly having first determined the inverse of the interaction matrix. Singham and Bohren (1988) reexamined the scattering-order technique, which was published earlier by Chiappetta (1980). To reduce computational roundoff error, Draine (1988) added several mathematical steps to the conjugate gradient technique for solving the interaction matrix. He also described how the computation time could be

reduced if the particle shape with respect to the incident plane wave was symmetric. Flatau et al. (1990) reported on the block-Toeplitz method for inverting the interaction matrix.

Motivation

Cloud and precipitation remote sensing at 94 GHz has become possible only recently by advances in microwave radar technology (Lhermitte, 1987). The pulsed Doppler radar enables the meteorologist to observe the motion and growth of small hydrometeors; this is not possible with radars that operate at centimeter wavelengths. For certain rainfall events, the backscattered signal is used for determining the clear air velocity (Lhermitte, 1988). Mie theory is used to calculate backscattering by spherical raindrops; however, it is not appropriate for calculating backscattering by nonspherical ice crystals. The coupled-dipole method is used to show that minima occur in the backscattered signal from ice crystals as a function of size parameter. As a result of the nonsphericity of the ice crystals that were modeled, these minima appear at different size parameters for different incident wave zenith angles. The minima also depend on ice crystal shape. Thus, it may be possible to use 94 GHz radar backscattered signal to estimate the shape and size distribution of ice crystals in the 1 to 4 mm size range. By decreasing the wavelength of

the radar, information about smaller ice crystals would be available (Lhermitte, 1990).

Organization

Since Purcell and Pennypacker first published the coupled-dipole method in 1973, its formulation has remained essentially unchanged. A general description of the model is presented in Chapter 2. Recently, the model has been extended to include particles of optically active material (Singham; 1986) and anisotropic material (Varadan et al., 1989).

An integral part of the coupled-dipole method is the effective-medium theory that provides the relationship between the polarizability of the dipolar subunits and the refractive index of the particle the array represents. The most widely used scheme for this is the Clausius-Mosotti relation. Draine (1988) added a radiative reaction term which guarantees that the polarizability will have an imaginary component even if the refractive index of the particle is purely real. This was done to avoid violation of the optical theorem. A complex polarizability can also be guaranteed by using the electric dipole term from Mie theory (Doyle, 1988). Incorporation of this scheme in the coupled-dipole method and consequent improvements in scattering calculations are described in Chapter 3 and Appendix A.

The coupled-dipole method provides values of the electric field scattered by an arbitrary particle. Chapter 4 describes how the input data has been manipulated to enhance the usefulness of the coupled-dipole method. Derivations of equations for calculating observable scattering parameters from the output data are also presented.

In remote sensing of the atmosphere, often only the backscattered signal is readily available. Chapter 5 reports the advantages, disadvantages, and limitations of using the couple-dipole method for determining backscattering by arbitrary particles. In the final section, application of the coupled-dipole method for determining the backscattered signal from ice crystals at 94 GHz (3.2 mm) is discussed.

Chapter 2

THE COUPLED-DIPOLE METHOD

The coupled-dipole method, which is based on a simple physical description of how a particle scatters electromagnetic waves, has remained essentially unchanged since it was published by Purcell and Pennypacker (1973). Its formulation is based on representing an arbitrary particle by an array of N dipolar subunits arranged on a lattice. The dipolar subunits are sufficiently small to give rise to only electric dipole radiation. Total scattering is then calculated by summing the electromagnetic waves scattered by each dipolar subunit excited by the incident wave as well as the waves scattered to it from all other dipolar subunits.

The coupled-dipole method can be thought of as an extension of the Rayleigh-Gans theory. Whereas interactions among the dipolar subunits are ignored in the Rayleigh-Gans theory, they form an integral part of the coupled-dipole method. Including interactions improves the accuracy of scattering calculations, but also necessitates solving a $3N \times 3N$ complex matrix. Gray (1916), Kirkwood (1936), and Cassim and Taylor (1965) published earlier investigations similar to the coupled-dipole method; however, Purcell and Pennypacker were apparently the first to apply the method to absorption and scattering by optically homogeneous particles and compare the results with an analytic solution.

The key to the coupled-dipole method is the interaction of the dipolar subunits. The following derivation of the electric dipole radiation field will provide a better understanding of these interactions. The derivation is similar to that by Jackson (1975, Chap 9); however, these equations are presented in SI units. Once the interactions are known, the solution may be obtained by direct inversion of the $3N \times 3N$ matrix or by numerical iteration. Several options are discussed in this chapter.

Formulation of the Dipole Interaction Equation

The vector potential \vec{A} is a function of the current density \vec{J} in the system:

$$\vec{A} = \frac{\mu_0}{4\pi} \int \vec{J}(\vec{x}') \frac{e^{ik_0|\vec{x}-\vec{x}'|}}{|\vec{x}-\vec{x}'|} d^3\vec{x}' \quad (2.1)$$

where μ_0 is the permeability of the material, k_0 is the free space wavenumber given by $k_0 = 2\pi/\lambda_0$, λ_0 is the free space wavelength, and \vec{x}' and \vec{x} are the locations of the charge and where the field is being evaluated, respectively. A sinusoidal time dependence $\exp\{-i\omega t\}$ of the current is assumed. Rapid spatial oscillation of the electromagnetic field allows the following approximation for the argument of the exponential term

$$|\vec{x} - \vec{x}'| \approx r - \hat{n} \cdot \vec{x}' \quad (2.2)$$

where $r = |\vec{x}|$ and \hat{n} is a unit vector in the direction of \vec{x} . For the far (radiation) zone the distance from the charge to the detector in the denominator may be replaced by r only. When the source dimensions d are small compared with the wavelength, $\exp\{-ik_0\hat{n} \cdot \vec{x}'\}$ may be expanded in powers of k . For electric dipole radiation only the first term of this expansion is kept, which simplifies the vector potential to

$$\vec{A} = \frac{\mu_0 e^{ik_0 r}}{4\pi r} \int \vec{J}(\vec{x}') d^3x' \quad (2.3)$$

Thus, the vector potential behaves like an outgoing spherical wave with a r^{-1} dependence. In fact, equation 2.3 is valid everywhere outside the source (Jackson, 1975, Sect 9.2). The only limiting assumption so far is $d \ll \lambda_0$.

Equation 2.3 can be further manipulated using integration by parts and by applying the continuity equation for current density. The vector potential becomes

$$\vec{A} = \frac{-i\mu_0 k_0}{4\pi c} \vec{p} \frac{e^{ik_0 r}}{r} \quad (2.4)$$

where \vec{p} is the electric dipole moment and c is the speed of light in vacuo.

The magnetic induction is given by: $\vec{B} = \vec{\nabla} \times \vec{A}$; while outside the source the electric field is $\vec{E} = i \frac{c}{k_0} \vec{\nabla} \times \vec{B}$. The electric field \vec{E} is now calculated

$$\vec{E} = \frac{k_0^2}{4\pi\epsilon_0} (\hat{n} \times \vec{p}) \times \hat{n} \frac{e^{ik_0 r}}{r} + \frac{[3\hat{n}(\hat{n} \cdot \vec{p}) - \vec{p}]}{4\pi\epsilon_0} \left(\frac{1}{r^3} - \frac{ik_0}{r^2} \right) e^{ik_0 r} \quad (2.5)$$

Each dipolar subunit has a dipole moment given by

$$\vec{p} = \alpha \vec{E} \quad (2.6)$$

where α is the polarizability of the dipole. Equations 2.5 and 2.6 are now combined to form a system of $3N$ equations; the resulting $3N \times 3N$ matrix is referred to as the interaction matrix. With N dipolar subunits, the exciting field \vec{E}_i at the i th dipole due to the incident radiation and the scattered radiation from the other dipolar subunits is:

$$\vec{E}_i = \sum_{j \neq i}^N [a_{ij} \alpha \vec{E}_j - b_{ij} (\alpha \vec{E}_j \cdot \hat{n}_{ij}) \hat{n}_{ij}] + \vec{E}_0 e^{i\vec{k}_0 \cdot \vec{r}_i} \quad (2.7)$$

where

$$a_{ij} = \frac{e^{ik_0 r_{ij}}}{4\pi\epsilon_0 r_{ij}} \left(k_0^2 + \frac{ik_0}{r_{ij}} - \frac{1}{r_{ij}^2} \right); \quad b_{ij} = 3a_{ij} - 2k_0^2, \quad (2.8)$$

\vec{E}_0 is the incident field, and $r_{ij} = |\vec{r}_i - \vec{r}_j|$ is the distance from the i th to the j th dipolar subunit. The polarizability α can be a complex tensor (Post, 1962), but here it is a scalar since only isotropic scatterers will be represented by arrays of spherical dipoles. The solution to equation 2.7 yields the resultant electric field at each dipole location with retardation taken fully into account.

The only limitation thus far is that the diameter of the dipolar subunits must be small enough compared with the wavelength. Since the dipolar

subunits are arranged on a simple cubic lattice and are touching (not penetrating) their neighbors, the dipolar subunit diameter may be taken to be the same as the lattice spacing. Therefore, the lattice spacing must also be smaller than the wavelength. This is equivalent to the restriction required when simplifying equation 2.3, i.e. $d \ll \lambda$. Purcell and Pennypacker (1973) expected good results when $k_0 d \leq 0.7$. From the method-of-moments literature the grid spacing should not exceed one-tenth of the wavelength ($k_0 d \leq 0.6$) (Massoudi et al., 1984). Yung (1978) placed a tighter restriction on the spacing, $k_0 d \leq 0.33$, citing the necessity for smaller phase difference of the incident wave between neighboring dipolar subunits. Recently, Draine (1988) considered the wavelength within the dipolar subunit and included the complex refractive index m of the material. To achieve 10% accuracy (based on a zero-frequency limit) his calculations suggested $k_0 d |m| \leq 1$. Table A.1 (page 111) contains examples of how the accuracy of scattering calculations using the coupled-dipole method generally decreases as $k_0 d |m|$ increases.

The derivation of the coupled-dipole method as described above is a heuristic approach founded on physical principles. A derivation of the method based on volume integrals using the free space Green's functions has been given by Lakhtakia (1990). The results of both derivations are identical, and the user is left to choose from several techniques to solve the overall scattering problem. Several techniques are described in the following section.

Solution Techniques

Equation 2.7 forms the basis of the coupled-dipole method by describing the electric dipole field radiated by each dipolar subunit. The task is to solve the $3N$ linear algebraic equations to yield the resultant field at all subunits. Several solution techniques are available, and most are standard matrix solution procedures. Purcell and Pennypacker (1973) used an iterative technique of successive substitution; Yung (1978) was the first to use the conjugate gradient technique for solving these simultaneous algebraic equations; Singham et al. (1986b) inverted the interaction matrix; Chiapetta (1980) and Singham and Bohren (1988) used an iterative technique known as the scattering-order technique; and Flatau et al. (1990) exploited the block-Toeplitz structure of the interaction matrix for rectangular particles. The two solution techniques of interest here are the matrix inversion and scattering-order. The advantages and disadvantages of these and some other techniques are now discussed.

Matrix Inversion Technique

The system of simultaneous equations arising from equation 2.7 may be expressed in the form $\mathbf{A} = \mathbf{XB}$, where \mathbf{X} is the $3N \times 3N$ interaction matrix, \mathbf{A} is the $3N \times 1$ vector containing the incident electric field components $\vec{E}_0(\mathbf{r}_i)$,

and \mathbf{B} is the $3N \times 1$ vector containing the unknown exciting field components \vec{E}_i . The matrix inversion technique solves for \mathbf{B} by inverting the interaction matrix: $\mathbf{X}^{-1}\mathbf{A} = \mathbf{B}$. By the physical nature of the problem an inverse exists, but since the matrix inversion technique is a computer-oriented routine, the inverse is obtained only if the matrix is algorithmically nonsingular. As will be discussed later, this technique offers an advantage because iterative techniques rely on mathematical series that do not always converge or converge quickly. The inverse is obtained using LINPACK¹ subroutines CGECO and CGEDI.

Another advantage of the matrix inversion technique is that the scattered field for the particle in different orientations can be calculated quickly (Singham et al., 1986b). When the coordinate system describing the particle remains fixed, the interaction matrix and its inverse remain the same. Thus, simulation of particle rotation is accomplished by rotating the incident field in the opposite sense.

The disadvantage of the matrix inversion technique is that it is very computer intensive in terms of storage requirements and computation time. For a particle represented by an array of N dipolar subunits, the $3N \times 3N$ complex interaction matrix must be stored. Compiling the program in single precision (COMPLEX * 8 on an IBM ES/3090-600) for a 250 dipolar array requires approximately 8.0 megabytes of memory. When the program is

¹LINPACK is a nonproprietary collection of subroutines amassed by the National Bureau of Standards and available at many computer facilities.

compiled in double precision rather than single precision, the scattering calculations differ by less than one percent for spheres with refractive indices between 1 and 2 and size parameters between 0.5 and 2.0. Thus, additional memory burden is avoided by not declaring the variables as COMPLEX * 16. This is not a general recommendation for not using double precision because, if the dipolar subunits are made very small compared with the incident wavelength and the incident field at adjacent dipolar subunits are nearly equal, error accumulation due to $\vec{E}_i \approx \vec{E}_{i+1}$ may require double precision. Since executable memory size increases as N^2 , this matrix solution technique cannot be used with small computers.

This solution technique may not be acceptable if CPU time is a limiting factor. The inverse matrix is determined by Gaussian elimination which, although a direct method of solution, is the slowest numerical method. Computer run time to invert a matrix associated with a 160-dipole array takes approximately 1 minute on an IBM ES/3090-600, which has a clock speed of 15 ns (six processors rated at about 65 MIPS). Since computation time is proportional to N^3 , increasing the array to 600 dipoles will increase computation time to nearly one hour. However, this technique may be attractive if the scattering response is to be calculated for multiple orientations of the particle.

Scattering-Order Technique

The second solution technique of interest is the scattering-order technique. This approach was first described by Chiapetta (1980) and independently reexamined by Singham and Bohren (1988). The advantage of using the scattering-order technique is that the interaction matrix is not required and a much larger dipolar array can be used. The scattering-order technique is based on internal scattering orders among the dipolar subunits. The following is a brief description of the scattering-order technique.

For the collection of N dipolar subunits the scattering-order technique still relies on equation 2.7, which uses the incident field and dipole interaction to calculate the electric field at each dipole; however, it can be rewritten as:

$$\vec{E}_i = \vec{E}_{0_i} + \sum_{i \neq j} C_{ij} \cdot \vec{E}_j \quad (2.9)$$

where the matrix C_{ij} is a function of a_{ij} , b_{ij} , α , and \hat{n}_{ij} . Equation 2.9 can be expressed as an infinite series in powers of C_{ij}

$$\begin{aligned} \vec{E}_i = & \vec{E}_{0_i} + \sum_{i \neq j} C_{ij} \cdot \vec{E}_{0_j} + \sum_{i \neq j} \sum_{j \neq k} C_{ij} \cdot C_{jk} \cdot \vec{E}_{0_k} \\ & + \sum_{i \neq j} \sum_{j \neq k} \sum_{k \neq m} C_{ij} \cdot C_{jk} \cdot C_{km} \cdot \vec{E}_{0_m} + \cdots \end{aligned} \quad (2.10)$$

Equation 2.10 is equivalent to a Born expansion for scattering and is described as a multiple scattering solution in the following fashion. The incident wave

hits the particle and excites the dipoles (0th scattering order or the first term on the right side of equation 2.10). The dipolar subunits then radiate to their neighbors for the first scattering order (second term of equation 2.10). The new field is calculated at each dipole location and the next scattering order is calculated--and so on until the series converges. This process can be carried out efficiently by recognizing that each higher order field may be obtained by using the results of the previous scattering order:

$$\vec{E}_i = \vec{E}_i^{(0)} + \sum_{i \neq j} C_{ij} \cdot \vec{E}_j^{(0)} + \sum_{i \neq j} C_{ij} \cdot \vec{E}_j^{(1)} + \sum_{i \neq j} C_{ij} \cdot \vec{E}_j^{(2)} + \dots \quad (2.11)$$

where $\vec{E}_i^{(k)} = \sum_{i \neq j} C_{ij} \cdot \vec{E}_j^{(k-1)}$, $k = 1, 2, 3, \dots$. Hence, each scattering order can be calculated using the previously determined fields and interaction matrix.

The scattered field is obtained by summing consecutively higher-order terms in the expansion until convergence is achieved. In this technique the field at each dipole is completely replaced for each scattering order. This reduces computer storage requirements since only a few small arrays are needed to calculate subsequent terms in the series; therefore, storage of the large $3N \times 3N$ interaction matrix is no longer necessary.

The disadvantage of the scattering-order technique is that convergence is not guaranteed. If the field amplitude at a dipole becomes greater than the incident field, successive orders may continue to increase and the series ultimately diverges (Singham and Bohren, 1988). The divergent behavior of the series depends on the particle's shape, size, and relative refractive index.

Convergence is more likely for elongated shapes, smaller size parameters, and relative refractive indices that are not much different from unity. For example, the series diverges for a sphere with a relative refractive index of $1.33 + i0.0$ when the size parameter exceeds about 3, and for a relative refractive index of $1.9 + i0.0$, divergence is observed at a size parameter of 1.7. This places a restriction on the particles that can be studied using the scattering-order technique.

When the series converges with little or no oscillation, the scattering-order technique is relatively fast. For a 160-dipole array, one iteration takes approximately 1 CPU second on an IBM ES/3090-600. Thus, if this series converges in less than 60 iterations the scattering-order technique would be more attractive than matrix inversion. By comparison the matrix inversion technique takes about 60 seconds to solve a 160-dipole array. Table 2.1 lists the number of terms in the series required to achieve convergence when modeling arrays of dipoles that represent a sphere with a refractive index of $1.9 + i0.0$. The convergence criterion is satisfied when three consecutive values of the calculated exciting field differ by less than an amount specified by the user. A tolerance value of 0.1% appears sufficient. However, this does not guarantee that the series has converged. It is also best to perform the convergence test on the backscattered field since convergence is slowest in the backward direction. Computation time for the scattering-order technique varies as N^2 . Thus, for larger arrays this technique may be more appealing

Table 2.1 An example of how the number of scattering orders necessary for series convergence increases with size parameter. The series is considered to have converged when three successive values of the backscattered field differ by less than 0.1%.

Size Parameter	Number of Dipoles	Time per iteration (sec)	Number of terms in series
0.7	461	9	7
1.2	1064	18	19
1.4	1357	23	24
1.6	1791	30	50

than the matrix inversion technique except when multiple orientations of the particle are required.

Other Techniques

Two other techniques to solve the interaction matrix are the conjugate gradient and the block-Toeplitz techniques.

Yung (1978) was the first to adapt the conjugate gradient algorithm for the coupled-dipole method. This is a nonlinear iterative technique that will reach a solution in $3N$ steps, but because the algorithm approaches the solution quickly, the series can be terminated early if a small error is acceptable (Strang, 1986, Chap 5). Computer time for an iteration is proportional to $N^2 \log N$. Like the scattering-order technique, the series within the conjugate gradient technique will not always converge.

Draine (1988) used the conjugate gradient technique to calculate scattering by particles with fourfold symmetry. Exploiting this symmetry will reduce computing time by an order of magnitude or more and ease storage requirements by about 40%. Unfortunately, not all particles have this symmetry, and even when they do, this computational short-cut is limited to only a few particle orientations.

Flatau et al. (1990) introduced the block-Toeplitz technique into the coupled-dipole method. This technique exploits symmetries of the interaction

matrix when the dipole array represents a cube or parallelepiped. Minimal storage requirements are the strong point of the block-Toeplitz technique, and while it is much faster than the matrix inversion technique, it is slightly slower than the conjugate gradient technique.

All matrix solution techniques have advantages that make one more attractive than another depending on the application. In this dissertation the matrix inversion and scattering-order techniques were chosen for particular purposes. The matrix inversion technique is used in Chapter 3 for testing a new method for determining the polarizability of the dipolar subunits. It is used again in Chapter 5 for calculating scattering by particles in multiple orientations. The scattering-order technique is also used in Chapter 5 to calculate scattering by particles that are represented by arrays too large for the matrix inversion technique.

Chapter 3

DOYLE'S METHOD FOR CALCULATION OF POLARIZABILITY

Purcell and Pennypacker (1973) formulated the coupled-dipole method to study scattering by arbitrary particles at non-zero frequencies. The arbitrary particle is represented by an array of polarizable subunits arranged on a simple cubic lattice. To solve the scattering problem one must choose a technique to solve the system of linear equations and also determine how to represent the polarizable subunits. Several solution techniques were discussed in Chapter 2; in this chapter a scheme to determine the electric-dipole polarizability of the dipolar subunits is described.

Splitting the homogeneous scatterer into smaller objects alters its electromagnetic description. To relate the discrete and continuous aspects of the particle, Purcell and Pennypacker used the Clausius-Mosotti (CM) relation. Like every effective-medium theory the CM relation is approximate, but it has been used by nearly all adherents of the coupled-dipole method. Here, based on work by Doyle (1989), an alternative method for calculating polarizability is presented.

No material is homogeneous in the absolute sense. A medium which is perceived as homogeneous is actually comprised of heterogeneities, i.e. charged particles. As long as the heterogeneities (referred to hereinafter as grains) are much smaller than the wavelength, the behavior of an electromagnetic wave

passing through such a medium can be described statistically by estimating the bulk optical property of the particle using an effective-medium theory (Bohren and Wickramasinghe, 1977). An effective-medium theory requires knowledge of the volume fraction of the embedded grains and the optical properties of the grains and the surrounding matrix.

When the grains are composed of many molecules, the material can be characterized by an effective dielectric function using the Maxwell Garnett (MG) theory (Maxwell Garnett, 1904; Bohren and Huffman, 1983, Sect 8.5):

$$\epsilon_{av} = \frac{(1-f)\epsilon_m + f\beta\epsilon}{1-f+f\beta}, \quad (3.1)$$

where ϵ_{av} , ϵ , and ϵ_m are the dielectric functions of the bulk medium, grains, and surrounding matrix, β is a function of grain shape, and f is the volume filling factor of the grains. If the grains are spherical, $\beta = 3\epsilon_m/(\epsilon + \epsilon_m)$, and equation 3.1 can be rewritten as

$$\epsilon_{av} = \epsilon_m \left[1 + \frac{3f \left(\frac{\epsilon - \epsilon_m}{\epsilon + 2\epsilon_m} \right)}{1 - f \left(\frac{\epsilon - \epsilon_m}{\epsilon + 2\epsilon_m} \right)} \right]. \quad (3.2)$$

Spheroidal dipolar subunits have been described in other applications of the coupled-dipole method (Singham, 1986). In the case of the coupled-dipole method, the dielectric function of the particle ϵ_{av} and the matrix ϵ_m are known

and the dielectric function of the grains ϵ must be determined. Rearrangement of equation 3.2 yields

$$\epsilon = \frac{2(1-f)\epsilon_m^2 - (2+f)\epsilon_m\epsilon_{av}}{(1-f)\epsilon_{av} - (1+2f)\epsilon_m}. \quad (3.3)$$

This form of the MG theory will be mentioned later in the chapter.

When the grains are too small to be assigned a dielectric function, the Clausius-Mosotti (CM) relation (also known as the Lorentz-Lorenz equation) may be used to determine the polarizability α of the grains

$$\alpha = \frac{3(\epsilon_{av} - \epsilon_m)}{N(\epsilon_{av} + 2\epsilon_m)} = \frac{3(m^2 - 1)}{N(m^2 + 2)}, \quad (3.4)$$

where N is the number density of the grains per unit volume ($N \propto f^{-1}$), and m is the complex relative refractive index. Even though the MG theory and CM relation give different physical properties, they are very similar. Barker (1973) published a derivation of the MG equation that is formally equivalent to the derivation of the CM relation.

In the coupled-dipole method the grains are the dipolar subunits. The means to estimate the dielectric function or the polarizability of the subunits are given in equations 3.3 and 3.4. The relationship between ϵ and α of the dipolar subunits is obtained by combining these equations to produce another form of the Clausius-Mosotti relation:

$$\alpha = 4\pi a^3 \frac{(\epsilon - \epsilon_m)}{(\epsilon + 2\epsilon_m)}, \quad (3.5)$$

where a is radius of the dipolar subunit. This brief discussion of effective-medium theory provides a basis for introducing Doyle's method for calculating the electric dipole polarizability of the dipolar subunits.

For a sphere in the longwave limit ($x \ll 1$, $|m|x \ll 1$, where x is the size parameter: $x = 2\pi a/\lambda_0$, with a being the radius and λ_0 the wavelength of electromagnetic radiation in free space) the scattering amplitude S_1 is given by (Bohren and Huffman, 1983, Sect 5.2)

$$S_1 = \frac{-ik^3 \alpha}{4\pi}. \quad (3.6)$$

Since the sphere is in the Rayleigh regime for scattering, the scattering amplitude can be expressed as $S_1 = (3/2)a_1$, where a_1 is the electric dipole coefficient from Mie theory. Thus, the polarizability can be written in terms of the electric dipole coefficient

$$\alpha = i \frac{6\pi}{k^3} a_1. \quad (3.7)$$

Since interactions between the dipolar subunits in the coupled-dipole method are due to electric dipole radiation, this expression may be appropriate for calculating the polarizability of the subunits. Equation 3.7 does not differ from

equation 3.5 in the zero frequency limit. If a_1 is expanded in terms of the size parameter x and the series truncated after the first term, then equation 3.7 is identical to equation 3.5.

Doyle (1989) used equation 3.7 for determining the reflectance of a composite of silver spheres in a transparent medium and obtained calculated values that agreed better with experimental values than if only the first term in the series had been used. The task now is to use this expression in the coupled-dipole method and see if it improves scattering calculations.

From this point on the calculation of the electric dipole polarizability using a_1 will be known as Doyle's method; equation 3.7 will be referred to as Doyle's expression. The value for a_1 , the electric dipole coefficient, is given by:

$$a_1 = \frac{m\psi_1(mx)\psi_1'(x) - \psi_1(x)\psi_1'(mx)}{m\psi_1(mx)\xi_1'(x) - \xi_1(x)\psi_1'(mx)} \quad (3.8)$$

where ψ and ξ are the Ricatti-Bessel functions given by:

$$\psi_1(x) = \frac{\sin(x)}{x} - \cos(x), \quad \psi_1'(x) = \frac{-\sin(x)}{x^2} + \frac{\cos(x)}{x} + \sin(x) \quad (3.9)$$

and

$$\xi_1(x) = -i\frac{e^{ix}}{x} - e^{ix}, \quad \xi_1'(x) = \frac{ie^{ix}}{x^2} + \frac{e^{ix}}{x} - ie^{ix} \quad (3.10)$$

Thus, Doyle's expression gives the exact value for the electric dipole polarizability.

Most applications of the coupled-dipole method use the CM relation as it appears in equation 3.4. In this form only the dielectric functions of the bulk particle and the surrounding medium are required. To use Doyle's method, the complex refractive index m of the dipolar subunits must be determined for equation 3.8 using equation 3.3 where $m = (\epsilon/\epsilon_m)^{1/2}$.

Scattering calculations using Doyle's expression to calculate polarizability in the coupled-dipole method are discussed in Appendix A beginning on page 104. The results are compared with two other methods for calculating the polarizabilities: the CM relation and an expression published by Draine (1988). Draine introduced a radiative reaction term to the CM relation which guarantees a non-zero imaginary part of the polarizability to account for attenuation when the refractive index of the material is real. The solutions using these three methods were compared with Mie theory (Bohren and Huffman, 1983, Appendix A). In all cases scattering calculations using Doyle's expression agreed with Mie theory better than when using the CM relation or Draine's radiative reaction term.

Another test for Doyle's expression occurs at a Fröhlich frequency. This is an absorption mode where the relative complex dielectric function approaches -2: $\epsilon/\epsilon_m \rightarrow -2 + i0$. At the Fröhlich frequency the CM relation yields an unbounded polarizability while Doyle's expression remains bounded.

A Fröhlich frequency occurs for quartz in the infrared part of the electromagnetic spectrum. Scattering calculations using the coupled-dipole method with Doyle's method were shown to agree favorably with measured data. A detailed discussion and results of using Doyle's expression at a Fröhlich frequency is found in Appendix A beginning on page 112.

Chapter 4

SCATTERING CALCULATIONS USING
THE COUPLED-DIPOLE METHOD

The description of the coupled-dipole method in Chapters 2 and 3 has been focused on its formulation, solution techniques for determining dipolar interactions, and a new scheme for determining the polarizability of the dipolar subunits. This chapter contains information on how the input data can be manipulated to enhance the usefulness of the program and includes derivations of some of the observable scattering parameters that are calculated by the program. A version of the coupled-dipole method computer program was obtained from Singham, and the modifications described in this chapter were made to serve the needs of the research presented here and in the future.

Particle Shape

An advantage of the coupled-dipole method over other methods used to calculate scattering by nonspherical particles is that a particle of any shape can be modeled. In the coupled-dipole method a particle is represented by an array of subunits located on a cubic lattice. However, caution is required when constructing the array or choosing the coarseness of the lattice spacing. For example, consider an array of eight dipolar subunits (hereinafter referred

to as dipoles) situated on the vertices of a cube centered about the origin. This simple array represents a cube; however, as will be described soon, it could also represent a sphere constructed of all the dipoles within $\sqrt{3}/2$ units of the origin. This ambiguity of shape must be minimized when building arrays of dipoles. Another example of poor particle representation is the depiction of a cylinder as a single string of dipoles. This configuration lacks adequate cross sectional area and no sagittal dipole interaction necessary to represent the cross section. Subroutines for several particle shapes are available in the coupled-dipole method; they are briefly described here, and their listings are found in Appendix B.

The unit of length used to describe the particle dimensions in this dissertation is the lattice space (ls). One lattice space is the distance from the center of one dipole to the center of an adjacent dipole. For determining the equivalent volume of a dipolar array, one dipole is considered to have unit volume.

Subroutine SPHERE builds a dipolar array to represent a spherical particle in the following manner. To model a sphere of radius a , the subroutine builds a cube with sides $2a$, centered at the origin. All lattice points within the cube that fall within a distance of the origin are included in the array. The position of the origin with respect to the lattice is optional; however, two logical choices exist. The origin can be centered on one dipole which will be referred to as the central dipole (0.0, 0.0, 0.0), or the origin can

lie in the midst of a core of eight dipoles that are offset by one-half dipole diameter into respective octants of the coordinate system ($\pm 0.5, \pm 0.5, \pm 0.5$). Many published papers use only the latter option, which reduces the number of arrays that can be used to represent a sphere. A sphere of each type is shown in Figure 4.1. The top array represents a sphere with the origin centered on a dipole and contains 251 dipoles. It is constructed by choosing a radius of 3.8 ls and has an effective radius of 3.91 ls. The bottom sphere has the origin centered in a core of eight dipoles and contains 304 dipoles. It is constructed by choosing a radius of 4.1 ls and has an effective radius of 4.17 ls. More will be said about the effective radius of particles in the section describing particle size, which begins on page 38. Scattering by a sphere calculated by the coupled-dipole method has been shown to compare favorably with Mie theory (e.g., Yung, 1978; Singham and Bohren, 1988).

Subroutine SPHEROID is similar to subroutine SPHERE except that criteria for including dipoles in the array are based on the principal radii of a spheroid. The subroutine is set up to build a prolate (oblate) spheroid with its major (minor) axis in the z-direction. The spheroid is automatically centered around the origin; thus the central dipole may or may not be located at the origin depending on whether the major and minor radii are represented by an odd or even number of dipoles. For this reason subroutine SPHERE is a separate entity and not a special case within subroutine SPHEROID.

Examples of spheroids are shown in Figure 4.2. The top array represents a

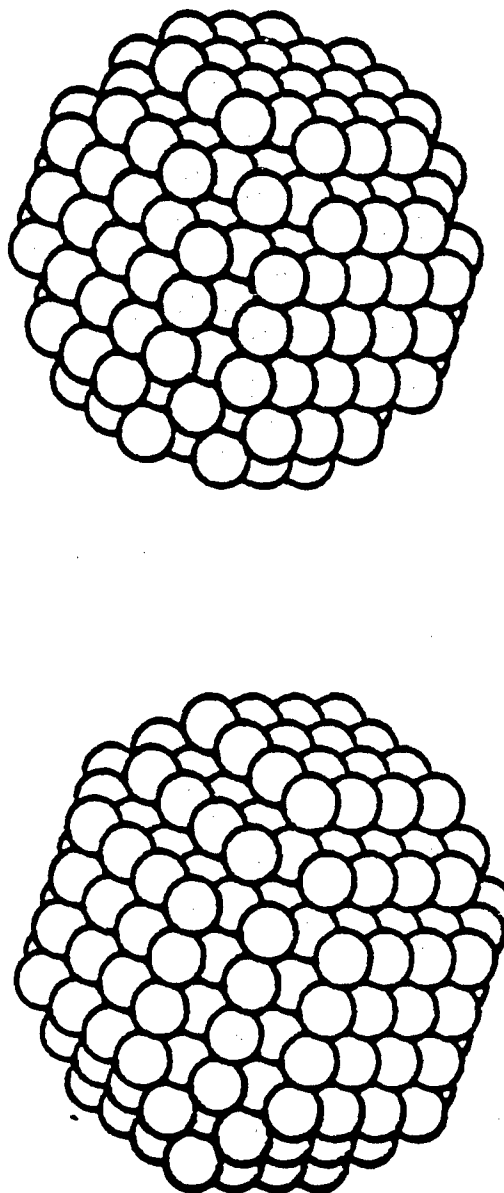


Figure 4.1 Arrays of dipoles arranged to represent spheres. The top array contains 251 dipoles and has an effective radius of 3.91 ls; the bottom array contains 304 dipoles and has an effective radius of 4.17 ls.

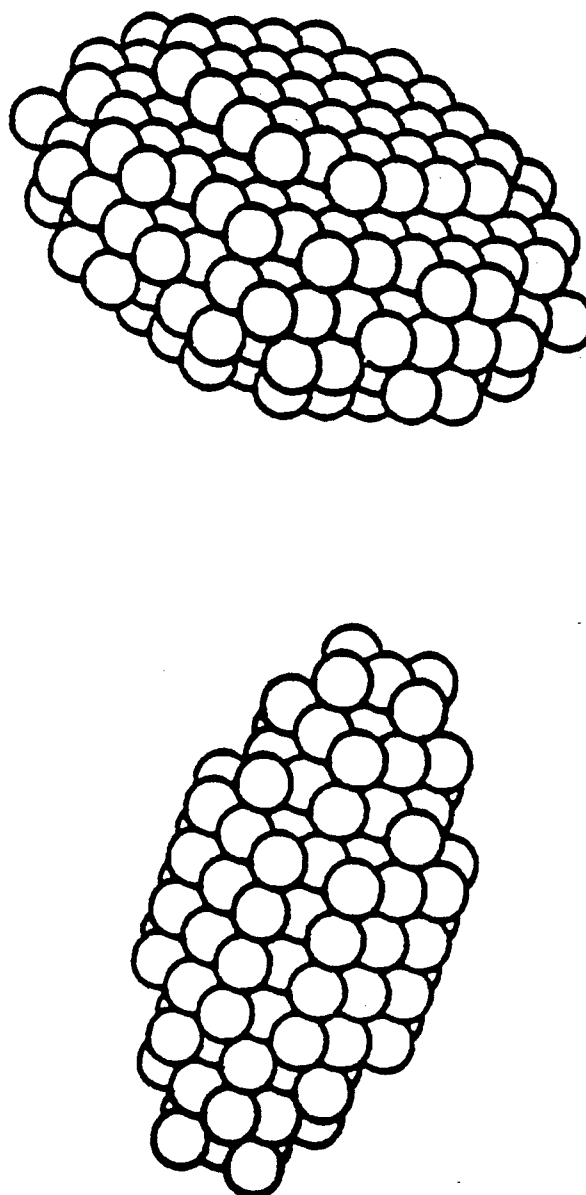


Figure 4.2 Arrays of dipoles arranged to represent spheroids. The top array contains 290 dipoles and represents a 2×1 oblate spheroid; the bottom array contains 128 dipoles and represents a 2×1 prolate spheroid.

2×1 oblate spheroid, contains 290 dipoles, and has an equivalent spherical radius of 4.11 ls. The bottom array represents a 2×1 prolate spheroid, contains 128 dipoles, and has an equivalent spherical radius of 3.21 ls. Unlike a sphere, scattering by spheroids and other particle shapes that will be discussed is orientationally dependent. Scattering by spheroids using the coupled-dipole method has been shown to compare favorably with the T-matrix method at low frequencies and low refractive indices (Goedecke and O'Brien, 1988).

The subroutine RECTSLD builds a dipolar array that represents a rectangular solid. The user specifies the x -, y -, and z -dimensions, and the subroutine centers the particle around the origin. This subroutine was written to compare results published by Purcell and Pennypacker (1973). The block-Toeplitz technique for solving the interaction matrix equation specifically handles particles of this shape (Flatau et al., 1990). Unfortunately, few applications in meteorology require knowledge of scattering by rectangular particles. An example of this type of particle is shown in the top part of Figure 4.3. The array is constructed with x -, y -, and z -dimensions of 4, 4, and 10, and contains 160 dipoles.

Subroutine CYLNDER constructs a cylinder with its longitudinal axis in the x direction. Input parameters for assembling the array include the length, the radius of the circular cross section, and whether the center dipole of the cross section is located on the x -axis ($x, 0.0, 0.0$) or if four dipoles are

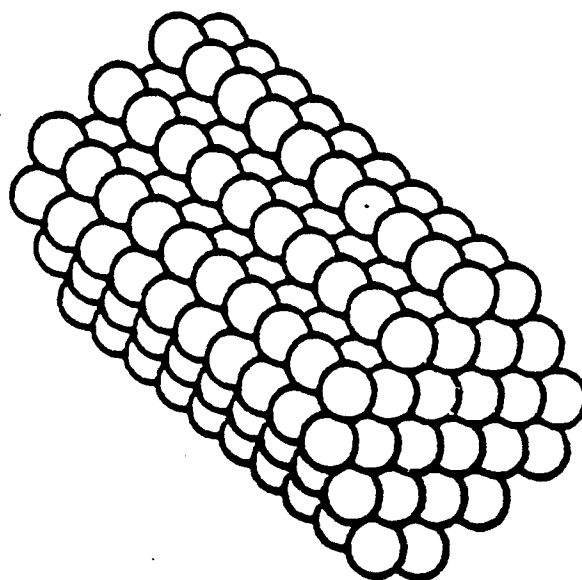
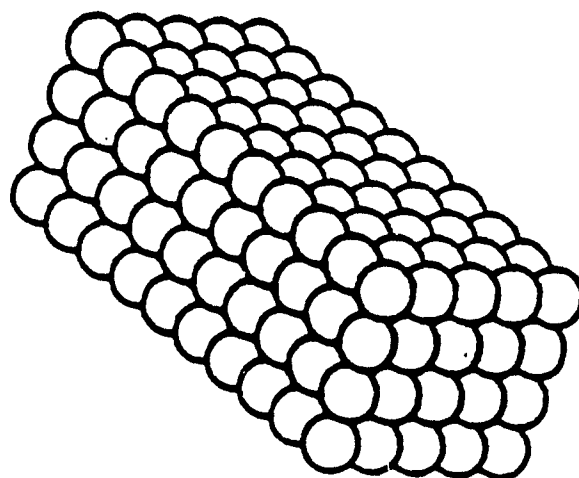


Figure 4.3 Arrays of dipoles arranged to represent a rectangular solid and a cylinder. The top array contains 160 dipoles and represents a $4 \times 4 \times 10$ rectangular solid; the bottom array contains 240 dipoles and represents a cylinder with a cross-sectional radius of 2.9 ls and a length of 10 ls .

centered around the x-axis $[(x, \pm 0.5, \pm 0.5)$ similar to the offset option in SPHERE]. An example of a cylindrical particle is shown in the bottom half of Figure 4.3. The array is constructed by choosing a cross-sectional radius of 2.9 ls, has a length of 10 ls, contains 240 dipoles, and has an effective circular cross-section radius of 3.04 ls. Scattering by a finite cylinder was compared with the results of an analytic solution for infinite cylinders, BHCYL (Bohren and Huffman, 1983, Appendix C). Approximations based on Fraunhofer diffraction theory indicate that cylinders with an aspect ratio greater than 10:1 may be regarded as effectively infinite (Bohren and Huffman, 1983, Sect 8.4.7). For such a cylinder, scattering calculations using the coupled-dipole method and BHCYL are in good agreement. For example, values of extinction efficiency per unit length for cylinders with a refractive index of $1.33 + i0.4$ are within 2%.

Subroutine FCC builds a sphere similar to SPHERE except that the dipoles are placed on a face-centered cubic lattice rather than simple cubic. The creation of FCC was to test a different dipole spacing scheme. Since a face-centered cubic lattice has 12 nearest neighbors rather than only 6 as with the simple cubic, and it has a packing fraction higher by a factor of $\sqrt{2}$ (Kittel, 1976), it was thought that a better representation of a sphere could be achieved with little effort. The disadvantage of this structure would be that with an increased number of dipoles, more computer storage and computing time is required to solve the interaction matrix for an equal-sized sphere.

Another concern with this structure is that mathematical approximations that hold for the simple cubic lattice may not be valid for the face-centered cubic lattice. Lorentz showed that for atoms on a simple cubic lattice the electric field resulting from the contributions of the nearest dipoles (\vec{E}_{near}) vanishes at any lattice site (Jackson, 1975, Section 4.5). Although face-centered cubic is not equivalent to simple cubic, the structure may be symmetric enough to assume $\vec{E}_{\text{near}} \approx 0$. If this approximation were not valid the CM relation (and Doyle's expression) would need to be reformulated. Scattering calculations were made using SPHERE and FCC and were compared with results from Mie theory. Since SPHERE compared more favorably with Mie than FCC it appears that the approximation $\vec{E}_{\text{near}} \approx 0$ may not be valid.

Subroutine HEXAGON constructs a hexagon crystal with its longitudinal axis lying in the x direction and two vertices aligned with the z axis. Depending on the input parameters, the array can represent either a hexagonal plate or column. Because the array is positioned on a simple cubic lattice, a regular hexagon is difficult to construct. Instead of 120° angles, the hexagon is constructed with 90° and 135° angles, and the cross-section dimensions are chosen to best represent an equilateral polygon. Figure 4.4 contains two examples of hexagonal particles. The top figure is a column and has an effective cross-sectional diameter of 5.98 ls, a length of 12 ls or an aspect ratio of about 2×1 , and contains 336 dipoles. The bottom figure is a

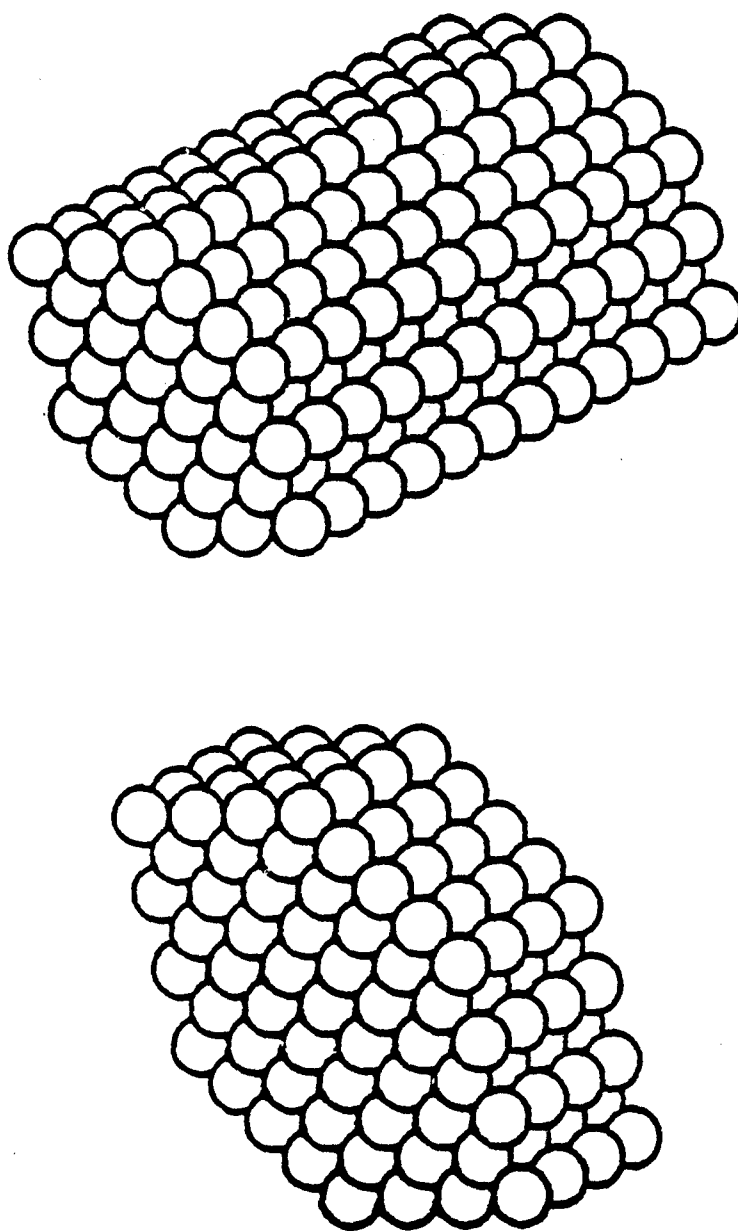


Figure 4.4 Arrays of dipoles arranged to represent hexagonal crystals. The top array contains 336 dipoles and represents a 2×1 hexagonal column; the bottom array contains 212 dipoles and represents a 2×1 hexagonal plate.

plate and has an effective cross-sectional diameter of 8.21 ls, a depth of 4 ls or an aspect ratio of about 2×1 , and contains 212 dipoles.

Particle Size

The subroutines described in the previous section can be used to construct arrays of dipoles that represent particles of various shapes. However, as a result of the discrete nature of the dipoles, only a discrete set of particle sizes can be represented unless additional modifications are made. The modifications to vary the particle size are based on either the effective radius or volume of particle that the array represents. If a particle of given size is to be modeled, the subroutines adjust the radii of the dipoles accordingly. The following exemplifies these modifications.

If SPHERE were used to build a particle of radius 3.0 ls with the origin at a central dipole, the resulting dipolar array would contain all the dipoles within 3.0 ls of the origin and consist of 123 dipoles. The volume of the scatterer is then N , the number of dipoles. The effective radius of the particle is given by

$$a_e = \left(\frac{3N}{4\pi} \right)^{1/3} . \quad (4.1)$$

In this case $a_e = 3.09$ ls. If the input parameter for radius had been 3.1 ls, the subroutine would have built the same 123-dipolar array. The next largest array would not occur until the input radius reached 3.2 ls which would result in an array of 147 dipoles; the effective radius for this sphere is 3.27 ls. Thus, a particle of radius between 3.09 and 3.27 ls cannot be built without further modifications to the subroutine. One modification has already been discussed: the option for repositioning the origin with respect to the lattice points. This option approximately doubles the number of arrays that can represent a sphere, but overall selection remains limited. Table 4.1 contains the complete list of spheres (of radius $3.0 \leq a \leq 4.5$) that can be represented using the SPHERE subroutine. The list contains information on arrays that have the origin at a central dipole or within a group of eight dipoles. It is observed in Table 4.1 that a spherical particle with an effective radius of 3.25 ls cannot be built. The following modification eliminates this restriction.

When a particle of specific size is required, the user is required to input the actual dimensions and the radius of the dipole is adjusted so the effective radius matches the desired value. For instance, if a sphere with an effective radius of 3.25 ls is to be modelled, the sphere containing 147 dipoles may be used, but the dipole radius will be reduced to 0.48 ls from 0.50 ls. The size of

Table 4.1 Physical characteristics of dipolar arrays that are constructed by subroutine SPHERE. Radius is the input parameter, eff rad is the effective radius based on equivalent volume sphere, and N is the number of dipoles in the array.

Origin not at a central dipole			Origin at a central dipole		
Radius	Eff Rad	N	Radius	Eff Rad	N
3.0	3.19	136	3.0	3.09	123
3.3	3.37	160	3.2	3.27	147
3.6	3.68	208	3.5	3.50	179
3.9	4.06	280	3.8	3.91	251
4.1	4.17	304	4.2	4.18	305
4.4	4.41	360	4.3	4.33	341

a spheroid is adjusted based on the radius of an equivalent sphere (equation 4.1). For a cylinder and hexagon the modification depends on the effective cross-sectional radius:

$$a_e = \left(\frac{N}{\pi} \right)^{1/2}. \quad (4.2)$$

In this manner particles of any size can be represented.

This ability to change the size of the dipoles is also important because backscattered radiation is highly dependent on particle shape. When more dipoles are used to represent a particle, the array becomes a truer representation of that particle. As will be discussed in Chapter 5, backscattering calculations can be improved by modelling particles with larger arrays of smaller dipoles.

Scattering Matrices

Two related matrices are encountered when calculating scattering of polarized light by a particle: the amplitude scattering matrix and the Mueller matrix. The amplitude scattering matrix provides the relation between the incident and scattered electric fields. The Mueller matrix is an expansion of the amplitude scattering matrix using a set of observable properties of

polarized light which are referred to as the Stokes vectors. Both matrices are calculated in the coupled-dipole method.

From this point on light will refer to plane wave radiation propagating in the $+z$ direction. Polarization in the context of polarized light is not to be confused with the polarizability of the dipolar subunits. The state of polarization describes the behavior of the electric field in the x - y plane as the wave propagates in the z direction. For example, parallel linearly polarized light refers to a linearly polarized plane wave whose electric field remains parallel to some arbitrary axis. Conventions for defining polarized light are not standard; the convention adopted here is that used by Bohren and Huffman (1983, Chap 2.11).

Singham et al. (1986a) analyzed the scattered light in terms of left- and right-circularly polarized light. The equations necessary to evaluate parallel and perpendicular linearly polarized light have been added to the coupled-dipole method; the derivation of these equations used to calculate the amplitude scattering matrix is now described.

The amplitude scattering matrix relates the parallel and perpendicular components of the incident (i) and scattered (s) electric fields

$$\begin{pmatrix} E_{\parallel s} \\ E_{\perp s} \end{pmatrix} = \frac{e^{ik(r-z)}}{-ikr} \begin{pmatrix} S_2 & S_3 \\ S_4 & S_1 \end{pmatrix} \begin{pmatrix} E_{\parallel i} \\ E_{\perp i} \end{pmatrix}, \quad (4.3)$$

where $S_j(j=1,4)$ is the amplitude scattering matrix (Bohren and Huffman, 1983, Sect 3.3). By expressing the parallel and perpendicular components of the incident field in terms of x and y : $\vec{E}_{\parallel i} = \vec{E}^x$, and $\vec{E}_{\perp i} = -\vec{E}^y$, where $\vec{E}^x = E_0 \hat{x}$, $\vec{E}^y = E_0 \hat{y}$, and $E_0 = 1$, the x and y component values for the incident field become: $E_{\parallel i}^x = -E_{\perp i}^y = 1$ and $E_{\parallel i}^y = E_{\perp i}^x = 0$. With this information, the matrix elements in equation 4.3 can be solved for in terms of x and y components of parallel and perpendicular linearly polarized scattered light:

$$S_3 = -\frac{E_{\parallel s}^y}{C} \quad S_2 = \frac{E_{\parallel s}^x}{C} \quad S_1 = -\frac{E_{\perp s}^y}{C} \quad S_4 = \frac{E_{\perp s}^x}{C}. \quad (4.4)$$

where $C = \exp\{ikr\}/-ikr$.

The electric field at a detector \vec{E}_d placed at distance r_d in the unit direction \hat{n}_d is obtained by summing the far-field amplitudes from the N dipoles

$$\vec{E}_d = \frac{k^2 e^{ikr_d}}{r_d} (\tilde{1} - \hat{n}_d \hat{n}_d) \sum_{j=1}^N e^{-ik\hat{n}_d \cdot \vec{r}_d} \alpha_j \vec{E}_j. \quad (4.5)$$

where $\tilde{1}$ is the identity matrix. Equation 4.5 is similar to equation 4.3. With minor algebraic manipulation the elements of the amplitude scattering matrix can be calculated using the coupled-dipole method.

The values for the amplitude matrix are passed into a subroutine where the 4×4 Mueller matrix is defined by

$$\begin{pmatrix} I_s \\ Q_s \\ U_s \\ V_s \end{pmatrix} = \begin{pmatrix} S_{11} & S_{12} & S_{13} & S_{14} \\ S_{21} & S_{22} & S_{23} & S_{24} \\ S_{31} & S_{32} & S_{33} & S_{34} \\ S_{41} & S_{42} & S_{43} & S_{44} \end{pmatrix} \begin{pmatrix} I_i \\ Q_i \\ U_i \\ V_i \end{pmatrix}. \quad (4.6)$$

(Bohren and Huffman, 1983, p 65). The Mueller matrix describes the relationship between the incident and scattered Stokes vector. The Stokes vector (I , Q , U , and V) is a description of the state of polarization of both incident (i) and scattered (s) light. Monochromatic light of any state of polarization can be represented by the Stokes vector. The I component represents the irradiance of the wave; V defines its handedness. Q is related to horizontally and vertically polarized light, and U is related to $\pm 45^\circ$ linearly polarized light. Horizontal and vertical are defined with respect to the direction of wave propagation. (See Bohren and Huffman, 1983, Section 2.11.1, for a more detailed derivation of the Stokes vectors.)

In Chapter 5, the scattering and detection of horizontally and vertically polarized light will be discussed. When a plane wave has been linearly polarized by an ideal linear polarizer, the electric field vector remains parallel to a particular axis called the transmission axis. The Mueller matrix for an ideal linear polarizer is

$$\frac{1}{2} \begin{pmatrix} 1 & \cos 2\xi & \sin 2\xi & 0 \\ \cos 2\xi & \cos^2 2\xi & \cos 2\xi \sin 2\xi & 0 \\ \sin 2\xi & \sin 2\xi \cos 2\xi & \sin^2 2\xi & 0 \\ 0 & 0 & 0 & 0 \end{pmatrix} \quad (4.7)$$

where ξ is the angle between the transmission axis and the horizontal plane (horizontal with respect to the direction of wave propagation). When a particle is illuminated with horizontally polarized light, the amount of backscattered light that is horizontally polarized can be determined by multiplying a series of Mueller matrices; these are shown in equation 4.8.

$$\frac{1}{2} \begin{pmatrix} 1 & 1 & 0 & 0 \\ 1 & 1 & 0 & 0 \\ 0 & 0 & 0 & 0 \\ 0 & 0 & 0 & 0 \end{pmatrix} (S_{ij}) \frac{1}{2} \begin{pmatrix} 1 & 1 & 0 & 0 \\ 1 & 1 & 0 & 0 \\ 0 & 0 & 0 & 0 \\ 0 & 0 & 0 & 0 \end{pmatrix} \begin{pmatrix} 1 \\ 0 \\ 0 \\ 0 \end{pmatrix} \quad (4.8)$$

The 4×1 matrix on the right is the incident Stokes vector representing normalized irradiance. Next to the Stokes vector is the Mueller matrix for a linear polarizer with a horizontal transmission axis ($\xi = 0^\circ$). The product of these two matrices yields the 4×1 Stokes vector that represents horizontally polarized light. (S_{ij}) is the Mueller matrix for the scatterer as obtained from the coupled-dipole method. To determine the amount of scattered light that is horizontally polarized, the Mueller matrix for a horizontal polarizer is required once more. The product of these matrices gives the Stokes vector for scattered light. The I_s component of the resulting Stokes vector represents the irradiance

of horizontally polarized light scattered by a particle that was illuminated by horizontally polarized light. This irradiance will be referred to as S_{HH} , and its analog for vertically polarized light will be called S_{VV} . The product of the appropriate Mueller matrices yields the following equations:

$$\begin{aligned} S_{HH} &= \frac{1}{4}(S_{11} + S_{12} + S_{21} + S_{22}) \\ S_{VV} &= \frac{1}{4}(S_{11} - S_{12} - S_{21} + S_{22}) \end{aligned} \quad (4.9)$$

Bickel and Bailey (1985) provide an illuminating characterization of scattered light in the context of Stokes vectors and Mueller matrices.

Cross Sections

If a particle is interposed between a source of electromagnetic radiation and a detector, the power received at the detector decreases. The decrease in power or extinction of the incident wave is due to scattering and absorption by the particle and depends on the particle's shape, size, and relative complex refractive index as well as the frequency and polarization state of the incident plane wave. Characterization of the extinction is usually denoted in terms of particle extinction C_{ext} , scattering C_{sca} , and absorption C_{abs} cross sections. For plane waves, each cross section can be determined independently, and agreement can be tested by considering energy conservation

$$C_{ext} = C_{abs} + C_{sca} . \quad (4.10)$$

The calculation of these cross sections in the coupled-dipole method is now briefly described.

Extinction

The extinction cross section is calculated using the optical theorem which indicates that extinction depends only on the scattering amplitude in the forward direction. This may seem counterintuitive since extinction accounts for both absorption in the particle and scattering in all directions by the particle. For plane waves, the extinction cross section is determined by calculating the work done by the incident electric field

$$C_{ext} = \frac{4 \pi k_0}{|\vec{E}_i|^2} \sum_{j=1}^N \text{Im}(\vec{E}_j^* \cdot \vec{p}_j) . \quad (4.11)$$

where \vec{p}_j is the dipole moment and \vec{E}_j is the incident electric field at the j^{th} dipole as calculated by the coupled-dipole method, * indicates the complex conjugate, and Im signifies that only the imaginary part of the argument be evaluated.

Scattering

The scattering cross section is determined by first calculating the time-averaged power radiated per unit solid angle (Jackson, 1975)

$$\frac{dC_{sca}}{d\Omega} = \frac{k^4}{8\pi |\vec{E}_i|^2} \sum_{j=1}^N |(\hat{n} \times \vec{p}_j) \times \hat{n}|^2, \quad (4.12)$$

where $dC_{sca}/d\Omega$ is sometimes called the differential scattering cross section.

This quantity represents the amount of light scattered into a unit solid angle in direction \hat{n} . Simpson's rule is used to integrate over the total solid angle to yield the scattering cross section. For a good estimate of scattering cross section, it is necessary to sum over a minimum of 33 theta (θ) and 12 phi (ϕ) values, where $d\Omega = \sin \theta d\theta d\phi$ (Draine, 1988).

The average cosine of the scattering angle, or the asymmetry parameter g , can be obtained while calculating the scattering cross section from equation 4.12 as

$$g \equiv \langle \cos \theta \rangle = \frac{k_0^3}{C_{sca} |\vec{E}_i|^2} \int d\Omega \hat{n} \cdot \vec{k} \left| \sum_{j=1}^N [\vec{p}_j - \hat{n}(\hat{n} \cdot \vec{p}_j)] e^{-ik_0 \hat{n} \cdot \vec{r}_j} \right|^2. \quad (4.13)$$

The asymmetry parameter ranges in value from -1 to +1. For a particle whose scattered power density is symmetric about the scattering angle of 90° , g vanishes identically. If the forward scattering is larger (smaller) than backscattering, then the asymmetry parameter is positive (negative).

Absorption

The absorption cross section is determined by summing the power absorbed by all the dipoles

$$C_{abs} = \frac{4\pi k_0}{|\vec{E}_i|^2} \sum_{j=1}^N \left\{ \text{Im} \left[\vec{p}_j \cdot \left(\frac{\vec{p}_j}{\alpha} \right)^* \right] - \frac{2}{3} k^3 \vec{p}_j \cdot \vec{p}_j^* \right\}. \quad (4.14)$$

The first term on the right is the expression used by Purcell and Pennypacker (1973). Draine (1988) added the second term (radiative reaction term) to account for effect of the radiation on the motion of the dipoles as prescribed by Jackson (1975, Chap 17). Including the second term improves calculation of C_{abs} when comparing absorption by spheres with Mie theory.

The accuracy of these equations that determine the three cross sections can be shown by comparing $C_{sca} + C_{abs}$ with C_{ext} . Table 4.2 shows these values for several spheres with different refractive indices.

Backscattering

The backscattering cross section is calculated using the traditional definition of the radar backscattering cross section (see Bohren and Huffman, 1983, Sect 4.6)

Table 4.2 Results from the three independent equations used to determine C_{sca} , C_{abs} , and C_{ext} . Conservation of energy dictates that $C_{sca} + C_{abs} = C_{ext}$. Values in table show excellent agreement. Values calculated by Mie theory are also presented: $C_{ext}(Mie)$. Size parameter of the modeled sphere is 1.6. Cross sections have units of area.

Refractive index	C_{sca}	C_{abs}	$C_{abs} + C_{sca}$	C_{ext}	$C_{ext}(Mie)$
1.14 + i0.26	5.87	27.00	32.87	32.88	33.23
1.33 + i0.05	11.09	7.65	18.74	18.75	19.22
1.55 + i0.005	33.84	1.00	34.84	34.84	37.32
1.39 + i0.42	17.77	40.14	57.91	57.91	57.99
1.7 + i0.1	47.78	19.23	67.01	67.02	72.43
1.9 + i0.0004	108.78	0.13	108.91	108.92	121.40
2.5 + i1.4	50.03	61.49	111.52	111.53	97.85
3.5 + i2.05	52.37	58.29	110.66	110.67	94.28
3.0 + i4.0	53.59	56.11	109.70	109.70	92.97

$$C_{back} = \frac{4\pi}{k^2} (|S_2(180^\circ)|^2 + |S_1(180^\circ)|^2), \quad (4.15)$$

where $S_2(180^\circ)$ and $S_1(180^\circ)$ are elements from the amplitude scattering matrix.

The cross section efficiencies Q are calculated by dividing the respective cross section by the geometric cross section of the particle G normal to the incident wave. For example, the extinction efficiency is determined by

$$Q_{ext} = C_{ext}/G.$$

Chapter 5

BACKSCATTERING CALCULATIONS

Light scattering is important in many fields of science: for example, inferring properties of interstellar dust (Draine, 1988), locating dust particles on computer chips (Taubenblatt, 1990), studying molecules by analyzing the polarization state of scattered light (Harris and McClain, 1985). In remote sensing of the atmosphere, often the only information available is the backscattered signal. The objective of this chapter is to investigate the advantages and disadvantages as well as the limitations of using the coupled-dipole method for determining backscattering by hydrometeors.

Although most solid particles in nature are not spherical, it has become too often the practice to model these particles as spheres using Mie theory. Thus, the modeler avoids using a more computer intensive, but in many cases more appropriate, model. Unfortunately, the assumption that randomly oriented, nonspherical particles scatter like equal-volume spheres has become the mindset of many modelers. Methods for calculating scattering by arbitrary particles are often used to identify circumstances under which the practice of using equal-volume spheres is least likely to lead to unacceptable errors, but it is done in a fashion that appears to condone this practice rather than condemn it. In this chapter, calculations for arbitrary particles will be compared with those for equivalent-volume spheres.

The first topic in this chapter is the shape sensitivity of the backscattered signal. Next, scattering results from modeling spherical particles using the coupled-dipole method are compared with Mie theory, and emphasis is placed on how accuracy depends on size parameter. This is followed by a brief discussion of how well a collection of dipoles on a cubic lattice can represent a solid sphere, and whether small variations of shape affect backscattering calculations. Next, backscattering by equal-volume particles of different shapes are compared. With information from the preceding analyses, backscattering of 94 GHz radar by ice spheres and crystals is investigated. First, scattering results from modeling spheres with the coupled-dipole method are compared with Mie theory to determine the accuracy of the model for the refractive index of ice at 94 GHz: $1.878 + i4.76 \times 10^{-4}$. Finally, hexagonal plates and columns are modeled. The impetus is to identify the advantages of using linearly polarized radar to distinguish shape and size dependencies in backscattering by ice crystals.

Shape and Size Dependency of Backscattering

Bad data can be made to look good with a suitable choice of statistics. In a similar fashion, numerical models can appear credible if only forward scattering calculations are compared with analytic solutions. The coupled-dipole method can be used to demonstrate why scattering is more critical in

the backward direction. The scattering light is the sum of all the radiated waves from the dipolar subunits, the intensity of the scattered light depends on the phase relation among all the radiated waves. The following argument appears in Bohren and Singham (1990).

The scattered field is the sum of the radiated waves by all the dipoles that represent the particle. Consider the phase difference $\Delta\phi$ of two waves scattered by two separate dipoles excited by the same wave as shown in Figure 5.1. Interaction between the dipoles is ignored. The phase difference depends on the distance between the dipoles d (in the direction of wave propagation), the wavelength of incident light, and the angle between the incident and scattered waves θ :

$$\Delta\phi = \frac{2\pi d}{\lambda}(1 - \cos\theta). \quad (5.1)$$

The phase difference dependence on the dipole separation is

$$\frac{\partial(\Delta\phi)}{\partial d} = \frac{2\pi}{\lambda}(1 - \cos\theta). \quad (5.2)$$

The phase difference is least sensitive to separation for scattering in the forward direction ($\theta = 0$) and most sensitive in the backward direction ($\theta = \pi$). What is true for two dipoles in this simplified example is true for N dipoles. Thus, in a general sense the cumulative separation of all the dipoles, i.e. the particle shape, is critical for determining the backscattered signal. This is also true when the dipole interactions are not ignored.

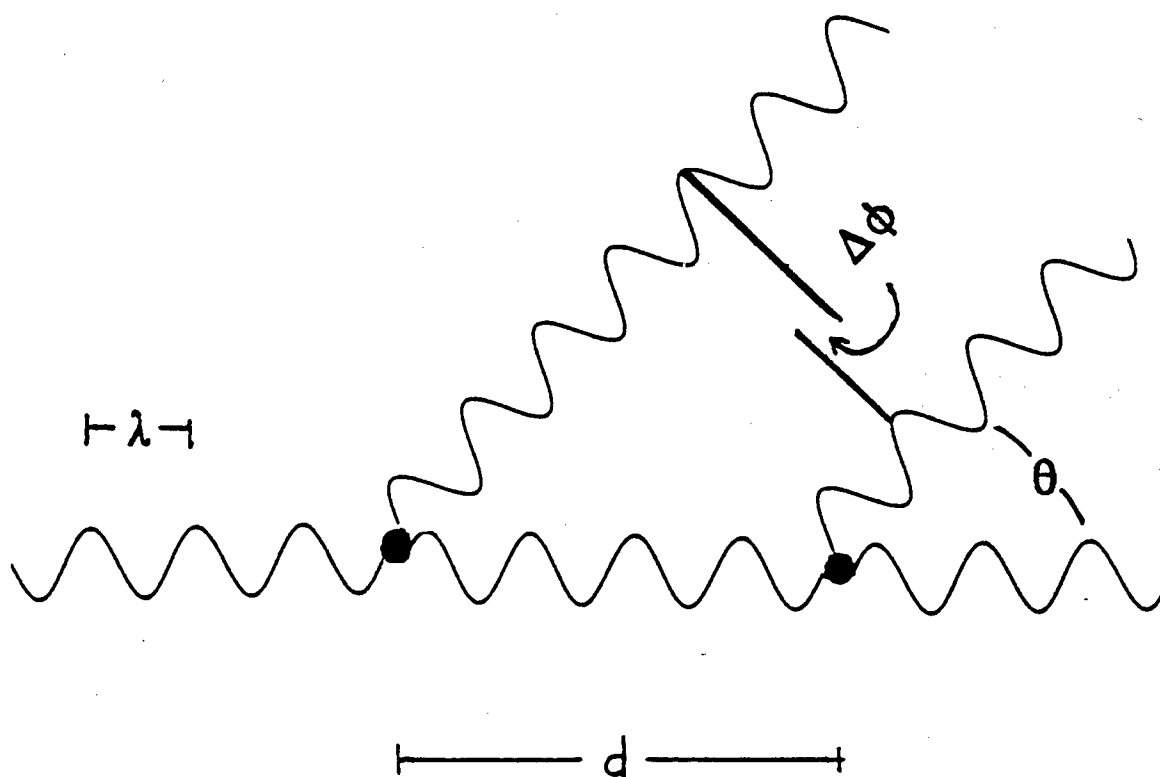


Figure 5.1 Diagram showing the relationship between the phase difference of two scattered waves and the distance between the scatterers.

For large particles when the phase difference of the incident light across the particle cannot be neglected, scattering is affected by interference among the radiated waves, which can be accounted for by the dipole interactions. Since the coupled-dipole method accounts for the interactions, it is expected to accurately compute backscattering. This is illustrated in Figure 5.2 where scattering results using the coupled-dipole method are compared with Mie theory. The sphere modeled has a refractive index of $1.33 + i0.05$ and a size parameter of 1.60. The array used in the coupled-dipole method contains 461 dipoles; computations were made using the scattering-order technique. The solid line represents Mie calculations. The dotted line is from the coupled-dipole method after the first iteration, which is equivalent to ignoring the dipole interactions; the dashed line represents a fully converged solution (14 iterations). Backscattering calculations are more sensitive to dipole interactions than forward scattering calculations. Thus, when judging model capability it is better to compare backscattering calculations, since forward scattering is least sensitive to shortcomings in the model.

The difficulty in accurately calculating the backscattered signal increases with size parameter. Figure 5.3 shows forward scattering (dashed line) and backscattering (solid line) as calculated by Mie theory for a sphere with refractive index of $1.33 + i0.05$ and illuminated by unpolarized light. For size parameters less than about 0.5 both scattered signals vary with the sixth power of particle radius, which is indicative of particles in the Rayleigh regime

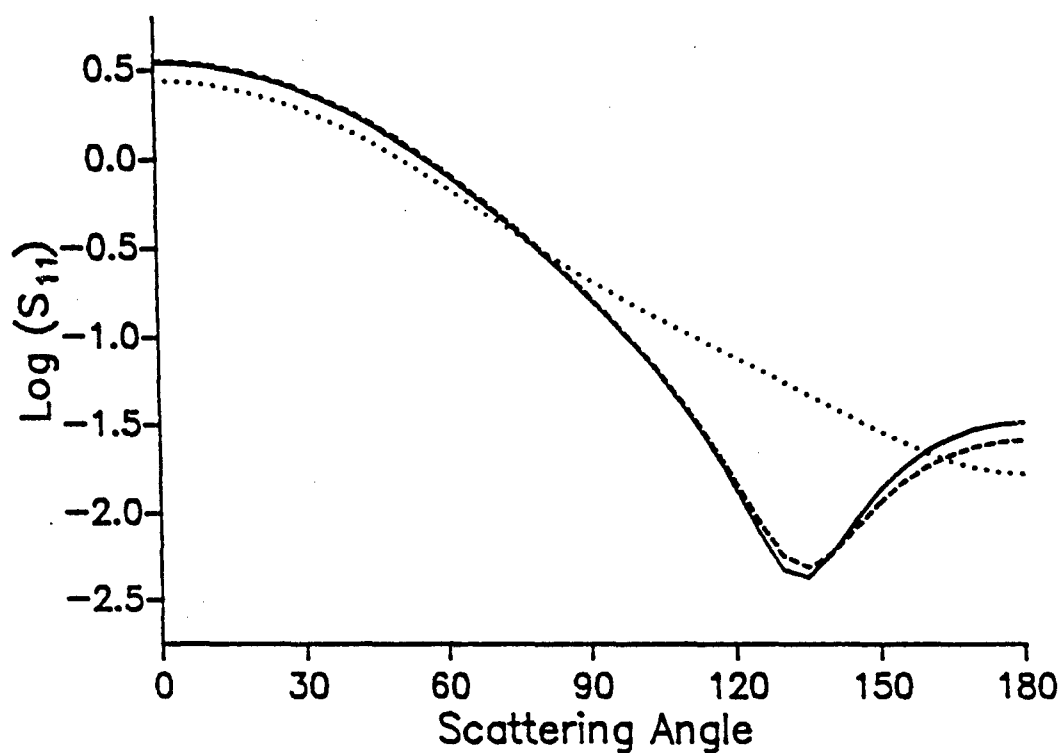


Figure 5.2 Importance of dipole interactions for backscattering calculations. A sphere with refractive index $1.33 + i0.05$ and size parameter of 1.60 was modeled. Solid line is from Mie theory. The other lines are from the coupled-dipole method using the scattering-order technique. The dotted line represents scattering values with no dipole interactions; the dashed line represents a fully converged solution that includes dipole interactions.

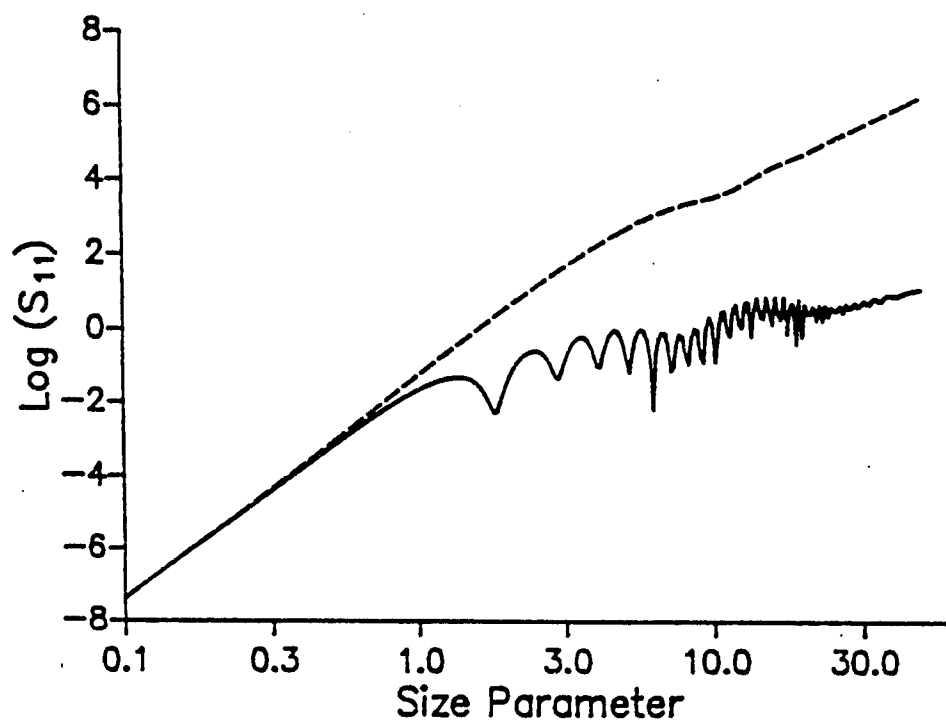


Figure 5.3 Forward scattering and backscattering by spheres of increasing size parameter. Spheres with refractive index $1.33 + i0.05$ and size parameters ranging from 0.1 to 50 were modeled. The dashed line represents forward scattering; the solid line represents backscattering.

(negligible phase shift of the incident wave across the particle). For larger particles, the effects of interference cause backscattering to fluctuate wildly; hence, small errors in particle size further reduce computational accuracy. The values in Figure 5.3 are obtained from Mie theory, which is a solution for a sphere with a well-defined radius. In the coupled-dipole method the representation of arbitrary particles by arrays of dipoles can make computing backscattering less precise. Limitations are now examined.

Limitations of The Coupled-Dipole Method

The ability of the coupled-dipole method to calculate backscattering depends on the particle's size and refractive index and how well the array of dipoles represents the particle's shape. Dependence on refractive index is addressed in Appendix A. Table A.1 shows that accuracy of scattering calculations from the coupled-dipole method decreases with increasing refractive index. This is due to the influence of higher order multipoles. In this section the effect of small variations in particle shape and of increasing the particle size will be examined.

Changing the particle size affects the accuracy of the scattering calculations using the coupled-dipole method. When the particle is small compared with the wavelength (size parameter less than 0.5) the phase difference of the incident light across the particle is negligible. In turn, the

dipoles are also small compared with the wavelength. Increasing the particle size requires either increasing the radius or number of dipoles. The latter option is permissible as long as the radius of the dipoles satisfies the criterion that $k_0 a |m| < 0.5$, and this criterion is not violated in the following analysis. A sphere with a refractive index of $1.33 + i0.05$ was modeled; its size parameter was varied from 1.0 to 2.0 by increasing the radius of the dipoles. The sphere was represented by three separate arrays: 251, 304, and 461 dipoles. The results in Figure 5.4 show good agreement with Mie theory until the size parameter exceeds 1.6. It is at this size parameter that the backscattered signal reaches its first minimum value (as shown in Figure 5.3). This poor agreement with Mie theory at size parameters above that which corresponds to the backscattering minimum also occurs for other refractive indices. These results are the same whether using the matrix inversion or scattering-order technique. To a lesser degree, but still occurring at the backscattering minimum, forward scattering calculations lose accuracy as shown in Figure A.2. Thus, for size parameters larger than that which corresponds to the first backscattering minimum, scattering calculations from the coupled-dipole method lose accuracy.

This loss of accuracy can be overcome somewhat by increasing the number of dipoles in the array while decreasing their size. Figure 5.5 shows the backscattering for a sphere with refractive index $1.33 + i0.1$ represented by arrays of 461, 739, 1064, and 2320 dipoles; results from Mie theory are

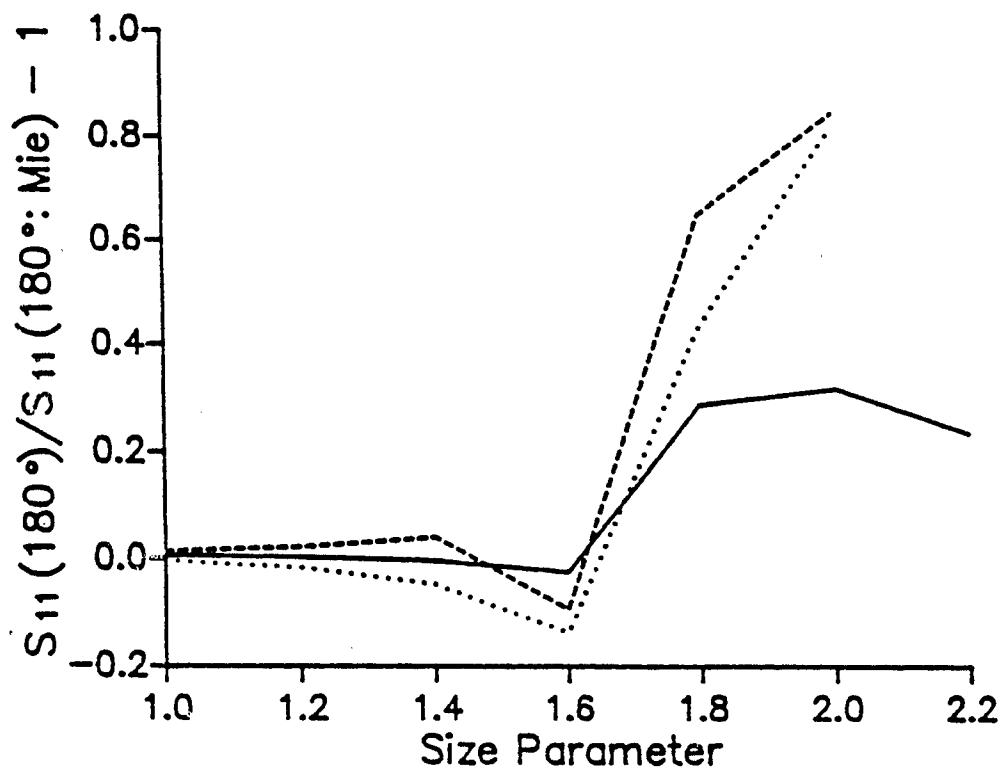


Figure 5.4 Comparison of coupled-dipole method with Mie theory for spheres of increasing size parameter. A sphere with refractive index $1.33 + i0.05$ was modeled. The particle size was increased by increasing the size of the dipoles. The solid line represents scattering by a 461 dipolar array, the dotted line by a 304 dipolar array, and the dashed line by a 251 dipolar array.

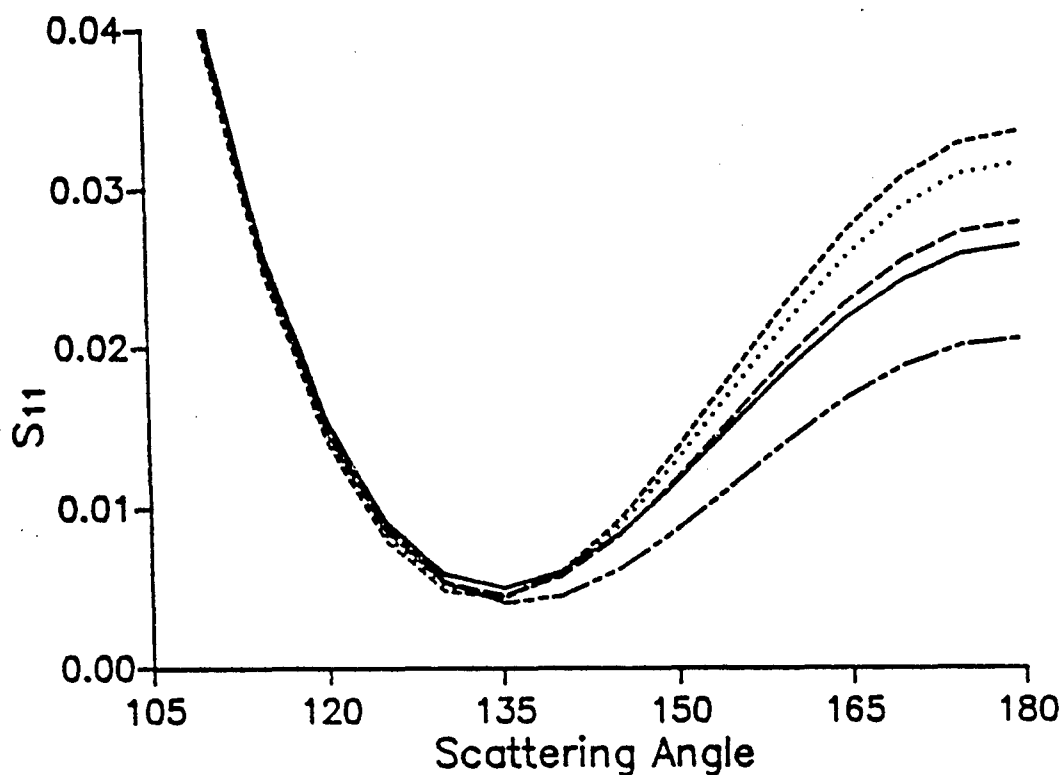


Figure 5.5 Improvement of backscattering by increasing the number of dipoles. A sphere with refractive index $1.33 + i0.1$ and a size parameter 1.60 was model. The solid line is Mie theory. The short-dashed line (- - -) represents scattering by a 461 dipolar array, the multiple-dashed line (— — —) by a 739 dipolar array, the dotted line by a 1064 dipolar array, and the long-dashed line (— — —) by a 2320 dipolar array.

depicted by the solid line. In general, backscattering calculations improve by increasing the number of dipoles; computation time always increases.

Increasing the number of dipoles in the array produces subtle changes in the shape of the array. The question of how well an array of dipoles on a simple cubic lattice represents a spherical particle is addressed in Appendix A beginning on page 116. Draine (1988) presented a formula for estimating the sphericity of an array of dipoles that represents a sphere. Table A.2 shows that small variations in sphericity may affect scattering when shape dependency is critical. As discussed in the previous section, backscattering is very shape dependent; therefore, if these small variations of sphericity are important they should affect backscattering calculations.

To check how backscattering depends on shape variations associated with representing a sphere by a lattice of dipoles, two spheres with refractive index $1.33 + i0.1$ were modeled; one had a size parameter of 0.84 and the other 1.60. Small variations in sphericity were obtained by representing each sphere with 13 arrays that varied in size from 280 to 515 dipoles. The effective radius of each array was held constant by varying the radius of the dipoles. Thus, the main difference between the arrays was the specific shape of each array. By Draine's criterion (1988), a perfect sphere has a radius of gyration of 1, and the value for radius of gyration increases as the particle departs from sphericity. Backscattering results are shown in Table 5.1. For the smaller sphere the backscattering values all agree with Mie theory to

Table 5.1 Effect of small variations in shape on backscattering calculations. Two spheres with refractive index of $1.33 + i0.1$ were modeled; their size parameters are 0.84 and 1.60. N is the number of dipoles in the arrays, ROG is the radius of gyration of the array (Draine, 1988). ROG is an estimate of the sphericity of the array--an exact sphere has a value of 1, deviation from 1 indicates nonsphericity. Rows are arranged by increasing ROG. The percent difference calculation is: $[S_{11}(180^\circ)/S_{11}(180^\circ; \text{Mie})]-1$. For the smaller sphere, effects of small variations in shape are not critical as for the larger sphere.

N	ROG	% diff when x = 0.84	% diff when x = 1.60
461	1.0006	0.6%	-2.6%
304	1.0012	0.6	9.1
280	1.0018	1.3	15.9
437	1.0019	1.1	17.0
485	1.0020	0.1	-10.3
480	1.0027	1.6	28.8
432	1.0031	0.6	-2.1
515	1.0034	0.6	-2.4
360	1.0035	0.2	8.2
389	1.0035	1.4	18.0
365	1.0039	0.9	8.1
341	1.0048	1.5	25.1
305	1.0060	1.1	8.2

within 2%; for the larger sphere, less than one-quarter of the values agree to within 3% while nearly half disagree by more than 10%. The poorer agreement for the larger particle is because its size is beyond the first backscattering minimum as discussed on page 58. At this size parameter backscattering becomes extremely shape dependent. A relation between increased sphericity and improved backscattering calculations is not observed in Table 5.1. Thus, Draine's criterion for radius of gyration does not generally aid in choosing an array that best represents a sphere. This criterion may have merit for calculations in the forward direction; however, for the more shape-dependent backward direction it provides no guidance for selecting arrays.

For particles that are larger than that which produces the first backscattering minimum, scattering calculations using the coupled-dipole method become suspect. Increasing the number of dipoles in the array generally improves the accuracy of these calculations.

Backscattering by Equal-Volume Particles

It was shown in the earlier sections of this chapter that accuracy of backscattering calculations using the coupled-dipole method is dependent on particle size and shape. This last sensitivity study examines whether the overall particle shape strongly affects backscattering calculations. The equal-volume particles modeled here are a prolate spheroid, rectangular solid,

cylinder, and hexagonal column; all have an aspect ratio (ratio of length to diameter) of 5:1 and size parameter of 1.0. An equal-volume sphere is included. Three refractive indices chosen are: $1.5 + i0.00$, $1.5 + i0.05$, and $1.5 + i0.50$; these values are representative of ice crystals in the wavelength range from 6 to 15 μm (peak outgoing terrestrial radiation) (Rusk et al., 1971).

Scattering calculations were made with these particles in orientations that simulate natural conditions. Except for very large sizes and under turbulent conditions, ice crystals are expected to fall without tumbling (Cho et al., 1981; Pruppacher and Klett, 1980); therefore, the long axis of the particles modeled here remain horizontal (in the x - y plane). The particles were allowed to rotate in the horizontal plane, but not spin about their longitudinal axis. To account for not spinning about the longitudinal axis, the particle was initially oriented in the position that yielded the average backscattering value. For instance, the rectangular solid was rotated 45° and the hexagonal crystal by 22.5° ; an initial rotation did not significantly alter backscattering by the prolate spheroid or the cylinder because of their symmetry. Several states of polarization of the incident wave were analyzed: S_{11} , S_{HH} , and S_{VV} (see page 47 for a description of these). Modeling results are shown in Figures 5.6 through 5.9.

Figure 5.6 shows $S_{11}(180^\circ)$ for zenith angles ranging from 0° to 90° (the angle is defined with the zenith at 0° and the horizon at 90°) for the five particles with refractive index $1.5 + i0.00$. The horizontal line represents

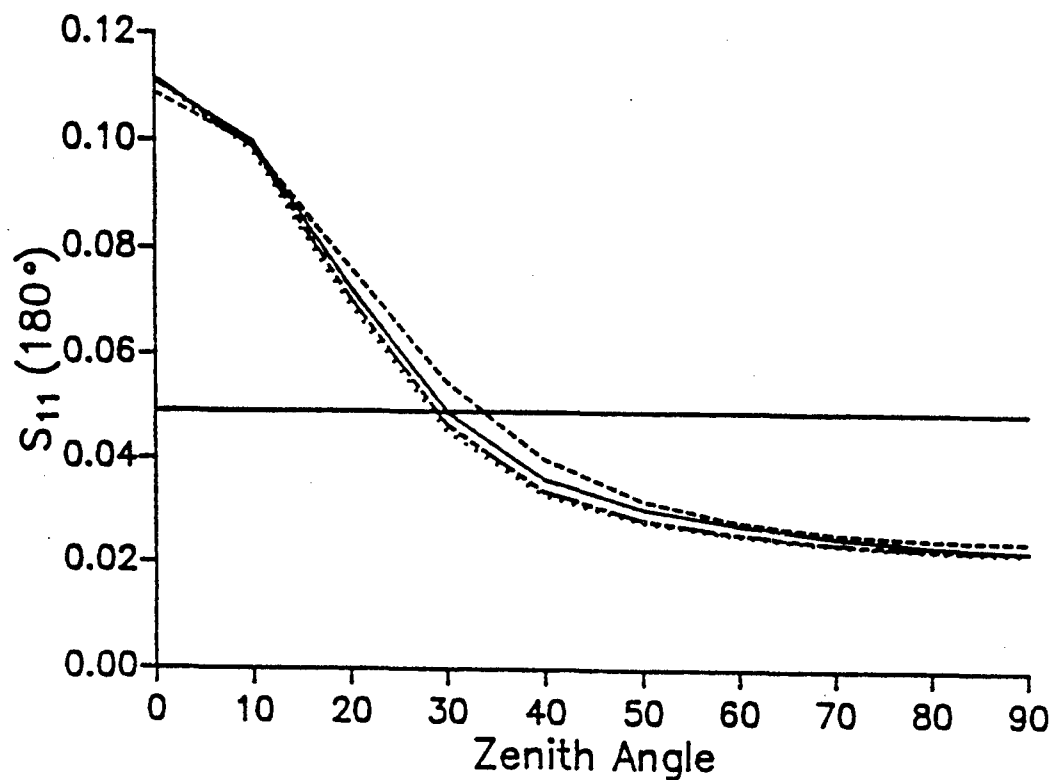


Figure 5.6 Backscattering of unpolarized light by equal-volume particles with aspect ratios of 5:1 and refractive index $1.5 + i0.00$. The solid horizontal line represents scattering by an equal-volume sphere. The other solid line represents scattering by a hexagonal column, the short-dashed line by a prolate spheroid, the dotted line by a cylinder, the multiple-dashed line by a rectangular solid.

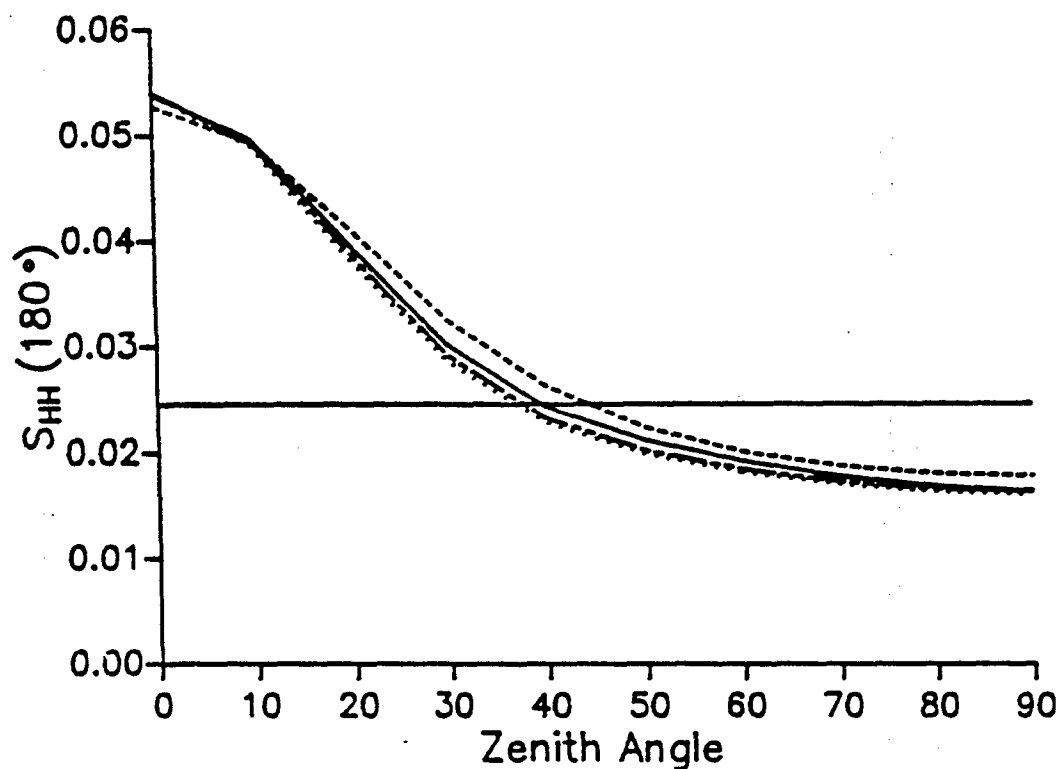


Figure 5.7 Backscattering of horizontally polarized light by equal-volume particles with aspect ratios of 5:1 and refractive index $1.5 + i0.00$. The solid horizontal line represents scattering by an equal-volume sphere. The other solid line represents scattering by a hexagonal column, the short-dashed line by a prolate spheroid, the dotted line by a cylinder, the multiple-dashed line by a rectangular solid.

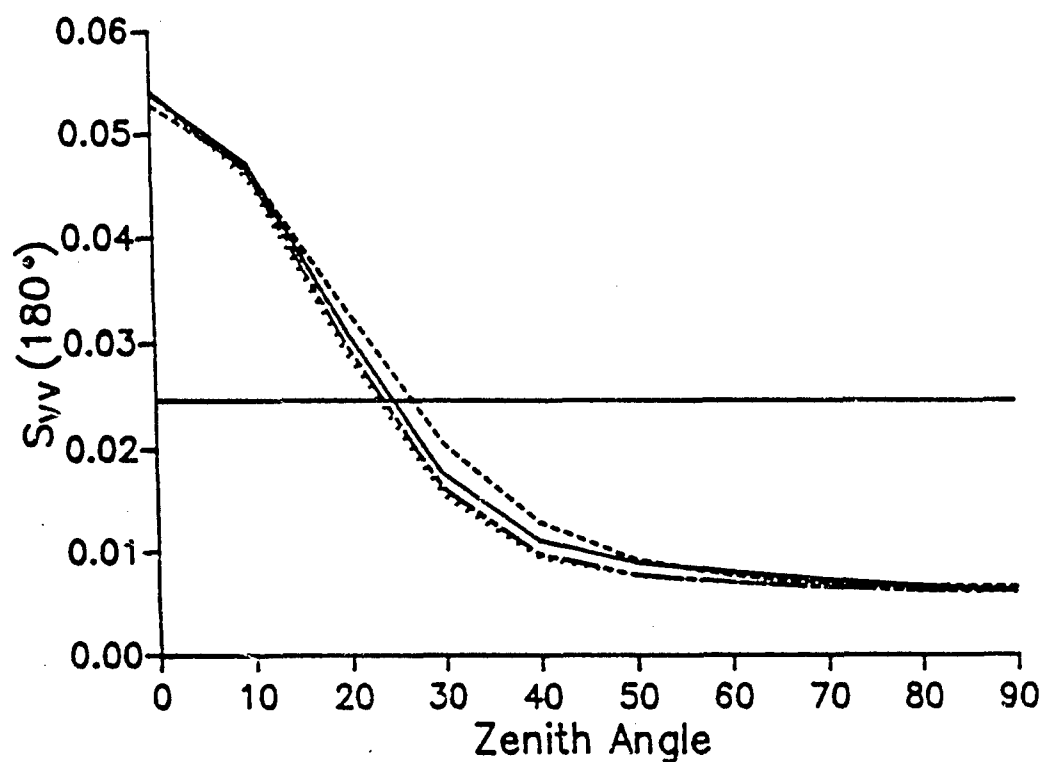


Figure 5.8 Backscattering of vertically polarized light by equal-volume particles with aspect ratios of 5:1 and refractive index $1.5 + i0.00$. The solid horizontal line represents scattering by an equal-volume sphere. The other solid line represents scattering by a hexagonal column, the short-dashed line by a prolate spheroid, the dotted line by a cylinder, the multiple-dashed line by a rectangular solid.

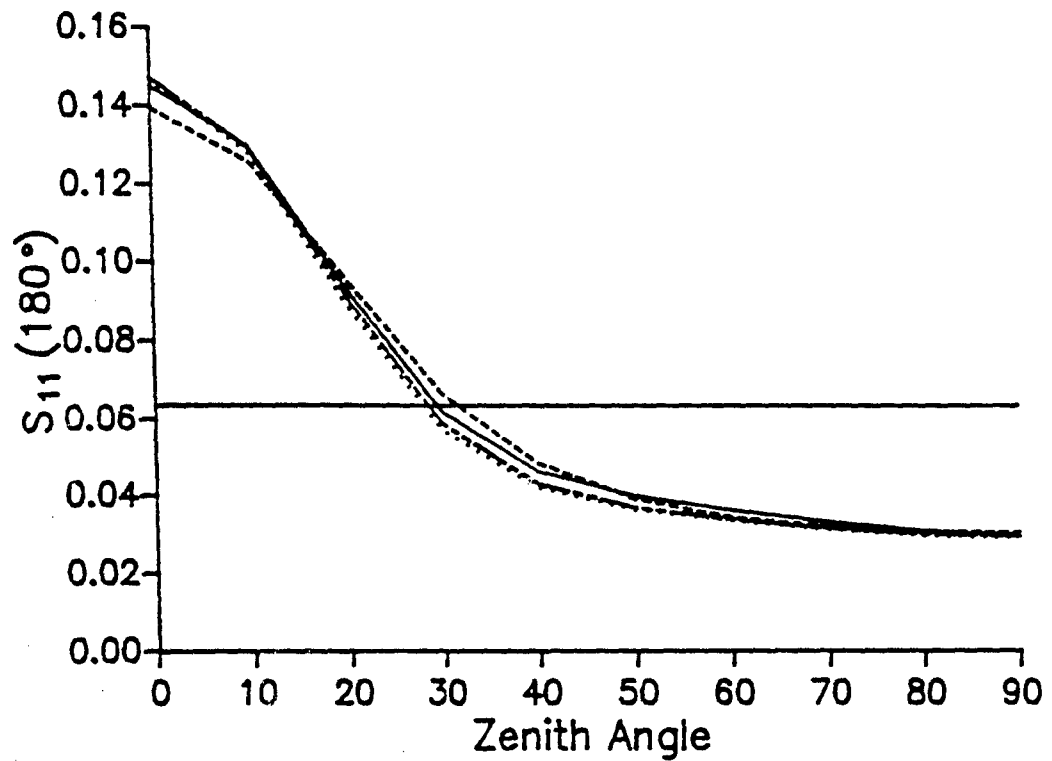


Figure 5.9 Backscattering of unpolarized light by equal-volume particles with aspect ratios of 5:1 and refractive index of $1.5 + i0.50$. The solid horizontal line represents scattering by an equal-volume sphere. The other solid line represents scattering by a hexagonal column, the short-dashed line by a prolate spheroid, the dotted line by a cylinder, the multiple-dashed line by a rectangular solid.

backscattering by the equal-volume sphere (no angle dependence). The remaining four particles display a similar relationship between zenith angle and backscattering. These results indicate that the overall particle shape is more important than subtle differences in the specific cross-section shape. Thus, for particles with aspect ratios of at least 5:1, analytic or numerical methods which treat elongated spheroids may be used to calculate backscattering by ice columns with only minor compromise to model accuracy (e.g. Yeh et al., 1982).

Figures 5.7 and 5.8 show $S_{HH}(180^\circ)$ and $S_{VV}(180^\circ)$ for the same particles and zenith angles as in Figure 5.6. At zenith angle of 0° , corresponding values of $S_{HH}(180^\circ)$ and $S_{VV}(180^\circ)$ are equal because at this angle the particles appear symmetric. With increasing zenith angle (looking down towards the horizon), the values of $S_{HH}(180^\circ)$ decrease slower than those for $S_{VV}(180^\circ)$. This too is expected because the horizontally polarized light excites the longer dimension of the particle. This difference between $S_{HH}(180^\circ)$ and $S_{VV}(180^\circ)$ is important, and it will be discussed later as a means to infer the size distribution of ice crystals by radar.

When the refractive index of these particles is changed to $1.5 + i0.05$, the backscattering calculations are similar to those shown in Figures 5.6 through 5.8 and are not presented. $S_{11}(180^\circ)$ values for these particles with refractive index $1.5 + i0.50$ are shown in Figure 5.9. Backscattering for all three refractive indices displays similar angle dependencies. The only differences of note are the higher values when the refractive index is

differences of note are the higher values when the refractive index is $1.5 + i0.50$. This is a consequence of the smaller penetration depth due to the larger imaginary part of the refractive index. Values for $S_{HH}(180^\circ)$ and $S_{VV}(180^\circ)$ at this refractive index behave similarly to those in Figures 5.7 and 5.8.

The mean value of $S_{11}(180^\circ)$ (averaged over all zenith angles) for the four elongated particles is similar to the backscattering by the equal-volume sphere. The percent difference between the mean values of $S_{11}(180^\circ)$ for the elongated particles and the backscattering value for the equal-volume sphere increases with increasing imaginary part of the refractive index (i.e., 3.6%, 3.8%, and 9.1% for these three refractive indices). Mugnai and Wiscombe (1980) noted that absorption *always* improves the agreement of backscattering by equivalent spheres; these calculations indicate the opposite. However, they modeled particles that had only a slight deviation (10%) from sphericity.

The backscattering calculations reported in this chapter show size and shape dependence. In addition, it is apparent that backscattering calculations using the coupled-dipole method lose accuracy when the particle size is larger than that associated with the first backscattering minimum. It also appears that for elongated particles, small variations in the particle's cross section are inconsequential. The last section addresses the size and shape dependence of the first backscattering minimum of ice crystals at 94 GHz.

Backscattering of 94 GHz Radar by Ice Crystals

The coupled-dipole method is applicable to studying backscattering of 94 GHz radar by ice crystals for several reasons. First, the coupled-dipole method can calculate scattering by ice crystals. Second, the wavelength of this radar is 3.2 mm; hence, the size parameter (or approximately the number of dipoles N needed to represent the particle) is not prohibitively large when modeling particles with linear dimensions of the order of one to five millimeters. Third, with $N < 300$ the matrix inversion technique can be used to rotate the particle through many orientations. Lastly, the refractive index of ice at this frequency is not too large to prevent use of the scattering-order technique for calculating scattering by larger ice crystals (when $N > 300$).

Of the models that calculate scattering by arbitrary particles, the coupled-dipole method is best suited for studying ice crystals. For example, the T-matrix method calculates scattering by rotationally symmetric particle with low aspect ratios; the ice crystals modeled here do not fit that description.

The relationship between particle shape and the first backscattering minimum is one of the interests for studying backscattering at 94 GHz. For falling raindrops, a backscattering minimum occurring at radius 0.83 mm provides an opportunity to remotely identify spherical raindrop size (Lhermitte, 1988). This identification is possible because the terminal velocity of raindrops increases with drop radius while backscattering by raindrops is at a local

minimum for drop radius 0.83 mm. Doppler radars measure the line-of-sight velocity of its targets (raindrops). When the radar is looking above the horizon (elevation angle greater than 0°), the Doppler shift is a result of both the horizontal and vertical forces acting on the target. The Doppler shift of a falling raindrop increases with drop size because terminal velocity varies with drop size. If the Marshall-Palmer (1948) raindrop size distribution is assumed, the relationship between the backscattering for each raindrop size and its respective Doppler shift can be determined. The crucial point is that the backscattering minima are also present in the Doppler shift spectrum. Since the terminal velocity of raindrops with radius 0.83 mm is known, the vertical component of the Doppler shift at that minimum can be determined. By removing the vertical component of the Doppler shift, the horizontal component remains. From the horizontal component one obtains a better estimate of the clear air velocity. This information about air motion may help to better understand cloud dynamics, cloud structure, and precipitation process.

This procedure is based on identifying the backscattering minimum which occurs for spheres. If a backscattering minimum is present for a size distribution of ice crystals this procedure could increase our understanding of ice clouds. Since ice crystals are nonspherical, Mie theory is not an applicable modeling tool; therefore, an alternative model such as the coupled-dipole method is required. Before calculating the backscattering of 94 GHz radar by

ice crystals, the accuracy of the coupled-dipole method will be estimated by first comparing scattering results for ice spheres with Mie theory.

Ice Spheres

The scattering-order technique was used to calculate backscattering by ice spheres, and the results were compared with Mie theory. The refractive index of ice (0° C) at 94 GHz is $1.878 + i4.76 \times 10^{-4}$. The number of dipoles in the arrays used to represent the sphere ranged from 461 for the smallest sphere to 2320 for the largest sphere. The number of dipoles was increased to keep the dipole radius small. This improves the accuracy of the calculations above the backscattering minimum, which occurs at a radius of 0.73 mm for ice. The results shown in Figure 5.10 indicate that calculations by the coupled-dipole method do fairly well at identifying the correct size parameter and magnitude of the backscattering response at the first minimum. The final step is to calculate backscattering by ice columns and plates.

Hexagonal Columns and Plates

The two ice crystals selected to be modeled are a hexagonal column and plate with aspect ratios 3.5:1 and 3.2:1, respectively. Hexagonal prismatic is the basic shape of ice crystals, although laboratory observations have revealed

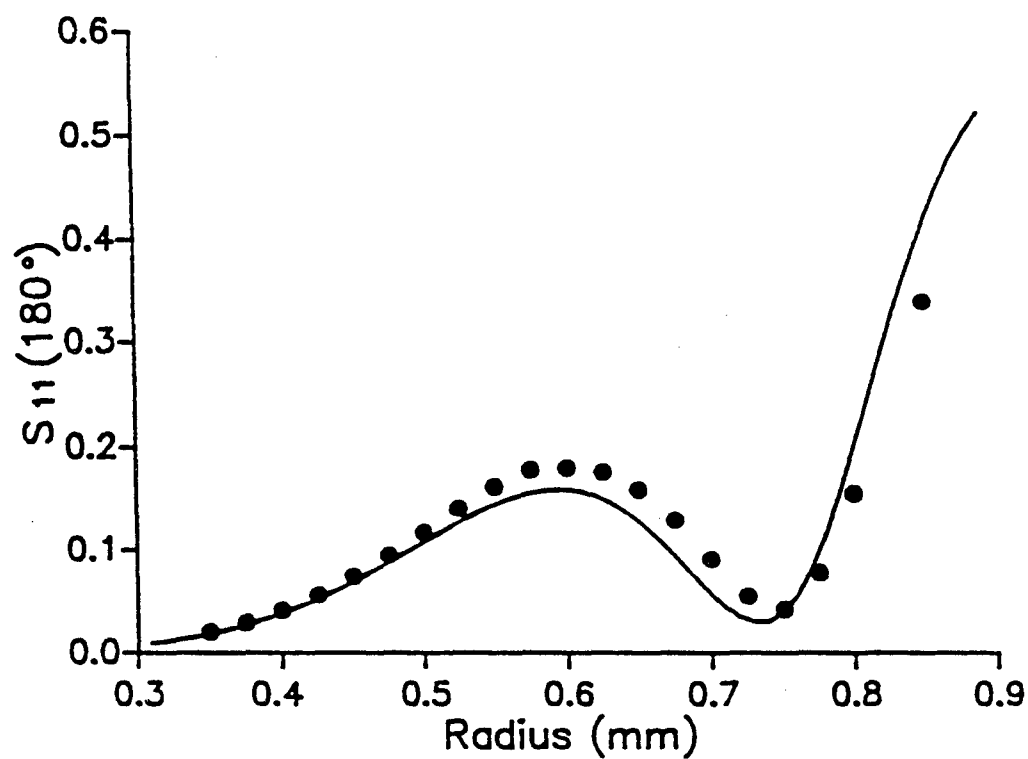


Figure 5.10 Comparison of coupled-dipole method with Mie theory for an ice sphere at 94 GHz ($m = 1.878 + i0.0005$). The solid line represents Mie theory; the dots represent coupled-dipole method.

a few other shapes (Pruppacher and Klett, 1980, Chap 2). The aspect ratio of 5:1 for the column would have been a better representation based on observations, but computer memory requirements restricted the size.

The matrix inversion technique was used to calculate backscattering by the ice crystals. The first set of calculations were made to dispel the notion that randomly oriented particles always scatter like equal-volume spheres.

Backscattering by the ice column and plate was calculated with the particles positioned in 100 orientations. The values for the column, plate, and sphere are shown in Figure 5.11. For size parameters less than 0.8 the difference between the backscattered signals is not too great. (This was observed in Figures 5.6 through 5.9 where the average backscattered signal from the randomly oriented particles with a size parameter of 1.0 was approximately equal to the backscatter from an equal-volume sphere.) At size parameters larger than 1.0 the backscattering signal of the sphere does not coincide with the minima for the other particles. Beyond this particle size, the backscattered signals differ by as much as a factor of six. Thus, at small size parameters and for particles of refractive indices close to unity, using an equal-volume sphere in place of randomly oriented particles may not be a bad assumption when calculating orientationally averaged backscattered signals; however, at larger size parameters the backscattering becomes very shape dependent, randomly oriented particles might no longer scatter like spheres.

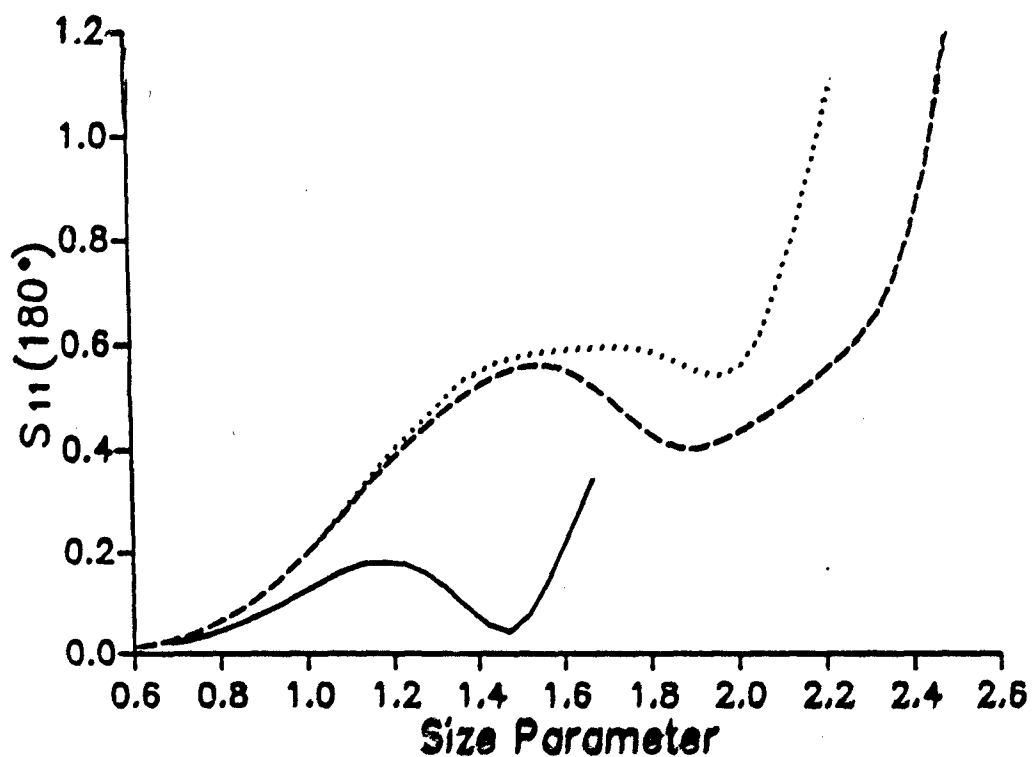


Figure 5.11 Backscattering of unpolarized light by randomly-oriented, equal-volume particles of increasing size parameter and with refractive index $1.878 + i0.0005$. Calculations were made with the coupled-dipole method. The solid line represents a sphere, the dashed-line represents a hexagonal column with aspect ratio of 3.5:1, and the dotted line represents a hexagonal plate with aspect ratio of 3.2:1.

The next set of calculations was made to determine a shape and size dependence of the first backscatter minimum for ice. For subsequent modeling the orientation of the crystals was assumed to be identical to that in the preceding section on backscattering by equal-volume particles: the particles do not tumble, and they are allowed to rotate within the horizontal plane.

Figures 5.12 through 5.16 show the dependence of backscattering by the hexagonal column (aspect ratio of 3.5:1) on size parameter, which is based on that of an equal-volume sphere. The values for size parameter range from 1.0 to 2.2 and correspond to column lengths of 2.1 to 4.6 mm. The five lines in the figures represent zenith angles of 10° , 30° , 50° , 70° , and 90° .

Unnormalized values of $S_{11}(180^\circ)$ are shown in Figure 5.12; in these and subsequent results the local maximum in the backscattering signal for 10° is about twice that for the other angles. In succeeding figures the local maximum has been normalized to 1.0 for comparing relative changes in the backscattering signal. Normalized values of $S_{11}(180^\circ)$ are shown in Figure 5.13. For the zenith angles 30° and 90° the relative difference between the local maximum and minimum is small, and it is largest for 50° and 70° . The shapes of the curves are somewhat different for values of $S_{HH}(180^\circ)$ and $S_{VV}(180^\circ)$ (shown in Figures 5.14 and 5.15). The relative difference between the local maximum and minimum for the $S_{HH}(180^\circ)$ curves are more pronounced for the smallest zenith angles. For $S_{VV}(180^\circ)$ the relative difference between local maximum and minimum is similar for all angle except 90° , but the noticeable

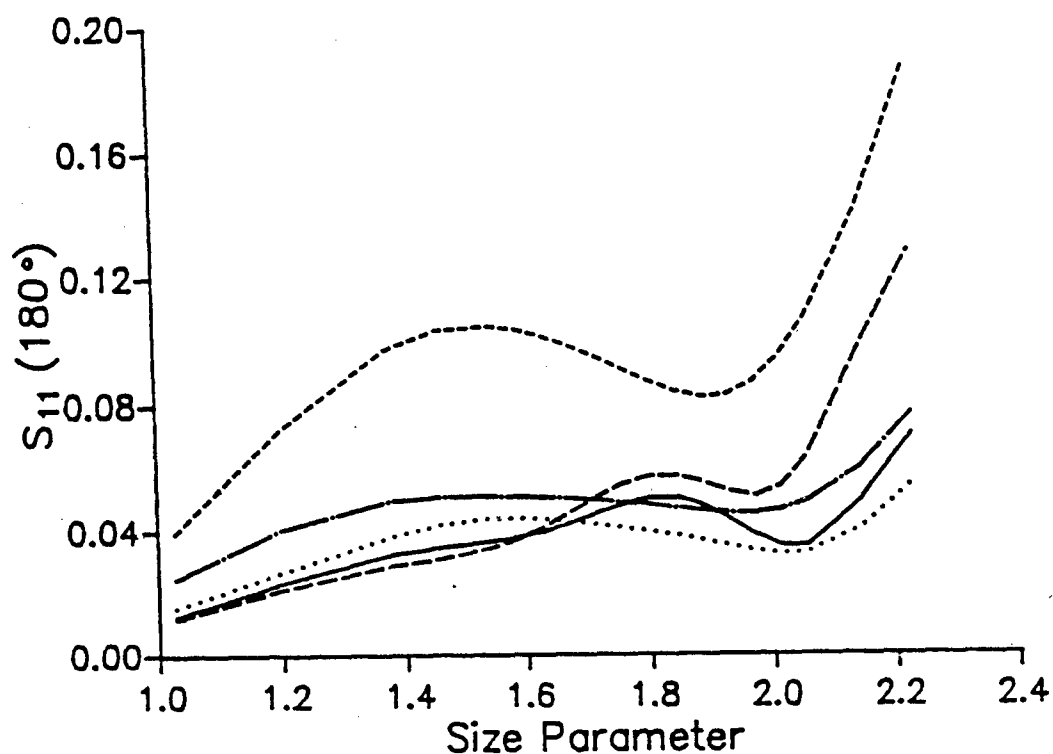


Figure 5.12 Backscattering of unpolarized light by ice columns of increasing size parameter at various zenith angles. The short-dashed line (---) represents a zenith angle of 10° , the dot-dash line (-·-·-) a zenith angle of 30° , the dotted line a zenith angle of 50° , the solid line a zenith angle of 70° , and the long-dashed line (— —) a zenith angle of 90° .

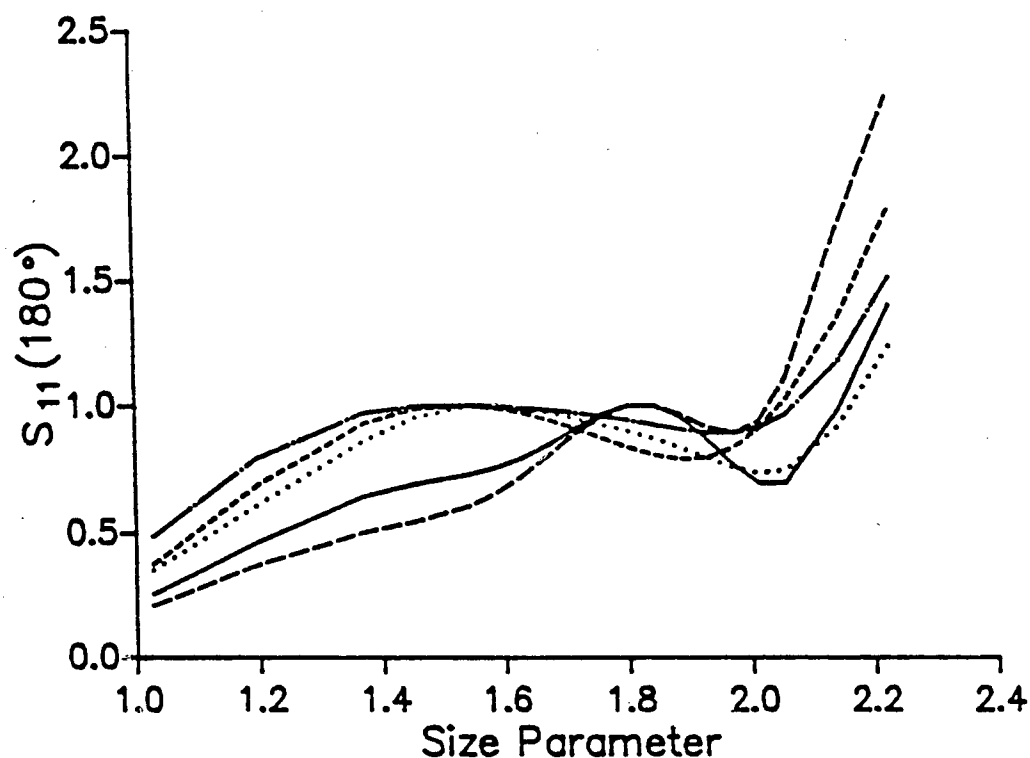


Figure 5.13 Backscattering of unpolarized light by ice columns of increasing size parameter at various zenith angles. Same as figure 5.10 except the local maximum value in the curves have been normalized to 1.0. The short-dashed line (---) represents a zenith angle of 10° , the dot-dash line (-.-.-) a zenith angle of 30° , the dotted line a zenith angle of 50° , the solid line a zenith angle of 70° , and the long-dashed line (——) a zenith angle of 90° .

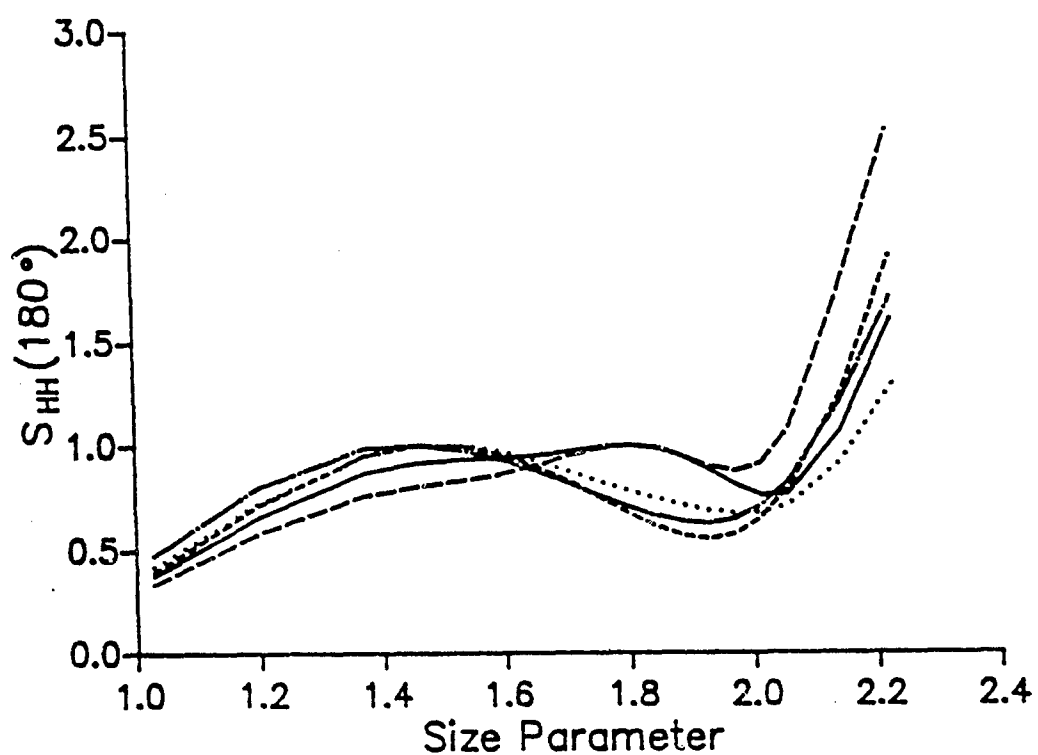


Figure 5.14 Backscattering of horizontally polarized light by ice columns of increasing size parameter at various zenith angles. The short-dashed line (---) represents a zenith angle of 10° , the dot-dash line (-.-.-) a zenith angle of 30° , the dotted line a zenith angle of 50° , the solid line a zenith angle of 70° , and the long-dashed line (— — —) a zenith angle of 90° .

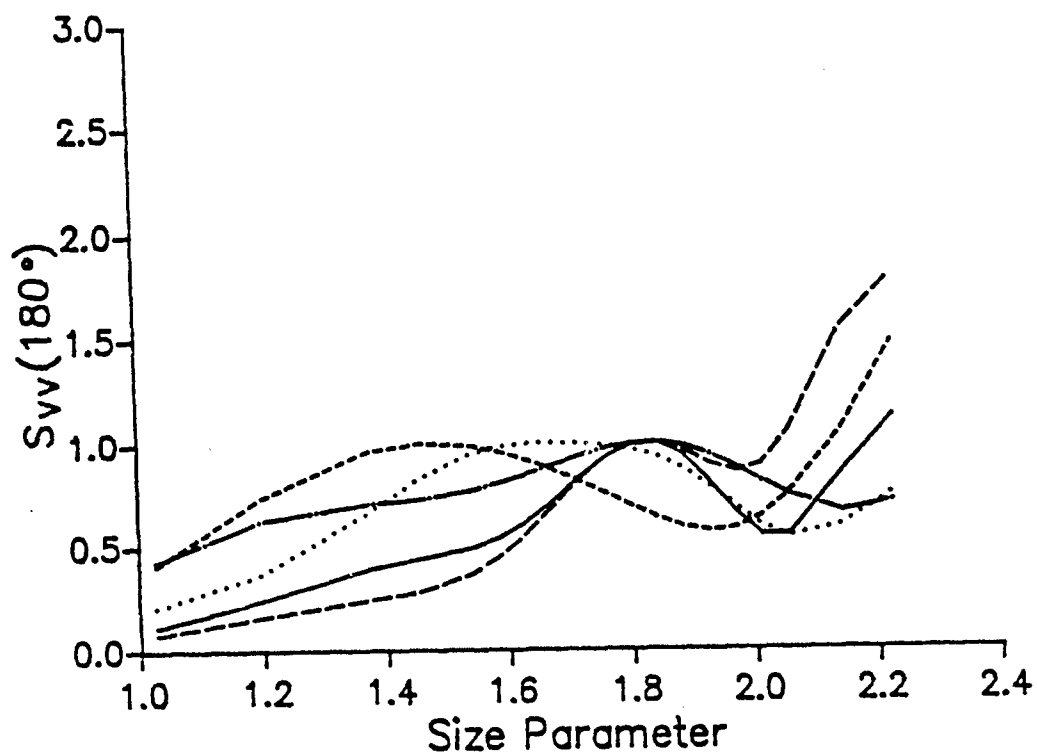


Figure 5.15 Backscattering of vertically polarized light by ice columns of increasing size parameter at various zenith angles. The short-dashed line (---) represents a zenith angle of 10° , the dot-dash line (-.-.-) a zenith angle of 30° , the dotted line a zenith angle of 50° , the solid line a zenith angle of 70° , and the long-dashed line (— — —) a zenith angle of 90° .

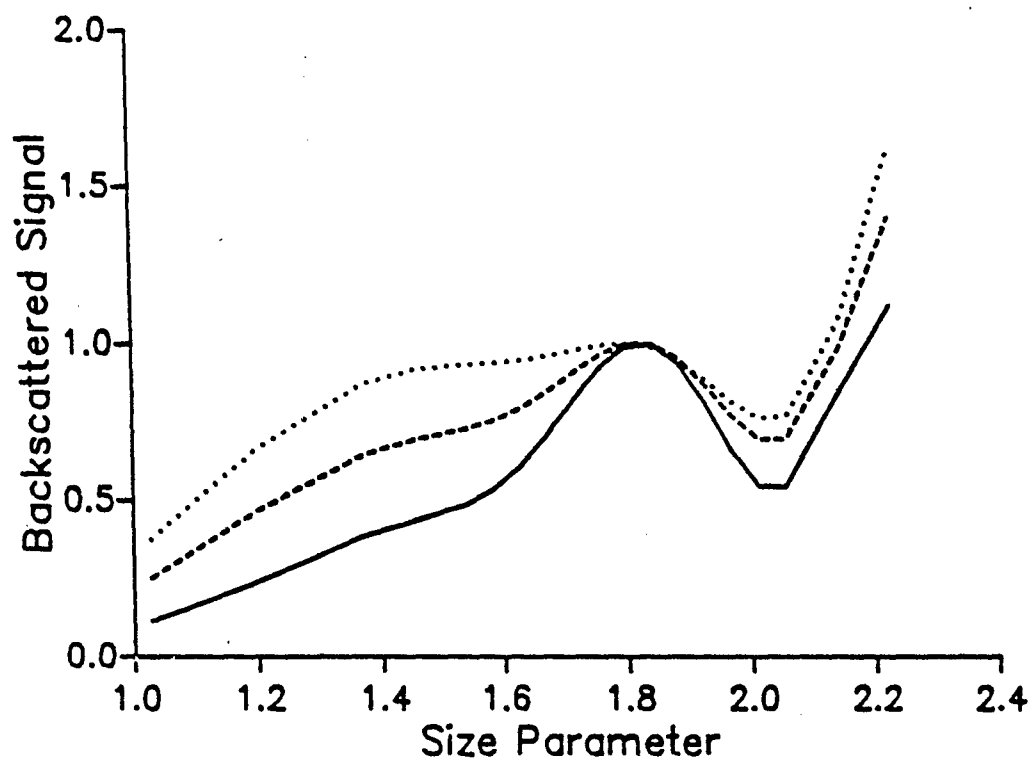


Figure 5.16 Backscattering by ice columns of increasing size parameter at zenith angle of 70° . The dashed-line represents unpolarized light, the dotted line represents horizontally polarized light, and the solid line represents vertically polarized light.

feature is the narrowing of the local maximum feature at the two largest zenith angles. A comparison of the backscattering signal at 70° for all three states of polarization is shown in Figure 5.16. The most pronounced local minimum is calculated to appear near a size parameter of 2.0 for $S_{VV}(180^\circ)$. The comparison of the backscattering signals in Figures 5.12 through 5.16 agrees with one's intuition that linearly polarized microwave radar (in particular S_{VV}) would produce better definition in the backscattering curves. This is also evident in backscattering by ice plates.

Figures 5.17 through 5.20 show the dependence of backscattering by the hexagonal plate (aspect ratio of 3.2:1) on size parameter. The size parameter calculation is again based on an equal-volume sphere. The values for size parameter range from 0.6 to 2.4 and correspond to plate diameters of 0.8 to 3.3 mm. The five lines in the figures represent zenith angles of 10° , 30° , 50° , 70° , and 90° . Normalized values of $S_{11}(180^\circ)$ are shown in Figure 5.17. Unlike the results for the hexagonal column, the backscattering minimum for the plate is spread over a larger range of size parameters, and it occurs at a lower size parameter for higher zenith angles. The relative difference between the local maximum and local minimum also decreases with increasing zenith angle. For values of $S_{HH}(180^\circ)$ and $S_{VV}(180^\circ)$ (shown in Figure 5.18 and 5.19) the shapes of the curves are again dissimilar. The main difference between $S_{HH}(180^\circ)$ and $S_{11}(180^\circ)$ is a slight deepening of the backscattering minimum at a zenith angle of 50° . The noticeable differences between $S_{VV}(180^\circ)$ and

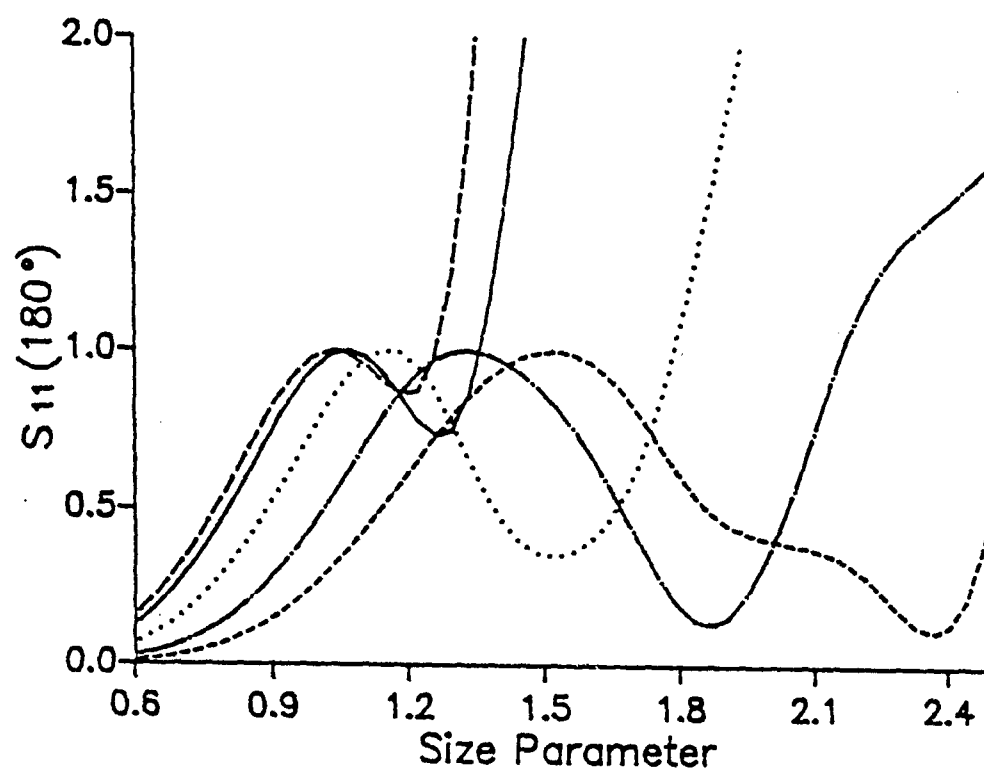


Figure 5.17 Backscattering of unpolarized light by ice plates of increasing size parameter at various zenith angles. The short-dashed line (---) represents a zenith angle of 10° , the dot-dash line (----) a zenith angle of 30° , the dotted line a zenith angle of 50° , the solid line a zenith angle of 70° , and the long-dashed line (— —) a zenith angle of 90° .

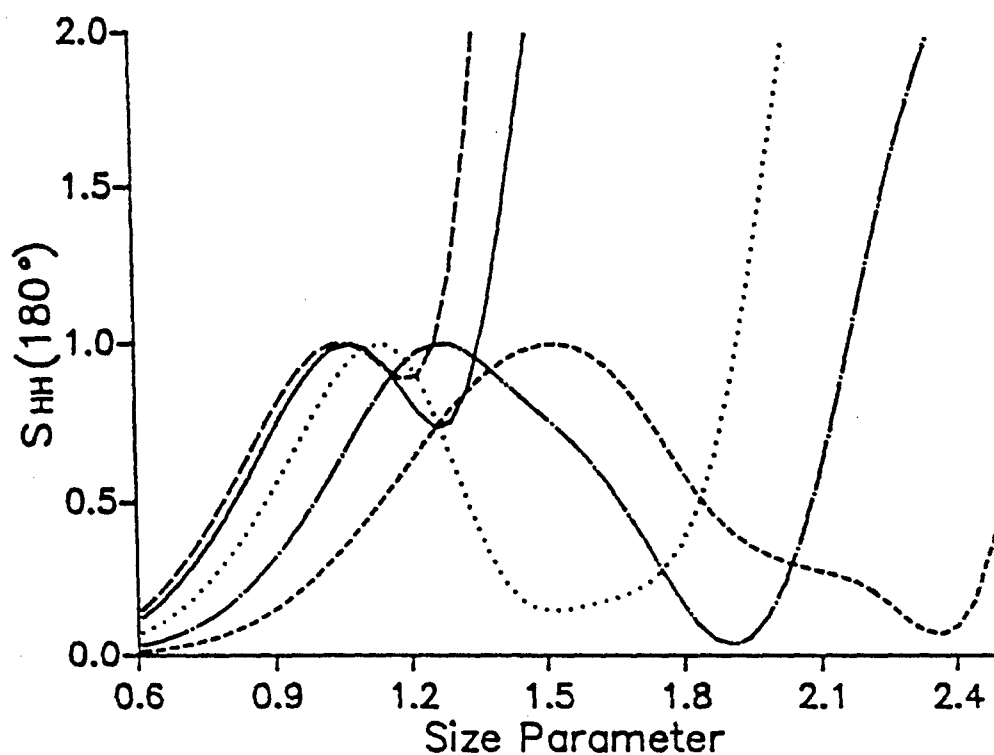


Figure 5.18 Backscattering of horizontally polarized light by ice plates of increasing size parameter at various zenith angles. The short-dashed line (---) represents a zenith angle of 10° , the dot-dash line (-.-.-) a zenith angle of 30° , the dotted line a zenith angle of 50° , the solid line a zenith angle of 70° , and the long-dashed line (——) a zenith angle of 90° .

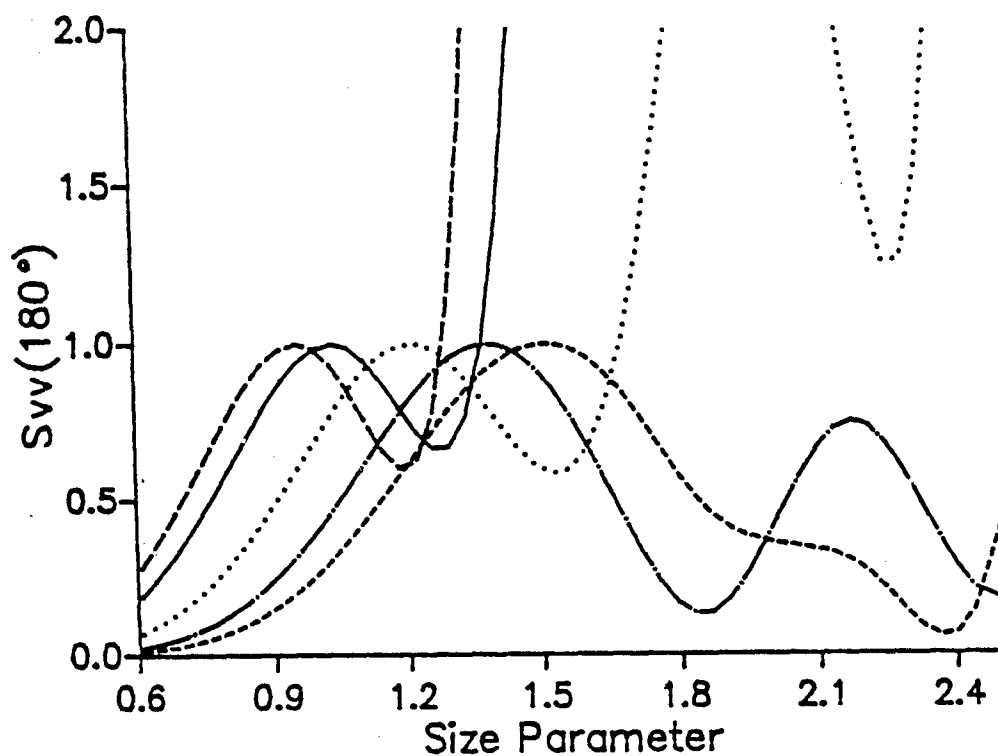


Figure 5.19 Backscattering of vertically polarized light by ice plates of increasing size parameter at various zenith angles. The short-dashed line (---) represents a zenith angle of 10° , the dot-dash line (-.-.-) a zenith angle of 30° , the dotted line a zenith angle of 50° , the solid line a zenith angle of 70° , and the long-dashed line (— — —) a zenith angle of 90° .

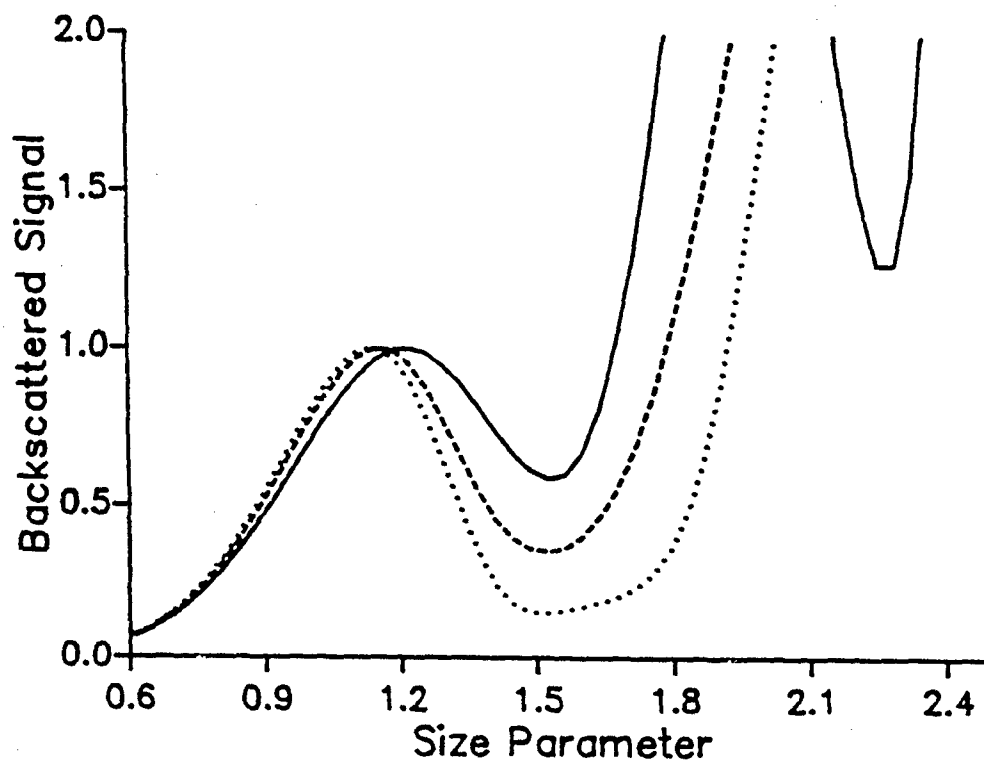


Figure 5.20 Backscattering by ice plates of increasing size parameter at zenith angle of 50° . The dashed-line represents unpolarized light, the dotted line represents horizontally polarized light, and the solid line represents vertically polarized light.

$S_{11}(180^\circ)$ are the shallower minimum at zenith angle of 50° and the presence of the second backscattering minimum for all zenith angles except 10° and 90° (a shallow minimum occurs at 70° , but it is out of range of the figure). A comparison of the backscattering signal at 50° for all three states of polarization is shown in Figure 5.20. In contrast with the results for the hexagonal column, $S_{HH}(180^\circ)$ produces the largest relative difference between the local maximum and minimum.

The backscattering minima for ice crystals have an added feature over their counterparts for spherical raindrops: a dependence on zenith angle. This dependence disappears if the ice crystals tumble as they fall; nonetheless, this could provide information about turbulence in the vicinity of the crystals. Thus, backscattered signals collected while the radar sweeps through zenith angles may be useful in remotely sensing the atmospheric environment.

Several areas within the realm of meteorology would benefit by having a better understanding of the crystal characteristics within ice clouds: climate modeling, atmospheric chemistry, and cloud physics (Vogelmann, et al., 1990). The transfer of infrared radiation through cirrus clouds is an issue in the debate over global warming. Modeling scattering by cirrus clouds can be improved if the size and shape distribution of the ice crystals are known. The scavenging or removal of atmospheric aerosols, including sulfates that contribute to acid precipitation, depends on the shape of the crystal. The scavenging efficiency of ice crystals appears to increase with surface to volume

ratio (Dungey, 1976). Crystal growth and aggregation are important mechanisms in the precipitation process. By analyzing backscattering signals from different levels within the atmosphere the growth of the ice crystals may be estimated.

Although identification of size and shape distributions of ice crystals using this procedure seems feasible, several contributing technological factors are still uncertain. The technology required to build millimeter-wavelength radar is relatively new. Present research and development of millimeter wave tubes is expected to result in construction of more powerful transmitters (Lhermitte, 1990), thereby increasing the sensitivity of the radar. The size range of ice crystals in this chapter is typical of falling snow. To identify the size distribution of smaller ice crystals, a shorter wavelength is required. A recently developed 1.4 mm (215 GHz) wavelength radar (Mead et al., 1989) has the potential for observing the first minimum in backscattering by smaller ice crystals; however, at this wavelength attenuation by atmospheric water vapor may (depending of the transmission power) limit the system's performance.

Identification of ice crystal size distribution depends on several other factors. First, the size distribution is assumed to be continuous. A discontinuous size distribution would produce gaps in the Doppler shift spectrum which could be mistaken as a backscattering minimum. Second, crystal aggregation should be a minimum. Backscattering calculations are

made only for plates and columns; scattering by aggregates may irretrievably obscure the desired backscattering minima. Third, the optical depth of the ice crystals is not too large, otherwise the backscattered signal will be a result of multiple scattering events. The procedure for identifying ice crystals is based on single scattering.

In this chapter, the ability of the coupled-dipole to calculate backscattering by nonspherical particles was demonstrated. For spheres smaller than the size which produces the first backscattering minimum, small shape variations in the dipolar array do not affect the accuracy of the backscattering calculation. Conversely, when the spheres are larger than the size which produces the first backscattering minimum, backscattering calculations lose accuracy. For particles with a large aspect ratio (at least 5:1) and small size parameter, the backscattering calculation is relatively insensitive to the exact shape of the particle, i.e. hexagonal column, cylinder, etc. Finally, backscattering calculations for hexagonal columns and plates have been presented. Although this is not a definitive work in radar meteorology, it is feasible that a size distribution of ice crystals could be estimated using remote sensing techniques. This can also be scaled down for observing cirrus crystals with an instrument operating at a shorter wavelength. In general, the size of the ice crystals will dictate the wavelength that will be best suited for obtaining the first backscattering minimum.

Chapter 6

SUMMARY AND CONCLUSION

The problem of light scattering by arbitrary particles can be approached a number of ways. One option too often taken is to assume that the particles are spherical. This assumption simplifies the computational task by allowing Mie theory to be used for the calculations; however, this oversimplification may lead to unacceptable errors. The other option is to appreciate the shape of the particles and choose an appropriate computer model to calculate the particle's scattering properties.

As described in this dissertation, the coupled-dipole method is applicable for modeling a considerable variety of arbitrary particles. First, a particle of any shape can be modeled using this method. Second, several solution techniques are available depending on the physical characteristics of the particle. If the size parameter of the particle is small (< 2 or 3 depending on shape or refractive index) or if the particle is to be modeled in numerous orientations, the matrix inversion technique may be used. If the relative refractive index of the particle is not too large (< 2), computer memory limitations can be avoided by using the scattering-order technique.

Another consideration in the coupled-dipole method is the relationship between the polarizability of the discrete dipolar subunits and the relative

refractive index of the particle being modeled. In most papers the Clausius-Mosotti (CM) relation or the CM relation with a radiative reaction term has been used. Since the formulation of the coupled-dipole method is based on subunits that radiate as dipoles, the conversion of relative refractive index to electric dipole polarizability (using the first term from Mie theory referred to as Doyle's method) was incorporated into the method. The results using Doyle's method show a better agreement with Mie theory than using the other schemes. Further calculations showed that Doyle's method can be used near a resonance mode (Fröhlich mode) for small particles and that the results compared favorably with measured data.

Input parameters for the coupled-dipole method have been added to accommodate a variety of particle shapes and sizes. Subroutines are available for constructing arrays of dipolar units that represent spheres, spheroids, rectangular solids, cylinders, and hexagonal crystals. The capability of specifying the size of particle has also been included. Output provides a number of useful scattering parameters: Mueller matrix elements for any scattering angle as well as scattering, absorption, and extinction cross sections.

The ability of the coupled-dipole method for determining backscattering calculations was investigated. A simple model was presented to show why scattering in the backward direction is most sensitive to particle size and shape. The sensitivity was shown to be a result of the phase relation of scattered waves from the dipolar subunits. Backscattering values using the coupled-

dipole method compare favorably with Mie theory for spheres which are smaller than the size parameter associated with the first backscattering minimum (e.g., size parameter of 1.6 for relative refractive index of $1.33 + i0.05$). At this and larger size parameters, backscattering becomes extremely shape dependent, and modeling results from the coupled-dipole method lose precision because an array of dipolar subunits arranged on a simple cubic lattice cannot adequately represent a solid sphere. Small variations in shape were shown to strongly affect backscattering calculations for spheres with size parameters which are near the size parameter associated with the first backscattering minimum. Agreement between the coupled-dipole method and Mie theory can be improved by increasing the number of dipolar subunits in the array; however, this also increases computer memory requirements and computation time.

Backscattering by equal-volume particles was investigated using the coupled-dipole method. A cylinder, rectangular solid, prolate spheroid, and hexagonal column of equal volume and with aspect ratio 5:1 were modeled, and the results were compared with those of an equal-volume sphere. Despite the difference in cross-sectional shape, the elongated particles displayed similar scattering properties for three different refractive indices. However, the size parameter of the particles was only 1.0. If the particles were larger than the size which corresponds to the first backscattering minimum, backscattering by the elongated particles might not agree so well because of the extreme shape

dependence as discussed above. The average backscattering value for the elongated shapes (this simulated random orientation of the particles) was approximately equal to that for the equal-volume sphere; however, agreement decreased with increasing refractive index.

Finally, backscattering of 94 GHz radar by ice crystals was examined. The accuracy of the coupled-dipole method in this application was shown to be good by comparing calculations of backscattering by ice spheres with Mie theory. Backscattering by randomly oriented ice columns and plates was compared with backscattering by equal-volume ice spheres. For small size parameters the backscattering values are in fair agreement; however, for larger size parameters they differ by as much as a factor of six.

The orientation of the ice columns and plates was then made more restrictive by modeling them as if they fell through the atmosphere without tumbling. The resulting backscattering calculations now contained a dependence on zenith angle. The first backscattering minima are present for both type crystals, but with noticeable differences. The relative difference between the local maximum and the first backscattering minimum for the ice plate is larger than that for the column, and the backscattering minimum for the plate is spread out over a larger range of size parameters. The use of horizontally and vertically polarized waves also enhance the magnitude of the first backscattering minima.

Backscattering minima by raindrops can be detected, and the information is used to determine additional features of the atmosphere. These variations in backscattering minima by ice crystals at 94 GHz may be used to remotely estimate their size and shape distributions. Knowledge of the ice crystal characteristics would benefit the areas of climate modeling, atmospheric chemistry, and cloud physics. Present research and development of millimeter radar technology will provide increased sensitivity, which makes this scheme for identifying ice crystals even more promising (Lhermitte, 1988).

In conclusion, scattering by arbitrary particles can be approximated by assuming their scattering properties are similar to that of equal-volume spheres. This practice has advantages and disadvantages. The calculations for scattering by equal-volume spheres are quick and inexpensive, and in many instances they provide a reasonable first-order estimate of the scattering properties of the arbitrary particles that may not have been initially apparent. But by using the equal-volume sphere approach, additional scattering information may be overlooked.

It was shown that scattering by an equal-volume sphere agrees favorably with that for small, tumbling ice crystals at 94 GHz (size parameter less than 0.8). Thus in this case the equal-volume sphere approximation will save computer time and costs while providing reasonable results. However, for size parameters larger than 1.0, the equal-volume sphere approximation will lead to large errors. Moreover, when the ice crystals are assumed to be not tumbling,

the scattering results take on additional features. The backscattered signal becomes dependent on zenith angle and on the polarization of the incident wave. These properties of scattering may help to identify the shape and size distributions of ice crystals, but they will never be present for spheres. Therefore, while calculating scattering by spheres may be a simple task and sometimes a fairly accurate approximation, important information could be omitted.

The next problem to be solved is that of inverting the backscattered signal to useful information about the size and shape of the ice crystals. Variations in backscattering for ice crystals of different aspect ratios should also be examined. The refractive index of ice at 94 GHz is sufficiently large to induce higher order multipoles in the ice crystals. It may be advantageous to incorporate the calculation of these multipoles in the coupled-dipole method to improve the accuracy of scattering calculations.

Appendix A

This appendix has been accepted for publication in the *Journal of the Optical Society of America A*. A slightly modified version of the paper is given here.

LIGHT SCATTERING BY NONSPHERICAL PARTICLES:
A REFINEMENT TO THE COUPLED-DIPOLE METHOD

Clifton E. Dungey[†] and Craig F. Bohren

Department of Meteorology, The Pennsylvania State University
University Park, Pennsylvania 16802

Abstract

In the coupled-dipole method an arbitrary particle is modeled as an array of N polarizable subunits each of which gives rise to only electric dipole radiation. The Clausius-Mosotti relation is widely used to calculate the polarizability of the subunits that corresponds to the dielectric function of the particle that the array represents. In this paper we replace the Clausius-Mosotti relation with an exact expression for the electric dipole polarizability and find improvement in extinction calculations for spheres as compared with Mie theory. Near a Fröhlich frequency the coupled-dipole method yields extinction cross sections for spheres and spheroids that compare favorably with the method of continuous distribution of ellipsoids and measured values.

[†]Captain Dungey is assigned to Penn State through the graduate meteorology program of the Air Force Institute of Technology.

Introduction

The coupled-dipole method was apparently first applied by Purcell and Pennypacker (1973) to calculate approximate cross sections of nonspherical particles. Partly owing to the enormous computer storage and CPU time required for modeling particles with large size parameters, this method never has had a great following. But in the past few years, with faster computers and more efficient programming techniques, an increasing number of people have begun using this relatively simple technique. For example, Draine (1988) has used it to study scattering by interstellar grains; Goedecke and O'Brien (1988) and Flatau et al. (1990) have examined scattering by ice crystals; S. B. Singham et al. (1986a) calculated differential scattering by chiral particles; and Varadan et al. (1989) computed scattering by anisotropic particles.

The coupled-dipole method has remained essentially unchanged since its inception. An arbitrary particle is divided into an array of N subunits located on a simple cubic lattice (Figure A.1). The dipolar subunits are sufficiently small to give rise to only electric dipole radiation. Total scattering is then calculated by summing the waves scattered by each dipolar subunit excited by the incident wave and by the waves scattered to it from all its neighbors. The coupled-dipole method originally was formulated (Purcell and Pennypacker, 1973) heuristically; however, a more formal mathematical derivation and a short review of the method has been published recently (Lakhtakia, 1990).

Some recent modifications made to the coupled-dipole method include more efficient means of calculating scattering by randomly oriented particles (Singham et al., 1986b) and improved solution algorithms (Draine, 1988; Flatau et al., 1990; Chiapetta, 1980; Singham and Bohren, 1988) that permit larger values of N . For scattering calculations in this paper we rely on the matrix inversion technique (Singham and Salzman, 1986) to solve the interaction

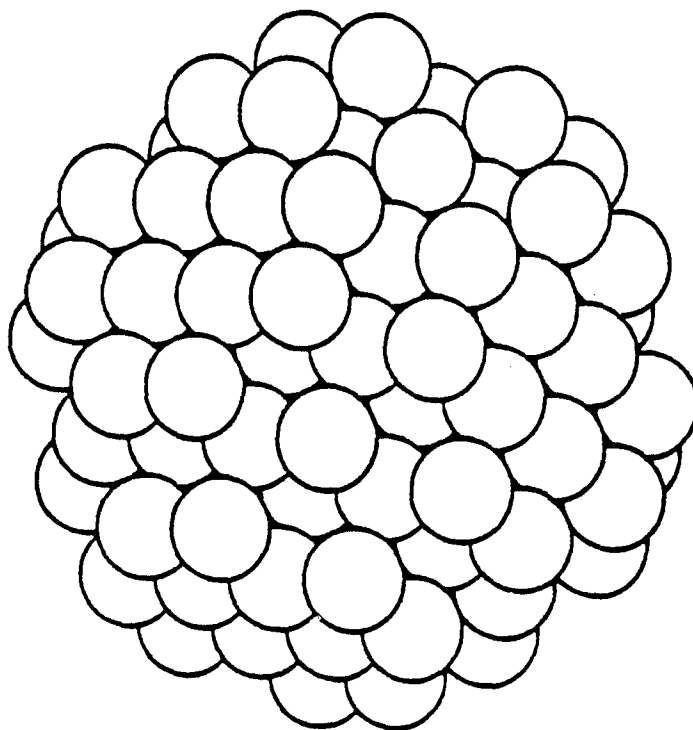


Figure A.1 A spherical particle which has been represented by an array of 136 dipolar subunits. The effective radius of the sphere is determined by $a_e = (3N/4\pi)^{1/3}$, where the dipolar subunits are assumed to have unit volume.

matrix directly. Although N is limited to 300 in this technique because of the need to store the matrix, we are guaranteed a solution provided that the matrix is algorithmically nonsingular. The matrix inversion method also permits the efficient calculation of extinction cross sections of nonspherical particles in random orientations (Singham et al., 1986b). In this paper we treat only isotropic scatterers.

An integral part of the coupled-dipole method is an effective-medium theory that provides the relationship between the polarizability of the individual dipolar subunits and the bulk dielectric function of the continuous medium that the array represents. The most widely used effective-medium theory for determining the polarizability has been the Clausius-Mosotti (CM) relation, in some instances with slight modifications (e.g. Draine, 1988).

In next section, following Doyle (1989), we calculate the electric dipole polarizability using an exact expression. Using this expression in the coupled-dipole method generally leads to calculated extinction cross sections more in accord with Mie theory.

In final section we test Doyle's method on particles in the neighborhood of a Fröhlich frequency. This is a strong absorption mode highly dependent on both particle size and shape. Extinction cross sections near the Fröhlich mode are computed for spheres and spheroids by using the coupled-dipole method and are compared with results from Mie theory, the method of continuous distribution of ellipsoids (CDE), and measured values (Huffman and Bohren, 1980). The nature of the shape-dependent extinction determined by the coupled-dipole method is used to analyze small discrepancies between results from modeling spheres with the coupled-dipole method and Mie theory.

Effective-Medium Theory

When dealing with a composite material consisting of small grains embedded in a homogeneous matrix, one must measure or estimate the dielectric function from a theory. If the optical properties of the embedded grains and the matrix are known, one uses an effective-medium theory to estimate the bulk characteristics of the composite. This problem is the converse of that faced by those using the coupled-dipole method for which the bulk dielectric functions of the particle (composite) and surrounding medium are known and the optical properties of the dipolar subunits (grains) must be calculated.

The Maxwell Garnett relation is an effective-medium theory that can be used to determine the dielectric function of the dipolar subunits. By assuming spherical dipolar subunits, we can reduce the Maxwell-Garnett relation (Bohren and Huffman, 1983, Sect 8.5):

$$\epsilon_{dip} = \frac{2(1-f)\epsilon_m^2 - (2+f)\epsilon_m\epsilon}{(1-f)\epsilon - (1+2f)\epsilon_m} \quad (A.1)$$

where ϵ_{dip} , ϵ , and ϵ_m are the dielectric functions of the dipolar subunits, the bulk particle, and its surrounding medium; and f is the volume filling factor. For spherical dipolar subunits on a simple cubic lattice with diameters equal to the lattice spacing $f = \pi/6$.

Purcell and Pennypacker (1973) used the CM relation to obtain the complex polarizability α of the dipolar subunits from the dielectric function of the material:

$$\alpha = \frac{3(\epsilon - \epsilon_m)}{N(\epsilon + 2\epsilon_m)} \quad (\text{A.2})$$

where N is the number of dipolar subunits per unit volume. Although the Maxwell-Garnett and CM relations yield different physical parameters, their formal derivations have been shown to be essentially identical (Barker, 1973). The relationship between α and ϵ_{dip} is obtained by combining equations (1) and (2) producing another form of the CM relation:

$$\alpha = 4\pi a^3 \frac{(\epsilon_{\text{dip}} - \epsilon_m)}{(\epsilon_{\text{dip}} + 2\epsilon_m)} \quad (\text{A.3})$$

where a is the radius of the dipolar subunits. Equations (1) and (3) will be referred to later, but next we briefly examine a shortcoming in the CM relation when it is used in the coupled-dipole method.

The optical theorem states that the extinction cross section C_{ext} for small spheres is determined from the imaginary part of its polarizability. When ϵ is purely real the CM relation produces a purely real α . Since C_{ext} cannot be zero because the incident wave must be attenuated by scattering, α must be complex. Draine (1988) and Goedecke and O'Brien (1988) provide methods that satisfy this criterion, we introduce a third.

When investigating the optical properties of small metal spheres suspended in a transparent medium, Doyle (1989) used an exact expression for the electric dipole polarizability

$$\alpha = i \frac{6\pi}{k^3} a_1 \quad (\text{A.4})$$

where $k = 2\pi a/\lambda$ and a_1 is the electric dipole coefficient from Mie theory:

$$a_1 = \frac{m\psi_1(mx)\psi_1'(x) - \psi_1(x)\psi_1'(mx)}{m\psi_1(mx)\xi_1'(x) - \xi_1(x)\psi_1'(mx)} \quad (\text{A.5})$$

with ψ_1 and ξ_1 being Riccati-Bessel functions and $x = ka$. In Doyle's application m is the ratio of the complex index of refraction of the metal spheres to that of the medium; for the coupled-dipole method it is the ratio of the index of refraction of the dipolar subunits to that of the medium. When using this exact expression for the electric dipole term, Doyle calculated reflectances of a composite that agreed better with experimental values than if only the first term in the series had been used.

The coupled-dipole method operates on the principle that the dipolar subunits are sufficiently small that they give rise to only electric dipole radiation. It was therefore appropriate to incorporate equations A.4 and A.5 into the coupled-dipole method. In what we now refer to as the Doyle expression, the polarizability of the dipolar subunits are calculated using this exact expression for the electric dipole polarizability. The value for m in equation A.5 is obtained from equation A.1 where $m^2 = \epsilon_{\text{dip}}/\epsilon_m$. In the small-particle limit, the Doyle expression reduces to the CM relation.

To guarantee a complex α , Draine used a radiative reaction term that is contained in the Doyle expression. If a_1 were expanded in a series of the size parameter x , the radiative reaction term would be the third in the series. The Doyle expression and Draine's radiative-reaction factor are similar in that they modify the entire interaction matrix. Goedecke and O'Brien (1988) use a self-term correction that modifies only the diagonal elements of the matrix. We now compare results from the coupled-dipole method by using the CM relation, Draine's radiation correction, and Doyle's expression. In our model all the dipolar subunits are spherical; most of the particles (dipolar arrays) that are modeled are also spherical. In our discussions we try to distinguish between the two.

In this section dipolar arrays representing spheres are modeled and the results are compared with BHMIE (Bohren and Huffman, 1983, Appendix A). For the first comparison the arrays range in size from 27 to 251 dipolar subunits. If the spacing of the lattice is considered to be 1 du (dipole unit) then the corresponding effective radii for the modeled spheres range from 1.86 to 3.91 du. A wavelength of 12.5 du was used. Figure A.2 shows relative values of Q_{ext} for two refractive indices using the three schemes to determine the dipolar subunit polarizability. For this comparison the Doyle expression agrees best with Mie theory.

One input variable remained constant for this comparison: the size parameter of the dipolar subunits. Purcell and Pennypacker (1973) state that if $ka < 0.35$, the coarseness of the array would not cause serious errors in the calculations. Yung (1978) claims reliable results when $ka < 0.17$. By also considering the wavelength of the electric field within the dipolar subunit Draine's guidance (1988) suggests $ka|m| < 0.5$ when an accuracy of 10% is desired, where $|m|$ is the modulus of the complex refractive index; for this comparison these values were 0.33 and 0.43.

In the second comparison the size of the dipolar subunit was varied. The range of $ka|m|$ was from 0.13 to 1.07. The sphere was represented by an array of 136 dipolar subunits; the wavelength was 12.5 du. As seen from Figure A.3, when the size parameter of the subunits is small, all three schemes for determining polarizability compare well with Mie theory. Over the entire range the Doyle expression is the most accurate. Note the increasing overprediction by all three schemes above $ka|m| = 0.8$, which occurs as Q_{ext} of the bulk sphere is reaching a maximum value of 3.7. Not only does the Doyle expression overpredict least, it is the only one to respond to the falling values of Q_{ext} at the largest size parameter indicated.

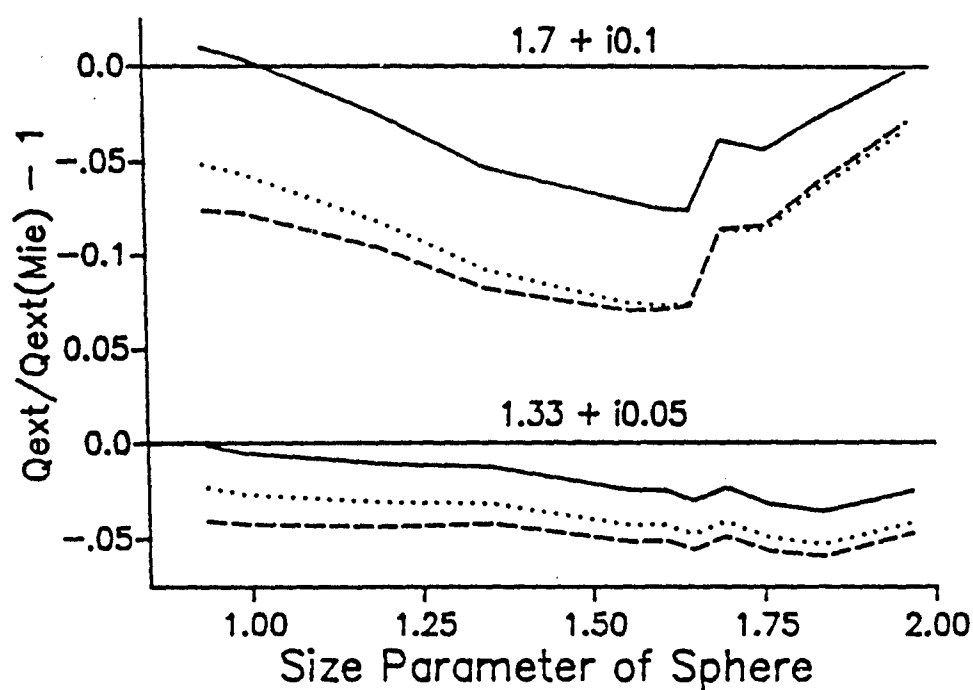


Figure A.2 Comparison between Mie theory and the coupled-dipole method using different schemes to calculate polarizability while varying the number of dipolar subunits. Calculations using the Doyle expression are represented by (—), Draine's radiative reaction term by ($\cdot \cdot \cdot$), and the Clausius-Mosotti relation by (- - -). N varies from 27 to 251; size of dipolar subunit remains constant. Results for two refractive indices are shown.

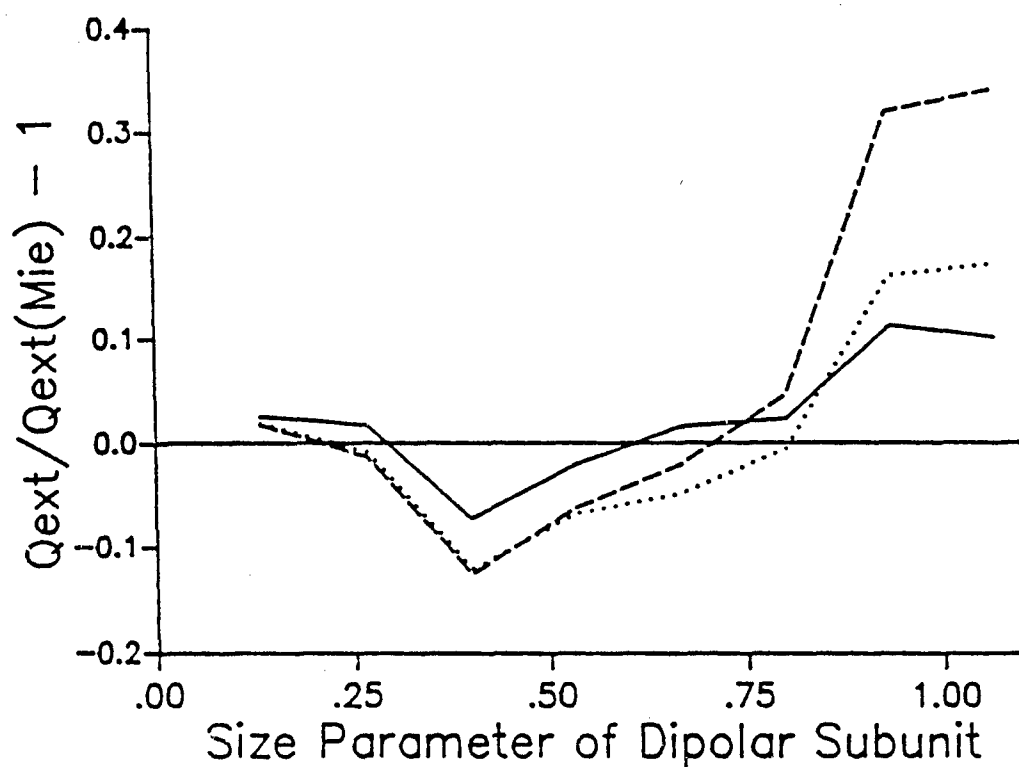


Figure A.3 Comparison between Mie theory and the coupled-dipole method using different schemes to calculate polarizability while varying the size of the dipolar subunits. Calculations using the Doyle expression are represented by (—), Draine's radiative reaction term by (· · · ·), and the Clausius-Mosotti relation by (- - -). N remains constant (136 dipolar subunits).

The index of refraction was varied in the third comparison. An array of 136 dipolar subunits was modeled; the effective radius of the particle remained constant and the wavelength was 12.5 du. Nine refractive indices were selected from earlier papers (Purcell and Pennypacker, 1973; Draine, 1988) and from various practical applications. As seen in Table A.1, agreement between the coupled-dipole method and Mie theory generally varies inversely with $ka|m|$. Among the different schemes the Doyle expression gives the best overall results. For instance, no improvement is noted for $m = 1.44 + i0.26$ but the coupled-dipole method already compares to within 1% of Mie theory. At the two largest refractive indices the Doyle expression does not compare best with Mie theory. It may be that the other schemes are near a crossover point as was the case in Figure A.2 near $ka|m| = 0.8$. However, the use of the coupled-dipole method in this particular application is not recommended because the higher order multipoles associated with the large refractive index are undoubtedly introducing error in the calculations. A better comparison would be made with a much array with a larger number of dipoles; unfortunately, the array size is limited in the matrix-inversion method.

When the coupled-dipole method is used appropriately ($ka|m| < 0.5$) the Doyle expression yields extinction efficiencies that agree better with Mie theory than the other two schemes do. Incorporation of the Doyle expression into the coupled-dipole method adds negligible computation time.

The refractive indices used in the previous comparisons are appropriate only for regions in which surface modes are not excited. A more stringent test of Doyle's expression is how well it enables the coupled-dipole method to calculate extinction near surface mode frequencies.

Table A.1. Comparison of Q_{ext} for nine spheres of different refractive indices as calculated by Mie theory and by the coupled-dipole method with either the Doyle expression, Draine's radiation reaction term, or the Clausius-Mosotti relation. Values shown are $[Q_{\text{ext}}/Q_{\text{ext}}(\text{Mie})-1]$. A 136-dipole array is used for the coupled-dipole calculations; effective radius of the sphere remains constant at 3.19 du. Rows are in order of increasing size parameter of the dipolar subunit.

Refractive Index	Doyle	Draine	Clausius-Mosotti	$ka m $
1.44 + i0.26	-1.0%	-1.0%	-1.0%	0.29
1.33 + i0.05	-1.7	-3.3	-5.0	0.34
1.55 + i0.005	-6.8	-11.1	-12.8	0.39
1.39 + i0.42	0.0	-1.1	-0.6	0.37
1.7 + i0.1	-7.1	-12.4	-12.8	0.42
1.9 + i0.0004	-10.3	-18.7	-18.4	0.48
2.5 + i1.4	14.1	16.0	16.7	0.72
3.5 + i2.05	17.3	19.7	15.3	1.02
3.0 + i4.0	30.0	18.1	36.9	1.26

Surface Modes

Resonance features known as surface modes can exist in small-particle absorption spectra even when none occur in the bulk material. Surface modes are caused by lattice vibrations in insulators and most commonly occur on the high-frequency side of bulk absorption bands. The absorption characteristics associated with a surface mode are highly shape dependent even though the particles are small compared with the wavelength.

The resonance is associated with the vanishing of the denominators of the Mie scattering coefficients. In the limit $x \rightarrow 0$ (finite $|m|$), the denominator of a_n vanishes if the following is satisfied (Bohren and Huffman, 1983, Sect 12.1):

$$m^2 = -\frac{n+1}{n}, \quad n = 1, 2, \dots \quad (\text{A.6})$$

For sufficiently small spheres the dominant coefficient is a_1 ; thus for $n = 1$ the resonance condition is $m^2 = -2$. With the refractive index of the medium close to unity the complex dielectric function of the particle for which resonance occurs is: $\epsilon = \epsilon' + i\epsilon'' = -2 + i0$. The frequency at which $\epsilon' = -2$ and $\epsilon'' = 0$ is called the Fröhlich frequency; the corresponding normal mode is known as a Fröhlich mode. Notice also from equation (1) that when $\epsilon_m = 1$, $\epsilon_{\text{dip}} = -2$ at the Fröhlich frequency. Thus according to the CM relation--either equation A.1 or A.3--the polarizability at a Fröhlich mode is infinite. It is under this condition we now test Doyle's expression for determining the polarizability.

An example of a Fröhlich mode appears in the infrared for quartz particles. The optical constants of quartz (Figure A.4) were determined by using the Lorentz oscillator model and published dispersion parameters

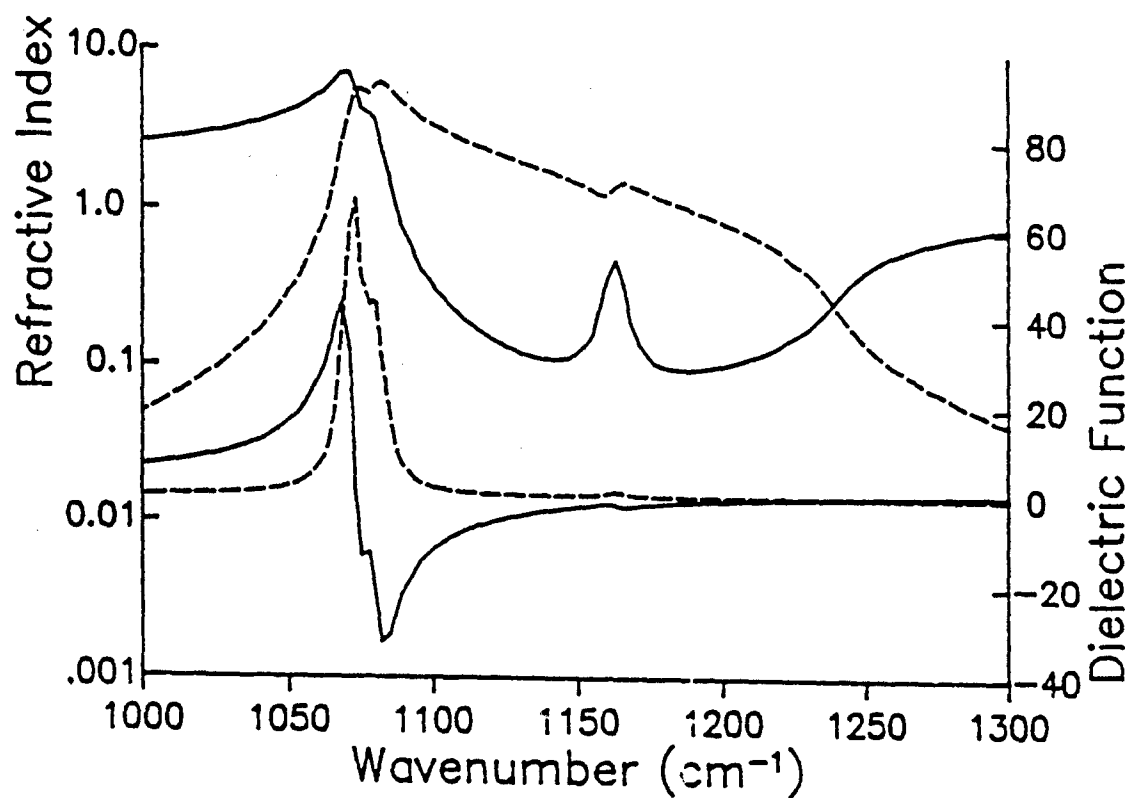


Figure A.4 Complex refractive index and dielectric function as a function of wavenumber (cm^{-1}) for quartz as obtained from the Lorentz oscillator model: upper curves are the refractive index, (—) represents the real part and (---) the imaginary part.

(Spitzer and Kleinman, 1961). As in Huffman and Bohren (1980) we used the so-called $\frac{1}{3}$ - $\frac{2}{3}$ rule to treat the anisotropy of quartz. ϵ' attains the value of -2 three times--at 1153, 1165, and 1169 cm^{-1} --with attendant values of ϵ'' being 0.39, 1.1, and 0.49 cm^{-1} , respectively. Although $\epsilon'' \neq 0$ when $\epsilon' = -2$, ϵ'' is sufficiently small to produce significant maxima in the extinction cross section, and we will still refer to these as Fröhlich modes. As seen in Figure A.4, the imaginary part of the refractive index, which is the usual first-order indicator of absorption, undergoes a slight inflection near 1160 cm^{-1} ; however, the resonance band is more pronounced than this indicates. Having all the necessary information to calculate the scattering parameters for quartz particles, our next step was to compare the coupled-dipole method by using the Doyle expression and the CM relation one last time.

Surface Modes for Spherical Particles

Replacing the CM relation with the Doyle expression to determine polarizability in the coupled-dipole method leads to extinction values that compare more closely with Mie theory. This was shown for several refractive indices where surface modes are not excited. However, when the calculations are made near the Fröhlich frequency, the CM relation does better than the Doyle expression. The following model comparison shows why.

Extinction efficiency was calculated for quartz spheres at the 1153 cm^{-1} Fröhlich frequency by using Mie theory and the coupled-dipole method. The variable of interest in this exercise was particle radius, which ranged from 0.1 to 100 μm when modeled by Mie theory. The coupled-dipole method was run twice, first with the CM relation and then with the Doyle expression, for each of nine spheres with radii ranging from 0.3 to 3.0 μm . For perspective, Mie theory was also used to calculate Q_{ext} for two other refractive indices. The results are shown in Figure A.5. The small-particle resonance associated

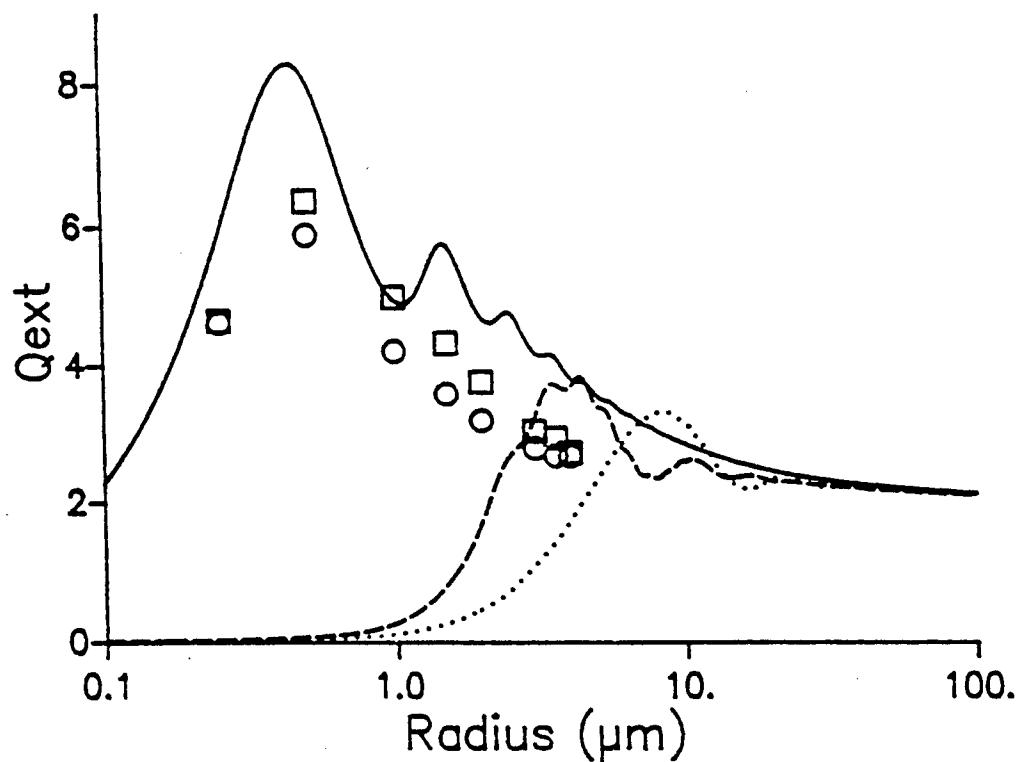


Figure A.5 Extinction efficiency as a function of particle radius (μm) obtained from Mie theory and the coupled-dipole method. Mie theory is represented by the continuous curves, each corresponds to a separate complex refractive index: — for $m = (0.1297, i1.444)$ (Fröhlich mode); \cdots for $m = (1.33, i0.05)$; and $---$ for $m = (1.7, i0.1)$. The coupled-dipole method is represented by \square when using the Clausius-Mosotti relation and \circ when using Doyle's expression; both are at the Fröhlich mode.

with the Fröhlich frequency is manifest as the highest Q_{ext} in the radius range from $3.0 \mu\text{m}$ and smaller. At larger radii ($> 3.0 \mu\text{m}$), the small-particle resonance diminishes and becomes obscured by the bulk properties of the sphere. In this size range, values of Q_{ext} for all three refractive indices approach the value of 2. It is in the size range between 0.3 and $3.0 \mu\text{m}$ for which the small-particle resonance is pronounced, and Q_{ext} obtained by using the CM relation more closely agrees with Mie theory calculation than does the Doyle expression.

It is observed that at radii of 0.3 and $3.0 \mu\text{m}$, the results from the coupled-dipole method with the CM relation or the Doyle expression are in agreement. It has been stated earlier that for small particles the Doyle expression reduces to the CM relation, which is why the two coupled-dipole method values agree at $0.3 \mu\text{m}$: both schemes yield identical polarizabilities. For particles larger than $3.0 \mu\text{m}$ the bulk extinction features become more important than the small-particle resonance. At these larger particle sizes the CM relation and the Doyle expression give different values for polarizability, but the calculated extinction efficiencies are nearly identical. (Larger spheres could not be run with the coupled-dipole method because of computer limitations.) Thus the discrepancy between the CM relation and the Doyle expression lies in the radius range from 0.3 to $3.0 \mu\text{m}$ and appears to be due to the small-particle resonance. This is not unexpected because the Doyle expression contains higher order terms of the size parameter that would have their greatest effect at limiting the resonance in this size range (according to the CM relation, polarizability is infinite at a true Fröhlich frequency, but it is not infinite by the Doyle expression). Consequently the larger polarizability from the CM relation leads to a higher Q_{ext} as seen between 0.3 and $3.0 \mu\text{m}$.

It may not be possible for the coupled-dipole method to duplicate the resonance peak of Mie theory at the Fröhlich frequency because the dipolar array cannot exactly represent a sphere. (More will be said about this below.)

The result will be a lower resonance peak. Using the CM relation in place of the Doyle expression yields a higher polarizability at a Fröhlich frequency, so we obtain a higher resonance peak. Thus conflicting inadequacies in the model permit the CM relation to produce extinction values at the Fröhlich frequency that more closely agree with Mie theory than does the Doyle expression.

For subsequent modeling the Doyle expression will be used. We feel that the elimination of the artificially high polarizability obtained with the CM relation near a Fröhlich mode should be avoided despite the fact that the CM relation agrees better with Mie theory. Replication of Mie theory is a goal when modeling spheres; however, in reality one might rather model a so-called near-sphere since spheres are more an anomaly in nature than modeling practices admit. We now examine extinction by quartz particles.

The extinction cross section per unit volume C_{ext}/v for a spherical quartz particle of radius $0.5 \mu\text{m}$ was calculated from wavenumber 1000 to 1300 cm^{-1} by using the optical constants shown in Figure A.4. For the coupled-dipole method, an array of 136 dipolar subunits was used to represent the sphere. The results appear in Figure A.6. Two major peaks appear in the Mie theory results that correspond to the Fröhlich frequencies--one peak is at 1153 cm^{-1} and the second is between 1165 and 1169 cm^{-1} . The coupled-dipole method also predicts extinction peaks near these frequencies; however, the peaks are not as high as those computed by Mie theory, and at 1153 cm^{-1} the extinction peak is shifted toward lower frequency and has a broader base. Both issues will be addressed; first is the extinction magnitude.

It was stated earlier that the resonance at a Fröhlich frequency is highly shape dependent. How well can a collection of dipoles on a cubic lattice represent a sphere at this frequency? Draine (1988) presented a criterion for estimating the sphericity of a dipolar array. By comparing the radius of gyration of an array of dipolar subunits with a sphere of equal volume, one

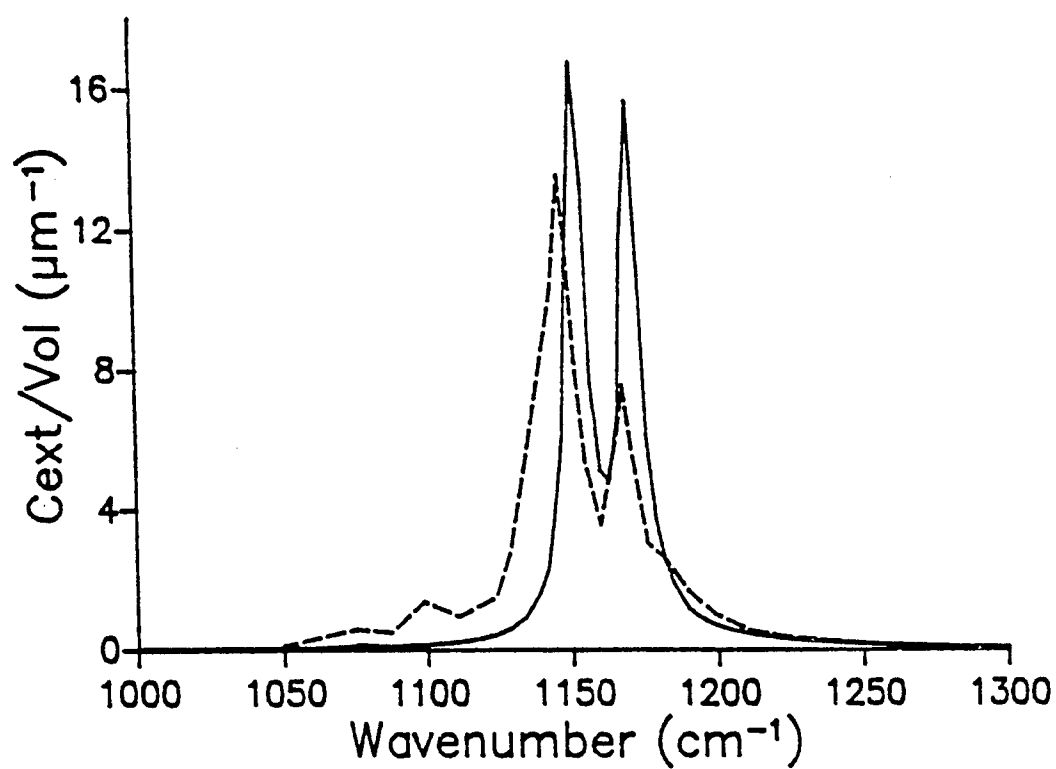


Figure A.6 Extinction cross section per unit volume (μm^{-1}) as a function of wavenumber (cm^{-1}) for spheres as obtained from Mie theory (—) and from the coupled-dipole method using the Doyle expression (- - -). Peaks correspond to the Fröhlich frequency for quartz.

can pick out a few values for N that best approximate a sphere. We adopted Draine's notation of $[f(N)]^{1/2}$ as the ratio of the radius of gyration of the dipolar array to that of a sphere. Thus as a measure of sphericity: $[f(N)]^{1/2} = 1$ for a perfect sphere. Draine contended that surface granularity, which is inversely proportional to the particle's sphericity, leads to numerical inaccuracies especially when the refractive index is large. We will investigate whether surface irregularity is the reason the coupled-dipole method cannot duplicate the peak extinction obtained from Mie theory at the Fröhlich frequency. If this were the case, the extinction cross section could be affected by small changes in the sphericity of a dipolar array.

Using the radius of gyration criterion, Draine considered the 136- and 160-dipole arrays to be good representations of spheres. (He also considered several larger arrays to be good representations, but the version of the coupled-dipole used here is limited to 300 dipolar subunits.) These dipole arrays have radii of 3.0 du and 3.5 du; however, the central dipoles of the arrays are displaced from the origin by 0.5 du. With the central dipole located at the origin, additional spherical approximations are obtained, for example: 123- and 179-dipole arrays (radii are 3.0 and 3.5 du). The sphericity of seven arrays was computed with the radius of gyration criterion and is listed in Table A.2. Note that the 136-, 160-, and 251-dipolar arrays have radii of gyration closer to unity than the remaining four arrays which implies that of the seven they best represent a spherical particle.

To determine if small changes in sphericity affects extinction near the 1153 cm^{-1} Fröhlich frequency, we eliminated the size difference of the seven arrays. The radii of the dipolar subunits of the seven arrays were adjusted so that the entire array represented a sphere with an effective radius a_e of $0.5 \mu\text{m}$. C_{ext}/v was then calculated for the seven arrays; the values are reported in Table A.2. At non-surface modes C_{ext}/v for spheres is unaffected by these variations in N (when a_e is held constant), but as seen in Table A.2 extinction

Table A.2. Comparison of C_{ext}/v among seven dipolar arrays; all represent a spherical particle of radius $0.5 \mu\text{m}$. Columns represent number of dipoles, radius of gyration, and maximum value of C_{ext}/v near the 1153 cm^{-1} Fröhlich frequency as calculated by the coupled-dipole method. Rows are in order of decreasing sphericity as determined by Draine's criterion. The corresponding C_{ext}/v calculated by Mie theory is $17.1 \mu\text{m}^{-1}$.

N	$[f(N)]^{1/2}$	C_{ext}/v
251	1.0015	14.40
136	1.0017	13.61
160	1.0021	14.94
179	1.0039	10.93
208	1.0069	11.58
147	1.0078	9.44
123	1.0112	10.12

values differ greatly at a Fröhlich mode. The three arrays that are the best representations of spheres according to Draine's criterion also have the highest values for extinction. This is not meant to be a definitive statement but it appears that extinction is dependent on how well the dipolar array represents a sphere. Unfortunately, larger arrays cannot be modeled with the matrix inversion method. The scattering order version can be used for arrays that contain greater than 1000 dipolar subunits, but that solution method diverges when the polarizability is too high (Singham and Bohren, 1988).

A corollary of this is that bigger arrays may not always be better: a sphere should not necessarily be represented by the largest array possible. For example, Table A.2 implies that the array that contains 136 dipolar subunits represents a sphere better than does the 208-unit array. This assertion is not conclusive, and needs further research.

Although sphericity of the dipolar array affects C_{ext}/v , it does not explain why values are lower than Mie theory by as much as 20%. This discrepancy of maximum calculated extinction may be inherent in the formulation of the coupled-dipole method. The coupled-dipole method is able to match the extinction computed by Mie theory at the Fröhlich frequency, but only when the dipolar subunits do not communicate their scattered fields to their neighbors. When the interactions between the subunits have been turned off, they scatter as individual spheres and the calculated C_{ext}/v becomes identical to that given by Mie theory. When the interactions are included, the values of C_{ext}/v decrease to what was shown in Table A.2. Thus the coupling of the dipoles appears to be the limiting factor: an array of dipolar subunits on a cubic lattice does not adequately represent a sphere when the shape dependence is as crucial as at a Fröhlich mode. We now will investigate the broadening of the extinction band shown in Figure A.6.

Shape Effects on Surface Modes

Mie theory predicts strong resonance peaks at Fröhlich frequencies for quartz crystals in the Rayleigh regime. The coupled-dipole method also shows extinction maxima at these frequencies as noted above; however, the height and width of the coupled-dipole extinction curve is different from that obtained with Mie theory. The reduction in height was explained by the inability of a finite array of dipolar subunits to represent a sphere. The widening of the extinction band may be explained in a similar fashion.

Resonance features are not limited to spheres. Whereas Mie theory is applicable only to spheres, the coupled-dipole method may be used to calculate extinction for any particle shape. To investigate nonspherical resonances near the Fröhlich frequency, we modeled the following shapes by using the coupled-dipole method: a 2×1 and a 4×1 oblate spheroid and a 2×1 and a 4×1 prolate spheroid comprised of 152, 136, 138, and 136 dipolar subunits, respectively. The spheroids were modeled with an equivalent radius of $0.5 \mu\text{m}$ as was done when modeling the 136-dipolar subunit sphere in the previous section. To simulate random orientation of the particles for comparison with measured data each spheroid was rotated in over 100 alignments. (The spheres in the previous section were also rotated but little effect on Q_{ext} was noted.)

Values of C_{ext}/v for the four spheroids and the 136-unit sphere are shown in Figure A.7. Near the Fröhlich frequencies, the spherical array exhibits the highest C_{ext}/v . Near wavenumber 1125 cm^{-1} , a larger value for extinction is calculated for both oblate spheroids and the 2×1 prolate spheroid than for the sphere suggesting the presence of a nonspherical resonance. Recalling Figure A.6, C_{ext}/v for the 136-dipole sphere was larger at 1125 cm^{-1} than that computed by Mie theory. Since the 136-dipole sphere was shown earlier to be slightly nonspherical, this nonspherical resonance could account for this larger extinction for the 136-dipole sphere. The proximity of the

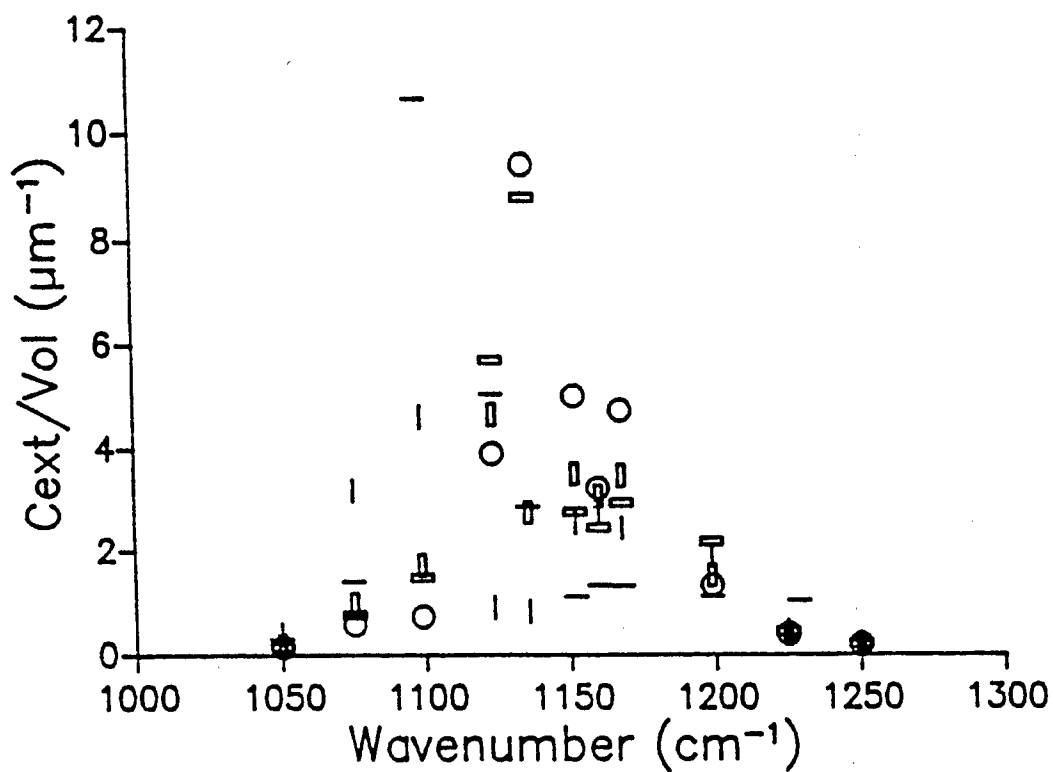


Figure A.7 Pictorial representation of small-particle extinction for quartz. Extinction cross section per unit volume (μm^{-1}) calculated by the coupled-dipole (Doyle expression) as a function of wavenumber (cm^{-1}). Five shapes are represented: \circ symbolizes a sphere, \parallel a 2×1 prolate spheroid, $|$ a 4×1 prolate spheroid, $=$ a 2×1 oblate spheroid, and $—$ a 4×1 oblate spheroid.

nonspherical resonance to the Fröhlich frequency of 1153 cm^{-1} thus widens the extinction band of the 136-dipole sphere towards lower wavenumbers as seen in Figure A.6. A similar broadening does not occur towards higher wavenumbers because, as can be seen from Figure A.7, the nonspherical resonances at 1200 cm^{-1} are weaker than those at 1125 cm^{-1} .

The results from modeling the sphere and spheroids with the coupled-dipole method are now compared with another theoretical method--the method of continuous distribution of ellipsoids CDE (Huffman and Bohren, 1980). This method is used to compute the absorption cross section per unit volume C_{abs}/v by integrating over a distribution of shape parameters in the Rayleigh-ellipsoid approximation. The CDE expression is simplified when all shapes within the ellipsoid distribution are equally probable:

$$\frac{C_{\text{abs}}}{v} = k \text{Im} \left(\frac{2\varepsilon}{\varepsilon - 1} \text{Log } \varepsilon \right). \quad (\text{A.7})$$

For comparison with the coupled-dipole results, extinction is taken to be nearly equal to absorption. This is not a bad assumption since the particles are small compared with the wavelength, and in the vicinity of the Fröhlich modes calculations from the coupled-dipole method show that the scattering cross section is approximately an order of magnitude smaller than the absorption cross section. To duplicate the equally-probable spheroid distribution used in the CDE method, we merely averaged the C_{ext}/v values from the coupled-dipole method for the sphere and spheroids. The modeling results are shown in Figure A.8. The agreement is good considering the CDE method represents a continuous distribution of spheroids and the coupled-dipole method only five arrays (four spheroids and a sphere). In turn, extinction measurements for submicron quartz crystals have been shown to be well predicted by the CDE method (Huffman and Bohren, 1980). Thus by the transitive property, this exercise has given credence to the ability of the coupled-dipole method

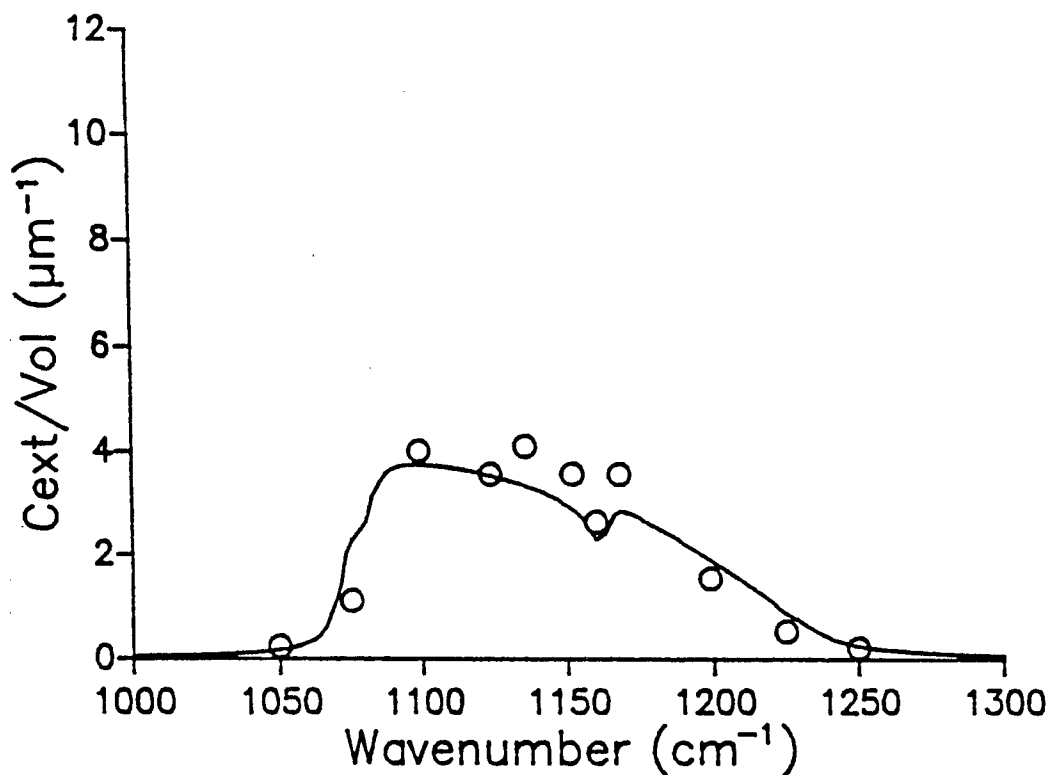


Figure A.8 Extinction cross section per unit volume (μm^{-1}) as a function of wavenumber (cm^{-1}) obtained from the Continuous Distribution of Ellipsoids method (—) and the coupled-dipole method (Doyle expression) using five spheroids (○): sphere, 2×1 and 4×1 oblate and prolate spheroids.

with the Doyle expression to treat extinction by nonspherical particles near a Fröhlich frequency.

As pointed out by a reviewer the coupled-dipole method may be overkill when comparing it with calculations based on electrostatics. However, because retardation is accounted for, the coupled-dipole method could (perhaps should) be used to investigate particles with larger size parameters near a Fröhlich mode whereas the CDE method could not. The purpose of this exercise was to introduce the Doyle expression. As for comparing the coupled-dipole method with an exact method such as the T-matrix, Goedecke and O'Brien (1988) have already shown agreement between the two, and, because of the size parameters of the spheroid as particles that we modeled, the use of the T-matrix for this study is unwarranted.

Conclusions

The coupled-dipole method relies on an effective-medium theory to provide the polarizability of the dipolar subunits. The CM relation is widely used in the coupled-dipole method, but because of the size of the dipolar subunits, it has an insufficient number of terms to account appropriately for the electric dipole polarizability. Doyle (1989) used the electric dipole term from Mie theory to obtain an exact expression for polarizability that afforded improved calculations of optical properties of a suspension of metal spheres. Incorporating Doyle's expression in the coupled-dipole method in place of the CM relation yielded improved extinction calculations at nonresonance frequencies.

Doyle's expression was further tested by calculating extinction by quartz particles near a Fröhlich mode. The small-particle absorption associated with this mode is highly shape dependent. Mie theory and the coupled-dipole method were compared by calculating the extinction by spherical particles;

differences were noted and examined. First, the peak extinction calculated by the coupled-dipole method was much lower than that obtained from Mie theory. This is because the shape dependency at the Fröhlich frequency is so critical that a spherical array of dipoles fails to represent a perfect sphere. Second, results from the coupled-dipole method indicated a wider absorption band than obtained from Mie theory. Further modeling with the coupled-dipole method indicated the broadening arises from nonspherical particle resonances. The calculated extinction by these nonspherical particles agrees with the results of another theoretical method, the CDE method, which in turn has been shown to agree with measured data (Huffman and Bohren, 1980).

Acknowledgements

We thank Shermila Singham who provided several versions of the coupled-dipole program that we adapted for use in this project. We also thank Keith Kendall and Andrew Vogelmann for their comments. This research was supported in part by NASA Grant NAS8-36194 and NSF Grant ATM-8810876.

Appendix B

SUBROUTINES FOR BUILDING DIPOLAR ARRAYS

This appendix contains source listings of the subroutines described in Chapter 4. The subroutines are used to build arrays which represent particles of several different shapes.

```

SUBROUTINE SPHERE (RAD,REALRAD,OFFSET,X,Y,Z,ITOT,RADEFF)
C
C THIS SUBROUTINE BUILDS A SPHERE OF DIPOLAR SUBUNITS.
C
C INPUT: RAD IS THE NUMBER OF DIPOLAR SUBUNITS IN THE RADIUS OF
C THE SPHERE; REALRAD IS THE RADIUS OF THE--IT IS USED TO ADJUST
C THE SIZE OF THE DIPOLAR SUBUNITS; OFFSET = 0.0 IF ORIGIN IS
C LOCATED WITH THE CENTRAL DIPOLE, OTHERWISE = 0.5.
C
C OUTPUT: ARRAYS X, Y, AND Z GIVE THE COORDINATES OF THE DIPOLAR
C SUBUNITS; ITOT IS THE NUMBER OF DIPOLES IN THE ARRAY; RADEFF IS
C THE EFFECTIVE RADIUS OF THE SPHERE
C
  DIMENSION X( * ), Y( * ), Z( * )
  OFFSET = 0.0
  ITOT = 0
  RAD2 = RAD*RAD
  ISIZE = IFIX(RAD+1.0)
C
  DO 30 JZ = -ISIZE,ISIZE,1
    ZJZ = FLOAT(JZ) + OFFSET
    DO 20 JY = -ISIZE,ISIZE,1
      YJY = FLOAT(JY) + OFFSET
      DO 10 JX = -ISIZE,ISIZE,1
        XJX = FLOAT(JX) + OFFSET
C
C DETERMINE IF THIS LATTICE POSITION FALLS WITHIN SPHERE'S RADIUS
C
        R = 1.0 * (XJX**2 + YJY**2 + ZJZ**2)
        IF (R.GT.RAD2) GO TO 10
C
        ITOT = ITOT + 1
        X(ITOT) = 1.0 * XJX
        Y(ITOT) = 1.0 * YJY
        Z(ITOT) = 1.0 * ZJZ
10      CONTINUE
20      CONTINUE
30      CONTINUE
C
  RADEFF = ((3*ITOT)/(4*PI))**(1/3) IN DIPOLE UNITS
  RADEFF = (0.238732415 * ITOT)**(1./3.)
C
  RAD = RADEFF
  IF (REALRAD.NE.0.0) RAD = REALRAD
C
  RETURN
  END

```

```

SUBROUTINE SPHROID (AAA,BBB,REALRAD,X,Y,Z,ITOT,RADEFF)
C
C   THIS SUBROUTINE BUILDS AN SPHEROID OF DIPOLAR SUBUNITS.
C
C   INPUT: AAA AND BBB ARE THE DIMENSIONS OF THE MAJOR AND MINOR AXES;
C   REALRAD IS THE RADIUS OF THE EQUIVALENT-VOLUME SPHERE. OFFSET IS
C   SET AUTOMATICALLY. CIRCULAR CROSS SECTION IS ORIENTED IN Y-Z
C   PLANE. OUTPUT: ARRAYS X, Y, AND Z GIVE THE COORDINATES OF THE
C   DIPOLAR SUBUNITS; ITOT IS THE NUMBER OF DIPOLES IN THE ARRAY;
C   RADEFF IS THE EFFECTIVE RADIUS OF THE EQUIVALENT-VOLUME SPHERE.
C
C   DIMENSION X( * ), Y( * ), Z( * )
C
C   IAA = IFIX(AAA - 1.0)
C   IBB = IFIX(BBB - 1.0)
C   DIAA = AAA/2.
C   DIAC = BBB/2.
C   ITOT = 0
C
C   DO 30 JX = -IBB,IBB,2
C     XJX = FLOAT(JX)/2.
C     DO 20 JY = -IAA,IAA,2
C       YJY = FLOAT(JY)/2.
C       DO 10 JZ = -IAA,IAA,2
C         ZJZ = FLOAT(JZ)/2.
C
C   C   DETERMINE IF THIS LATTICE POSITION FALLS WITHIN RADIUS
C   C   RAD = ((ZJZ/DIAA)**2 + (YJY/DIAA)**2 + (XJX/DIAC)**2)
C   C   IF (RAD.GT.1.0) GO TO 10
C
C   C   ITOT = ITOT + 1
C   C   X(ITOT) = 1.0 * XJX
C   C   Y(ITOT) = 1.0 * YJY
C   C   Z(ITOT) = 1.0 * ZJZ
10  CONTINUE
20  CONTINUE
30  CONTINUE
C
C   RADEFF = ((3*ITOT)/(4*PI))**(1/3)
C   RADEFF = (0.238732415*ITOT)**(1./3.)
C
C   RAD = REALRAD
C   IF (REALRAD.NE.0.0) RAD = REALRAD
C
C   RETURN
C   END

```

SUBROUTINE RECTSLD (AAA,BBB,CCC,REALRAD,X,Y,Z,ITOT,RADEFF)

```

C
C   THIS SUBROUTINE BUILDS A RECTANGULAR SOLID OF DIPOLAR SUBUNITS.
C
C   INPUT: AAA, BBB, CCC ARE THE X, Y, Z, DIMENSIONS; REALRAD IS THE
C   RADIUS OF THE EQUIVALENT-VOLUME SPHERE.
C
C   OUTPUT: ARRAYS X, Y, AND Z GIVE THE COORDINATE OF THE DIPOLAR
C   SUBUNITS; ITOT IS THE NUMBER OF DIPOLES IN THE ARRAY; RADEFF
C   IS THE EFFECTIVE RADIUS OF THE EQUIVALENT-VOLUME SPHERE.
C
C   DIMENSION X( * ), Y( * ), Z( * )
C
C   ITOT = 0
C   IAA = IFIX(AAA - 1.0)
C   IBB = IFIX(BBB - 1.0)
C   ICC = IFIX(CCC - 1.0)
C
C   DO 30 JZ = -ICC,ICC,2
C     DO 20 JY = -IBB,IBB,2
C       DO 10 JX = -IAA,IAA,2
C         ITOT = ITOT + 1
C         Z(ITOT) = FLOAT(JZ)/2.
C         Y(ITOT) = FLOAT(JY)/2.
C         X(ITOT) = FLOAT(JX)/2.
10      CONTINUE
20      CONTINUE
30      CONTINUE
C
C   RADEFF = ((3*ITOT)/(4*PI))**(1/3)
C   RADEFF = (0.238732415 * ITOT)**(1./3.)
C
C   RAD = REALRAD
C   IF (REALRAD.NE.0.0) RAD = REALRAD
C
C   RETURN
C   END

```

```

SUBROUTINE CYLNDER (RAD,HGHT,REALRAD,OFFSET,X,Y,Z,ITOT,RADEFF)
C
C THIS SUBROUTINE BUILDS A CYLINDER OF DIPOLAR SUBUNITS.
C
C INPUT: RAD IS THE NUMBER OF DIPOLAR SUBUNITS IN THE RADIUS OF THE
C CROSS SECTION; HGHT IS THE LENGTH OF THE CYLINDER; REALRAD IS THE
C RADIUS OF THE EQUIVALENT-AREA CIRCLE OF THE CROSS SECTION;
C OFFSET = 0.0 IF THE CENTRAL DIPOLES ARE LOCATED ON THE X AXIS,
C OTHERWISE =0.5. CYLINDER IS ORIENTED ALONG X AXIS.
C
C OUTPUT: ARRAYS X, Y, AND Z GIVE THE COORDINATES OF THE DIPOLAR
C SUBUNITS; ITOT IS THE NUMBER OF DIPOLES IN THE ARRAY; RADEFF IS
C THE EFFECTIVE RADIUS OF THE EQUIVALENT-AREA CIRCLE OF CROSS
C SECTION.
C
C DIMENSION X( * ), Y( * ), Z( * )
C ITOT = 0
C RAD2 = RAD * RAD
C ISIZE = IFIX(RAD + 1.0)
C LSIZE = IFIX(HGHT - 1.0)
C
C DO 30 JY = -ISIZE,ISIZE,1
C   YJY = FLOAT(JY) + OFFSET
C   DO 20 JZ = -ISIZE,ISIZE,1
C     ZJZ = FLOAT(JZ) + OFFSET
C     R = (YJY**2 + ZJZ**2)
C     IF (R.GT.RAD2) GO TO 20
C     DO 10 JX = -LSIZE,LSIZE,2
C       ITOT = ITOT + 1
C       Z(ITOT) = ZJZ
C       Y(ITOT) = YJY
C       X(ITOT) = FLOAT(JX)/2.
C     CONTINUE
C   CONTINUE
C CONTINUE
C
C RADEFF=(ITOT/(HGHT*PI))**1/2 OF THE CYLINDER'S RADIUS
C RADEFF = (ITOT/(HGHT * 3.141592654))**.5
C
C RAD = RADEFF
C IF (REALRAD.NE.0.0) RAD = REALRAD
C
C RETURN
C END

```



```

C      SUBROUTINE FCC (RAD,REALRAD,OFFSET,X,Y,Z,ITOT,RADEFF)
C
C      THIS SUBROUTINE BUILDS A SPHERE OF DIPOLAR SUBUNITS ON A FACE-
C      CENTERED CUBIC LATTICE RATHER THAN SIMPLE CUBIC LATTICE.
C
C      INPUT: RAD IS THE NUMBER OF DIPOLOAR SUBUNITS IN THE RADIUS OF
C      THE SPHERE; REALRAD IS THE RADIUS OF THE SPHERE; OFFSET = 0.0
C      IF THE ORIGIN IS LOCATED WITH THE CENTRAL DIPOLE, OTHERWISE = 0.5.
C
C      OUTPUT: ARRAYS X, Y, AND Z GIVE THE COORDINATES OF THE DIPOLAR
C      SUBUNITS; ITOT IS THE NUMBER OF DIPOLES IN THE ARRAY; RADEFF IS
C      THE EFFECTIVE RADIUS OF THE SPHERE.
C
C      DIMENSION X( * ), Y( * ), Z( * )
C      ITOT = 0
C      ROOT2 = SQRT(2.)
C      FACE = ROOT2 * 0.5
C      RAD2 = RAD * RAD
C      ISIZE = IFIX(RAD + 2.0)
C
C      DO 50 JZ = -ISIZE,ISIZE,1
C        DO 40 JY = -ISIZE,ISIZE,1
C          DO 30 JX = -ISIZE,ISIZE,1
C            XJX = ROOT2 * FLOAT(JX) + OFFSET
C            YJY = ROOT2 * FLOAT(JY) + OFFSET
C            ZJZ = ROOT2 * FLOAT(JZ) + OFFSET
C            DO 20 I = 1,4
C              R = 1.0 * (XJX**2 + YJY**2 + ZJZ**2)
C              IF (R.GT.RAD2) GO TO 10
C              ITOT = ITOT + 1
C              X(ITOT) = 1.0 * XJX
C              Y(ITOT) = 1.0 * YJY
C              Z(ITOT) = 1.0 * ZJZ
C              IF (I.EQ.1) THEN
C                XJX = XJX - FACE
C                YJY = YJY - FACE
C              ELSE IF (I.EQ.2) THEN
C                XJX = XJX + FACE
C                ZJZ = ZJZ - FACE
C              ELSE
C                XJX = XJX - FACE
C                YJY = YJY + FACE
C              END IF
C            CONTINUE
C          CONTINUE
C        CONTINUE
C      CONTINUE
C
C      RADEFF = ((3*ITOT)/(4*PI))**(1/3)
C      RADEFF = (0.238732415 * ITOT/ROOT2)**(1./3.)
C
C      RAD = RADEFF
C      IF (REALRAD.NE.0.0) RAD = REALRAD
C
C      RETURN
C      END

```

```

SUBROUTINE HEX (AAA,BBB,REALRAD,X,Y,Z,ITOT,RADEFF)
C
C   THIS SUBROUTINE BUILDS A HEXAGON SOLID OF DIPOLAR SUBUNITS.
C
C   INPUT: THE PARTICLE IS ALIGNED ALONG THE X AXIS WITH TWO OF THE
C   VERTICES LYING IN THE X-Z PLANE.  AAA IS THE NUMBER OF DIPOLES
C   IN THE WIDTH (Y DIRECTION); BBB IS THE NUMBER OF DIPOLES IN THE
C   LENGTH (X DIRECTION); REALRAD IS THE RADIUS OF THE EQUIVALENT-
C   AREA CIRCLE REPRESENTED BY THE CROSS SECTION OF THE PARTICLE.
C
C   OUTPUT: ARRAYS X, Y, AND Z GIVE THE COORDINATES OF THE DIPOLAR
C   SUBUNITS; ITOT IS THE NUMBER OF DIPOLES IN THE ARRAY; RADEFF
C   IS THE EFFECTIVE RADIUS OF THE CROSS SECTION.
C
C   DIMENSION X(*),Y(*),Z(*)
C   ITOT = 0
C   IAA = IFIX(AAA - 1.0)
C   IBB = IFIX(BBB - 1.0)
C
C   DETERMINE Z DISTANCE WHICH BEST APPROXIMATES EQUAL LENGTH FACES
C
C   ICC = NINT(SQRT(2.) * ((AAA-1.)/2.))
C
C   DO 30 JX=-IBB,IBB,2
C
C   BUILD THE CENTER SQUARE/RECTANGLE
C
C   IND = 0
C   DO 20 JY = -IAA,IAA,2
C     DO 10 JZ = -ICC,ICC,2
C       ITOT = ITOT + 1
C       Z(ITOT) = FLOAT(JZ)/2.
C       Y(ITOT) = FLOAT(JY)/2.
C       X(ITOT) = FLOAT(JX)/2.
10     CONTINUE
20   CONTINUE

```

```

C
C   BUILD THE UPPER AND LOWER TRIANGLES
C   DETERMINE HOW MANY LINES OF DIPOLES (NOL) TO ADD:
C
      NOL = IFIX(AAA/2.)
      DO 40 I = 1,NOL
C
C   START BUILDING NEW LINES REMEMBERING TO INDENT ONE EACH TIME
C
      IND = IND + 2
      JZ = ICC + IND
      DO 50 JY = -IAA+IND, IAA-IND, 2
        ITOT = ITOT + 1
        Z(ITOT) = FLOAT(JZ)/2.
        Y(ITOT) = FLOAT(JY)/2.
        X(ITOT) = FLOAT(JX)/2.
        ITOT = ITOT + 1
        Z(ITOT) = FLOAT(JZ)/(-2.)
        Y(ITOT) = FLOAT(JY)/2.
        X(ITOT)=FLOAT(JX)/2.
50      CONTINUE
40      CONTINUE
30      CONTINUE
C
C   RADEFF=(ITOT/(BBB*PI))*1/2 OF THE CYLINDER'S RADIUS
C   RADEFF = (ITOT/(BBB*3.141592654))*0.5
C
      RAD = RADEFF
      IF (REALRAD.NE.0.0) RAD = REALRAD
C
      RETURN
      END

```

REFERENCES

- Asano, S. and G. Yamamoto. 1975. Light scattering by a spheroidal particle, *Applied Optics*, 14: 29-49.
- Barber, P. and C. Yeh. 1975. Scattering of electromagnetic waves by arbitrarily shaped dielectric bodies, *Applied Optics*, 14: 2864-2872.
- Barker, A. S. 1973. Infrared absorption of localized longitudinal-optical phonons, *Physics Review*, B7: 2507-2520.
- Bickel, W. S. and W. M. Bailey. 1985. Stokes vectors, Mueller matrices and polarized scattered light, *American Journal of Physics*, 53: 468-478.
- Bohren, C. F. and D. R. Huffman. 1983. *Absorption and Scattering of Light by Small Particles*, Wiley-Interscience, New York.
- Bohren, C. F. and S. B. Singham. 1990. Backscattering by nonspherical particles: a review of methods; suggested new approaches, *GLOBE edition of Journal of Geophysical Research*.
- Bohren, C. F. and N. C. Wickramasinghe. 1977. On the computation of optical properties of heterogeneous grains, *Astrophysics and Space Science*, 50: 461-472.
- Cassim, J. Y. and E. W. Taylor. 1965. Intrinsic birefringence of a poly- γ -benzyl-L-glutamate, a helical polypeptide, and the theory of birefringence, *Biophysical Journal*, 5: 531-552.
- Chiappetta, P. 1980. Multiple scattering approach to light scattering by arbitrarily shaped particles, *Journal of Physics A*, 13: 2101-2108.
- Chiappetta, P. and B. Torresani. 1988. Electromagnetic scattering from a dielectric helix, *Applied Optics*, 28: 2085-2091.
- Cho, H. R., J. V. Iribarne and W. G. Richards. 1981. On the orientation of ice crystals in a cumulonimbus cloud, *Journal of the Atmospheric Sciences*, 38: 1111-1114.
- Doyle, W. T. 1989. Optical properties of a suspension of metal spheres, *Physical Review B*, 39(0): 9852-9858.

- Draine, B. T. 1988. The discrete-dipole approximation and its application to interstellar graphite grains, *The Astrophysical Journal*, 333: 848-872.
- Drolen, B. L. and C. L. Tien. 1987. Absorption and scattering of agglomerated soot particulate, *Journal of Quantitative Spectroscopy and Radiative Transfer*, 37: 433-448.
- Dungey, C. E. 1976. The effect of rainfall intensity on the removal of atmospheric sulfate, MS Thesis, Department of Meteorology, Pennsylvania State University, University Park, PA.
- Evans, K. F. and J. Vivekanandan. 1990. Multiparameter radar and microwave radiative transfer modeling of non-spherical atmospheric ice particles, *IEEE Geoscience and Remote Sensing*, 423-437.
- Flatau, P. T., G. L. Stephens, and B. T. Draine. 1988. Scattering on hexagonal ice crystals: discrete dipole and anomalous diffraction approximations, *Proceedings of the International Radiation Symposium*, 72-75, Lille, France.
- Flatau, P. T., G. L. Stephens, and B. T. Draine. 1990. Light scattering by rectangular solids in the discrete dipole approximation: a new algorithm exploiting the block-Toeplitz structure, *Journal of the Optical Society of America A*, 7: 593-600.
- Goedecke, G. H. and S. G. O'Brien. 1988. Scattering by irregular inhomogeneous particles via the digitized Green's function algorithm, *Applied Optics*, 27: 2431-2438.
- Gray, F. 1916. The optical activity of liquids and gases, *Physical Review*, VII: 472-486.
- Harris, R. A. and W. M. McClain. 1985. On the manifestation of retardation effects in diagonally polarized light scattering, *Journal of Chemical Physics*, 82: 658-663.
- Huffman, D. T. and C. F. Bohren. 1980. Infrared absorption spectra of non-spherical particles treated in the Rayleigh-ellipsoid approximation, in *Light Scattering by Irregularly Shaped Particles*, D. Schuerman ed., Plenum, New York, 103-111.
- Jackson, J. D. 1975. *Classical Electrodynamics*, Second Edition, Wiley and Sons, New York.

- Jones, A. R. 1979. Electromagnetic wave scattering by assemblies of particles in the Rayleigh approximation, *Proceedings of the Royal Society of London (A)*, 366: 111-127.
- Kattawar, G. W., C. Hu, M. E. Parkin, and P. Herb. 1987. Mueller matrix calculations for dielectric cubes: comparison with experiments, *Applied Optics*, 26: 4174-4180.
- Kirkwood, J. G. 1936. On the theory of dielectric polarization, *Journal of Chemical Physics*, 4: 592-601.
- Kittel, C. 1976. *Solid State Physics*, Fifth Edition, Wiley and Sons, New York.
- Lakhtakia, A. 1990. Macroscopic theory of the coupled dipole approximation method, *Optics Communication* (to be published).
- Lhermitte, R. 1987. A 94 GHz Doppler radar for cloud observations, *Journal of Atmospheric and Oceanic Technology*, 4: 36-48.
- Lhermitte, R. M. 1988. Cloud and precipitation remote sensing at 94 GHz, *IEEE Transactions on Geoscience and Remote Sensing*, 26: 207-216.
- Lhermitte, R. 1990. Attenuation and scattering of millimeter wavelength radiation by clouds and precipitation, *Journal of Atmospheric and Oceanic Technology*, 7: 464-479.
- Logan, N. A. 1965. Survey of some early studies of the scattering of plane waves by a sphere, *Proceedings of the IEEE*, 53: 773-785.
- Marshall, J. S. and Palmer, W. M. 1947. The distribution of raindrops with size, *Journal of Meteorology*, 5: 165-168.
- Massoudi, H., C. H. Durney, and M. F. Iskander. 1984. Limitations of the cubical block model of man in calculating SAR distributions, *IEEE Transactions on Microwave Theory and Techniques*, MTT-32: 746-752.
- Mead, J. B., R. E. McIntosh, D. Vandemark, and C. T. Swift. 1989. Remote sensing of clouds and fog with a 1.4-mm radar, *Journal of Atmospheric and Oceanic Technology*, 6: 1090-1097.
- Mie, G. 1908. Beitrage zur optik trüber Medien speziell kolloidaler Metallösungen, *Annals of Physics*, 25: 377-445.

- Mugnai, A. and W. J. Wiscombe. 1980. Scattering of radiation by moderately nonspherical particles, *Journal of the Atmospheric Sciences*, **37**: 1291-1307.
- O'Brien, S. G. and G. H. Goedecke. 1988. Scattering of millimeter waves by snow crystals and equivalent homogeneous symmetric particles, *Applied Optics*, **27**: 2439-2444.
- Oguchi, T. 1973. Attenuation and phase rotation of radio waves due to rain: calculations at 13.4 and 34.8 GHz, *Radio Science*, **8**: 31-38.
- Post, E. J. 1962. *Formal Structure of Electromagnetics, General Covariance and Electromagnetics*, Amsterdam, North-Holland Pub. Co., New York.
- Pruppacher, H. R. and J. D. Klett. 1980. *Microphysics of Clouds and Precipitation*, D. Reidel Publishing Company, Dordrecht, Holland.
- Purcell, E. M. and C. R. Pennypacker. 1973. Scattering and absorption of light by nonspherical dielectric grains, *The Astrophysical Journal*, **186**: 705-714.
- Rayleigh, Lord. 1881. On the scattering of light by small particles, *Philosophy Magazine*, **41**: 447-454. (reprinted in *Scientific Papers by Lord Rayleigh*, Vol I, Dover, New York, 1964).
- Rusk, A. N., and D. Williams, and M. R. Querry. 1971. Optical constants of water in the infrared, *Journal of the Optical Society of America*, **61**: 895-903.
- Singham, M. K., S. B. Singham, and G. C. Salzman. 1986b. The scattering matrix for randomly oriented particles, *Journal of Chemical Physics*, **85**(7): 3807-3815.
- Singham, S. B. 1986. Intrinsic optical activity in light scattering from an arbitrary particle, *Chemical Physics Letters*, **130**: 139-144.
- Singham, S. B. and C. F. Bohren. 1988. Light scattering by an arbitrary particle: the scattering-order formulation of the coupled-dipole method, *Journal of the Optical Society of America A*, **5**(11): 1867-1872.
- Singham, S. B., C. W. Patterson, and G. C. Salzman. 1986a. Polarizabilities for light scattering from chiral particles, *Journal of Chemical Physics*, **85**(2): 763-770.

- Singham, S. B. and G. C. Salzman. 1986. Evaluation of the scattering matrix of an arbitrary particle using the coupled-dipole approximation, *Journal of Chemical Physics*, **84**(5): 2658-2667.
- Spitzer, W. G. and D. A. Kleinman. 1961. Infrared lattice bands of quartz, *Physical Review*, **121**(5): 1324-1335.
- Strang, G. 1986. *Introduction to Applied Mathematics*, Wellesley-Cambridge Press, Wellesley, MA.
- Taubenblatt, M. A. 1990. Light scattering from cylindrical structures on surfaces, *Optics Letters*, **15**: 255-257.
- Varadan, V. V., A. Lakhtakia, and V. K. Varadan. 1989. Scattering by three-dimensional anisotropic scatterers, *IEEE Transactions of Antennas and Propagation*, **37**(6): 800-802.
- Vogelmann, A. M., T. P. Ackerman, and C. E. Dungey. 1990. Nonspherical particle scattering in cirrus clouds, *Extended Abstracts of the Seventh Conference on Atmospheric Radiation*, San Francisco, CA, July 23-27.
- Waterman, P. C. 1965. Matrix formulation of electromagnetic scattering, *Proceedings of the IEEE*, **53**: 805-812.
- Waterman, P. C. 1971. Symmetry, unitarity, and geometry in electromagnetic scattering, *Physics Review*, **D3**: 825-839.
- Wright, E. L. 1987. Long-wavelength absorption by fractal dust grains, *The Astrophysical Journal*, **320**: 818-824.
- Wright, E. L. 1988. The ultraviolet extinction from interstellar graphitic onions, *Nature*, **336**: 227-228.
- Yeh, C. 1964. Perturbation approach to the diffraction of electromagnetic waves by arbitrarily shaped dielectric obstacles, *Physical Review*, **135**: A1193-A1201.
- Yeh, C., R. Woo, A. Ishimaru, and J. Armstrong. 1982. Scattering by single ice needles and plates at 30 GHz, *Radio Science*, **17**: 1503-1510.
- Yung, Y. L. 1978. Variational principle for scattering light by dielectric particles, *Applied Optics*, **17**(23): 3707-3707.

VITA

Clifton E. Dungey was born on 29 July 1952 in Kingston, Pa. In 1970, he graduated from Dallas Area High School, Dallas, Pa. He completed his B.S. in Mathematics at Wilkes College, Wilkes-Barre, Pa in 1974, and his M.S. in Meteorology at The Pennsylvania State University in 1976. From 1976 to 1977, he was an instructor of Earth and Environmental Science at Wilkes College. From 1978 to 1983, he was employed as a meteorologist/ environmental scientist at Argonne National Laboratory, Argonne, IL. In 1983, he joined the U.S. Air Force. In 1987, he was assigned to the graduate program in meteorology of the Air Force Institute of Technology. He studied light scattering at The Pennsylvania State University under the supervision of Professor Craig F. Bohren.